Synthetic layered silicates as a basis for high-performance gas barrier coatings

DISSERTATION

zur Erlangung des akademischen Grades eines

Doktors der Naturwissenschaften (Dr. rer. nat.)

in der Bayreuther Graduiertenschule für Mathematik und Naturwissenschaften (BayNAT) der Universität Bayreuth

vorgelegt von

Dominik David Schuchardt

geboren in Hamburg

Bayreuth, 2023

Die vorliegende Arbeit wurde in der Zeit von Oktober 2019 bis Mai 2023 in Bayreuth am Lehrstuhl für Anorganische Chemie I unter Betreuung von Prof. Dr. Josef Breu angefertigt.

Vollständiger Abdruck der von der Bayreuther Graduiertenschule für Mathematik und Naturwissenschaften (BayNAT) der Universität Bayreuth genehmigten Dissertation zur Erlangung des akademischen Grades eines Doktors der Naturwissenschaften (Dr. rer. nat.).

Form der Dissertation: kumulativ

Dissertation eingereicht am: 22.05.2023

Zulassung durch das Leitungsgremium: 07.06.2023

Wissenschaftliches Kolloquium: 05.02.2024

Amtierender Direktor: Prof. Dr. Jürgen Köhler

Prüfungsausschuss:

Prof. Dr. Josef Breu	(Gutachter)
Prof. Dr. Seema Agarwal	(Gutachterin)
Prof. Dr. Rainer Schobert	(Vorsitz)
Prof. Dr. Markus Retsch	

„Ich glaube, wir sollten ruhig und gelassen sein und genießen, was wir haben. Wie lange, das steht in den Sternen, das weiß keiner. Und an die schöne Zeit zurückdenken, die wir gehabt haben.“ – Uwe Seeler

I dedicate this thesis to my family for all their support and love.

Content

List of Abbreviations

0WL	Zero water layer
1D	One-dimensional
1WL	One water layer
2D	Two-dimensional
2WL	Two water layer
α	Aspect ratio
BIF	Barrier improvement factor
Bis-GDA	Bisphenol A glycerolate diacrylate
CV	Coefficient of variation
d	Thickness of the filler
D	Diffusion coefficient
EDX	Energy dispersive X-ray spectroscopy
f	Initiator efficiency
FTIR	Fourier-transform infrared spectroscopy
HDPE	High density polyethylene
J	Diffusion flux of the permeant
k_c	Constant of chain transfer
k_d	Constant of initiator dissociation
k_p	Constant of chain propagation
k_t	Constant of termination
l	Pathway of a permeant through an unfilled barrier film
l‘	Pathway of a permeant through a filled composite
LDPE	Low density polyethylene
<*N*>	Mean number of fillers
NMF	*N*-Methylformamide

μ	Geometrical factor
OP	Oxygen permeability
OTR	Oxygen transmission rate
P	Permeability
PE	Polyethylene
PEGDA	Poly(ethylene glycol) diacrylate
PLA	Polylactic acid
PP	Polypropylene
PS	Polystyrene
PVOH	Poly(vinyl alcohol)
PVC	Poly(vinyl chloride)
PVDC	Poly(vinylidene dichloride)
PVP	Polyvinylpyrrolidone
ϕ	Filler content (in volume-%)
S	Solubility
SAXS	Small angle X-ray scattering
τ	Tortuosity
T_g	Glass temperature
TR	Transmission rate
TEM	Transmission electron microscopy
v_c	Reaction rate of chain transfer
v_i	Reaction rate of the initiation
v_p	Reaction rate of chain propagation
v_t	Reaction rate of termination
WVP	Water vapor permeability
WVTR	Water vapor transmission rate

XRD	X-ray diffraction

1. Summary

Gas impermeable layered silicates are known to improve the gas barrier properties of polymers. In this work, highly filled polymer nanocomposite coatings as well as glass-like all-inorganic coatings were prepared and then investigated for their properties, especially with respect to their gas permeabilities.

In the first two parts of this work, highly filled polymer nanocomposites were prepared by polymerization of diacrylates in the interlayer space of synthetic hectorite. Thin wet coatings of homogeneous suspensions of delaminated hectorite and monomer were prepared and subsequently polymerized. Ideally, the polymerization freezes the structure of the homogeneous suspension and allows the synthesis of highly ordered, one-dimensional crystalline nanocomposites (hybrid Bragg stacks).

In the first part, osmotically swollen Na-hectorite was combined with poly(ethylene glycol) diacrylate (PEGDA) of two different molecular weights. Thin (< 5 µm), highly filled (75 wt%), water-based, and biocompatible gas barrier coatings could be prepared. X-ray diffraction (XRD) experiments showed that single-phase materials could not be achieved for any of the PEGDA nanocomposites, but the combination of the higher molecular weight PEGDA with hectorite was less susceptible to humid air. Accordingly, the nanocomposite with higher molecular weight PEGDA exhibited better barrier properties. The oxygen barrier was improved by a factor of up to 4.23×10^7 compared to neat PEGDA without any filler. Overall, it was shown that these water-based gas barrier coatings are an excellent alternative to conventional halogen-containing and poorly degradable polymer coatings such as polyvinylidene dichloride.

As the nanocomposites of the first part showed phase segregation, the second part of the work, further focused on the preparation of hybrid Bragg stacks. For synthesizing hybrid Bragg stacks, delamination of the hectorite into individual nanosheets in the same medium in which the polymer matrix is soluble is essential. In addition, the enthalpy gain from the interactions between the hectorite surface and the polymer matrix must exceed the entropy loss due to the confinement of the polymer chains in the interlayer space. So far, three systems have been discovered to form such Bragg stacks. However, the hygroscopic interlayer cation Na^+ in these nanocomposites caused swelling of the layered structure and thus produced a collapse of the gas bar-

rier. To potentially shift the onset of swelling to higher humidities, the Na^+ was exchanged for a more hydrophobic functional organocation. This allowed osmotic delamination of the exchanged hectorite in *N*-methylformamide (NMF). Mixed with bisphenol A glycerolate diacrylate (Bis-GDA), which is soluble in NMF, copolymerization with the modifier resulted in one-dimensional crystalline hybrid Bragg stacks. This was demonstrated by XRD experiments as well as transmission electron microscopy. Thus, a hybrid Bragg stack material consisting of a polyanionic layered silicate with a polycationic polymer could be prepared by copolymerization. Such combination cannot be achieved by mixing these components in solution, where heterocoagulation of a disordered composite would occur. The results of the gas barrier measurements showed a significant improvement compared to the unfilled polymer matrix, but the onset of swelling could neither be shifted to higher humidities by the hydrophobic organocation nor by the strong electrostatic bonding of the polymer matrix to the hectorite layers.

In the third part of this work, thin nanoglass coatings of hectorite were produced without the addition of polymers. The gas impermeable layers with extremely high aspect ratio form band-like structures due to overlapping of large areas when they are processed from delaminated suspensions by spray coating. For application as a gas barrier coating, however, the swelling of sodium hectorite with humid air is a problem, as the gas barrier breaks down with high humidities. Collapsing the interlayer space and fixing the interlayer height to less than 3 Å, which is smaller than the kinetic diameter of oxygen, by ion exchange of the hygroscopic Na^+ for the flat-lying, more hydrophobic guanidinium was expected to block diffusion of permeates along the interlayer space. Despite oxygen transmission rates as low as 0.32 $cm^3\ m^{-2}\ day^{-1}\ atm^{-1}$ at harsh conditions of 38 °C and 90 % relative humidity the guanidinium hectorite coating failed to block oxygen diffusion completely, which was attributed to structural defects revealed by TEM cross-sections. For water vapor a transmission rate as low as 3.74 $g\ m^{-2}\ day^{-1}$ (38 °C/90 % relative humidity) was measured. The significant improved water vapor permeability of guanidinium hectorite compared to sodium hectorite indicated that the suppressed swelling and the, therefore, small interlayer height successfully impeded diffusion of water molecules along the interlayer space. The gas barrier performance and their optical properties render these waterborne coatings competitive to vapor-deposited inorganic gas barrier coatings.

2. Zusammenfassung

Gas impermeable Schichtsilikate sind seit langem dafür bekannt die Gasbarriereeigenschaften von Polymeren verbessern zu können. In dieser Arbeit wurden hochgefüllte Polymernanokompositbeschichtungen sowie glasähnliche vollständig anorganische Beschichtungen hergestellt und anschließend auf ihre Eigenschaften insbesondere ihrer Gasbarriere untersucht.

In den ersten zwei Teilen dieser Arbeit wurden hochgefüllte Polymernanokomposite mittels Polymerisation von Diacrylaten im Zwischenschichtraum hergestellt. Die Polymerisation von Monomeren zwischen individuellen Schichtsilikatplättchen in dünnen Beschichtungen aus homogenen Suspensionen mit delaminiertem Hectorit wurde verwendet, um hochgefüllte Polymernanokomposite herzustellen. Idealerweise friert die Polymerisation die Struktur der homogenen Suspension ein und ermöglicht die Synthese von hochgeordneten, eindimensional kristallinen Nanokompositen (hybrid Bragg stacks).

Im ersten Teil wurde osmotisch gequollener Na-Hectorit mit Poly(ethylen glycol) diacrylat (PEGDA) zweier verschiedener Molekulargewichte kombiniert. Dabei konnten dünne (< 5 µm), hochgefüllte (75 wt%), wasserbasierte, biokompatible und gleichzeitig abbaubare Gasbarriebeschichtungen hergestellt werden. Röntgenbeugungsexperimente (XRD) zeigten, dass für keines der PEGDA-Nanokomposite einphasige Materialien hergestellt werden konnten, jedoch die Kombination des höher molekularen PEGDA mit Hectorit weniger anfällig für Luftfeuchtigkeit war. Entsprechend wies das Nanokomposit mit höher molekularem PEGDA die besseren Barriereigenschaften auf. Die Sauerstoffbarriere konnte dabei um einen Faktor von bis zu 4.23×10^7 im Vergleich zu einer Beschichtung ohne Füllstoff verbessert werden. Insgesamt konnte gezeigt werden, dass diese wasserbasierten Gasbarrierebeschichtungen eine exzellente Alternative zu herkömmlichen halogenhaltigen und schwer abbaubaren Polymerbeschichtungen wie Polyvinylidendichlorid sind.

Nachdem die Nanokomposite des ersten Teils Phasensegregation aufzeigten, wurde im zweiten Teil dieser Arbeit der Fokus weiter auf die Herstellung von hybriden „Bragg Stacks“ gelegt. Für die Synthese von hybriden „Bragg Stacks“ ist die Delaminierung des Hectorits in einzelne Schichten im selben Medium, in dem auch die Polymermatrix

löslich ist unabdingbar. Zusätzlich muss der Enthalpiegewinn aus den Wechselwirkungen zwischen der Hectoritoberfläche und der Polymermatrix den Entropieverlust durch die räumliche Eingeschränktheit der Polymerketten im Zwischenschichtraum überwiegen. Bisher konnten drei Systeme entdeckt werden, die solche Bragg stacks bilden. Allerdings sorgte das hygroskopische Zwischenschichtkation Na^+ in diesen Nanokompositen für eine Quellung der Schichtstruktur und erzeugte somit einen deutliche Verminderung der Gasbarriere. Um das Einsetzen der Quellung zu höheren Luftfeuchten zu verschieben wurde in dieser Arbeit Na^+ gegen ein hydrophoberes funktionales Organokation ausgetauscht. Dies ermöglichte die osmotische Delaminierung des ausgetauschten Hectorits in *N*-Methylformamid (NMF). Gemischt mit dem in NMF löslichen Bisphenol A Glycerolat Diacrylat (Bis-GDA) führte eine Copolymerisation mit dem Modifikator zu eindimensional kristallinen hybrid Bragg stacks. Dies konnte mit Hilfe von XRD Experimenten sowie Transmissionselektronenmikroskopie nachgewiesen werden. Somit konnte ein hybrides „Bragg Stack“ Material bestehend aus einem polyanionischen Schichtsilikat mit einem polykationischen Polymer mittels Copolymerisation hergestellt werden. Solch eine Kombination kann nicht durch Mischen dieser Komponenten in Lösung erzielt werden, da es sonst zur Heterokoagulation eines ungeordneten Komposits kommt. Die Ergebnisse der Gasbarrieremessungen zeigten zwar eine deutliche Verbesserung im Vergleich zur ungefüllten Polymermatrix, allerdings konnte der Beginn der Quellung weder durch das hydrophobere Organokation noch durch die starke elektrostatische Anbindung der Polymermatrix an die Hectoritschichten zu höheren Luftfeuchten verschoben werden.

Im dritten Teil dieser Arbeit wurden dünne Nanoglasschichten aus Hectorit ohne den Zusatz von Polymeren hergestellt. Die gasundurchlässigen Schichten mit extrem hohem Aspektverhältnis bilden durch Überlappung großer Flächen bandartige Strukturen, wenn sie aus delaminierten Suspensionen mittels Sprühbeschichtung verarbeitet werden. Für die Anwendung als Gasbarrierebeschichtung ist jedoch die Quellung des Natrium-Hectorits mit feuchter Luft ein Problem, da die Gasbarriere bei hoher Luftfeuchtigkeit einbricht. Ein Kollabieren des Zwischenschichtraums auf einen Schichtabstand kleiner als der kinetische Durchmesser von Sauerstoff durch Ionenaustausch des hygroskopischen Na^+ gegen das flachliegende, hydrophobere Guanidinium sollte die Diffusion von Gasmolekülen entlang des Zwischenschichtraums blockieren. Trotz einer Sauerstoffdurchlässigkeit von nur 0.32 $cm^3\ m^{-2}\ day^{-1}\ atm^{-1}$ bei 38 °C und 90 % relativer Luftfeuchtigkeit konnte der Guanidinium-Hectorit die Sauerstoffdiffusion nicht

vollständig blockieren, was auf strukturelle Defekte, die in TEM Querschnitten erkennbar waren, zurückführen war. Für Wasserdampf wurde eine Transmissionsrate von nur 3.74 g m^{-2} day^{-1} (38 °C/90 % relative Luftfeuchtigkeit) gemessen. Die deutlich verbesserte Wasserdampfpermeabilität von Guanidinium-Hectorit im Vergleich zu Natrium-Hectorit deutet darauf hin, dass die unterbundene Quellung und der dadurch geringe Zwischenschichtabstand die Diffusion von Wassermolekülen entlang des Zwischenschichtraums erfolgreich beeinträchtigt haben. Die Gasbarriereeigenschaften und ihre optischen Eigenschaften machen diese wasserbasierten Beschichtungen konkurrenzfähig zu aufgedampften anorganischen Gasbarrieren.

3. Introduction

3.1. Challenges in the application of layered silicates as gas barrier

Two-dimensional (2D) layered materials have a long history. The discovery of graphene by Greim and Novoselov lead to an enormous research development in 2D layered materials.[1, 2] Since then many different 2D materials, like transition metal dichalcogenides or layered double hydroxides, have been developed and investigated, showing their potential for all kinds of applications.[3] However, 2D layered silicates were already in the focus of research since the development of nanocomposites in the Toyota Research labs by incorporation of layered silicates into a polymer matrix in the early 1990s.[4-6] For these nanocomposites, incorporation of the clay is known to enhance the material properties. Already low amounts of filler can result in improved mechanical properties,[6-8] thermal properties,[9, 10] flame retardancy,[11, 12] electrical properties, and gas barrier properties.[13] An important factor regarding the improvement of the properties is the interface between the layered silicate and the polymer.[14] Therefore, the quality of dispersion of the filler in the polymer matrix is crucial.[14] As for many applications, like gas barriers, the aspect ratio of the filler is highly important. A gentle separation into individual nanosheets before the preparation of the nanocomposite gives the most promising fillers. For synthetic hectorite, one-dimensional (1D) dissolution results in homogeneously swollen, liquid crystalline dispersions of individual nanosheets with extremely high aspect ratio.[15] Low-tech applications like food packaging need transmission rates (TR) from 10^{-1} to 10^{5} for oxygen and 10^{-1} to 10^{4} for water vapor.[16] Therefore, commodity polymers like polyethylene (PE), polystyrene (PS), polyvinyl chloride (PVC), or polyvinylidene dichloride (PVDC) are used for such packaging applications. For some sensitive goods, metalized polymer foils are used. The problem with these packaging solutions is their poor recyclability and degradability. Nanocomposites of layered silicates and degradable polymers can offer a more eco-friendly solution for such packaging applications. Further, the use of water-soluble polymers and layered silicates can decrease the use of environmentally concerning organic solvents during the processing of the packaging materials. Due to the delamination of the layered silicate solution-based processing allows for simple application of nanocomposites with high filler content. This is more important for high-tech applications like the encapsulation of organic light-emitting diodes (OLEDs) as ultra-high gas barriers (TR

< 10^{-6}) can only be achieved by high filler contents and large aspect ratios of the layered material. Additionally, high filler contents can lead to 1D crystalline structures, also called hybrid Bragg stacks, where one or two polymer chains are in severe confinement between two silicate lamellas. Such materials allow for direction dependant characterization of elastic moduli by Brillouin light scattering and show further unique properties like highly anisotropic heat transport or strongly increased T_g.[17-19] The gas barrier properties can be improved even further than the “tortuous path” theory by Cussler is predicting.[20] So far only three combinations of synthetic hectorite and polymers are known to form these 1D nanostructures.[17, 19, 21] Therefore, new ideas and innovative approaches have to be explored. A promising approach is the polymerization of monomers between individual clay nanosheets in delaminated suspensions. This process could allow freezing in the structure of the homogenous mixtures to produce new hybrid Bragg stack materials. Recently, the delamination of synthetic hectorite could be extended to different organic solvents.[22] As polymer nanocomposites with clay show a certain humidity threshold at which swelling is triggered, the use of organic solvents opens up the idea of polymerization between the individual clay nanosheets to more hydrophobic monomers that could enable a significant shift in the water sensitivity. High-end gas barriers often use an alternative approach to the “tortuous path” by using thin vapor-deposited inorganic layers of Al_2O_3 or SiO_x that block gas diffusion due to the dense packing of the inorganic layers.[23] These inorganic barriers, however, are brittle to some extent, and mechanical stress may cause pinholes and defects that deteriorate the barrier performance.[24] As the layered silicate is the impermeable component in those nanocomposites, gas barriers purely consisting of the layered silicate without any polymer as a binder could be an alternative by combining the two approaches. To block the diffusion of permeates along the interlayer space the space between the clay sheets needs to be minimized and fixed to an interlayer height smaller than the kinetic diameter of the permeates by ion exchange. In the past, there were several approaches to creating flexible gas barriers from binder-free layered silicates. But the insufficient delamination and low aspect ratios of the material resulted in limited success of the barrier performance. High aspect ratio synthetic hectorite that delaminates spontaneously into strict monolayers when immersed in water might offer sufficient properties to overcome these limitations seen in the past.

3.2. Layered silicates

3.2.1. Fundamentals and properties of layered silicates

Layered silicates also referred to as phyllosilicates are a broad class of materials. As indicated by their name they are build up by individual lamellas.[25] The structure of these lamellas differs. For clay minerals a 1:1 layered silicate or a 2:1 layered silicate is considered.[26] 1:1 layered silicates, e.g. kaolinite, consist of one tetrahedral layer and one octahedral layer alternating along the direction perpendicular to the layers. The tetrahedral layer is built by SiO_4 tetrahedra, which are linked to each other via basal oxygen atoms. The apical oxygen atom of each tetrahedron is connected to the octahedral layer, which consists of octahedra that are linked via edges. The octahedra have a central metal cation, e.g. Mg^{2+}, Al^{3+}, or Li^{+}, which is coordinated by six anions, e.g. OH^{-}, O^{2-} or F^{-}. For 2:1 layered silicates, e.g. hectorite or montmorillonite, a lamella consists of one octahedral layer and two tetrahedral layers (Figure 1).[25-27] Isomorphic substitution in the octahedral or tetrahedral layer can cause a layer charge.[25] If the individual layers carry a charge, this is compensated by an interlayer cation, e.g. Na^{+} or Ca^{2+}.[28]

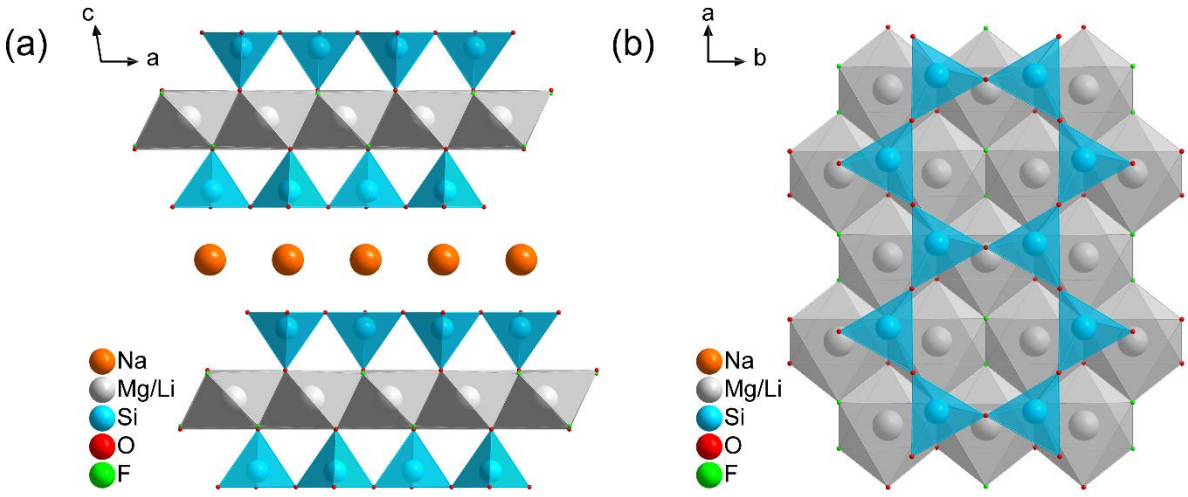

Figure 1: Structure of sodium hectorite. (a) Two hectorite platelets consisting of an octahedral layer surrounded by two tetrahedral layers with sodium in the interlayer space. (b) Top view onto a hectorite platelet (perpendicular to the layers).

Layered silicates occur naturally, but can also be produced synthetically. Natural layered silicates are mined in large quantities. They are, therefore, comparatively inexpensive. Their natural formation, however, causes impurities and inconsistent charge distribution within the layers.[25] Synthetically produced layered silicates, therefore, can

be synthesized without any impurities and consistent charge density leading to superior properties including the rare phenomenon of osmotic delamination that will be discussed in **chapter 3.2.4**.[29-31]

3.2.2. Synthetic sodium hectorite

In the course of this work, mainly synthetically produced sodium hectorite was used. This 2:1 layered silicate has the formal composition $Na_{0.5}Mg_{2.5}Li_{0.5}Si_4O_{10}F_2$ and is produced by melt synthesis.[29] The melt synthesis is carried out at 1750 °C in a molybdenum crucible for one hour. This first step is followed by annealing of the material for six weeks at 1045 °C. During this annealing the isomorphic substitution leads to a phase pure layered silicate with a homogeneous charge density. A very low coefficient of variation (CV, < 0.75), calculated according to Bailey,[32] indicates a well-defined d-spacing with very little interstratification.[31] The crystals of the sodium hectorite from this melt synthesis have a lateral extension of ≈ 20 µm.[31] Because of its purity and homogeneous charge density the synthetic sodium hectorite has an excellent intracrystalline reactivity and swelling behavior. Crystalline swelling already takes place with low relative humidities and occurs in distinct steps. In the dried state, an interlayer distance of 9.6 Å is realized.[31] With the first water layer, it rises to 12.4 Å (1WL) and the second water layer increases the interlayer distance to 15.5 Å (2WL).[31] When immersed in water the hectorite osmotically swells to a nematic phase of single platelets.[33] This gentle delamination preserves the lateral extension of the clay leading to extremely large aspect ratios (≈ 20000) compared to exfoliation by shear forces that can affect the aspect ratio.[31] For this process a low ionic strength is necessary as a concentration of 0.02 M or higher prevents the delamination of the hectorite.[33] This rare phenomenon is not restricted to water as a solvent. The sodium hectorite is also able to delaminate in several binary and ternary solvent mixtures.[34, 35] By complexing the sodium in the interlayer space with crown ethers it is further possible to osmotically swell the hectorite without the use of water in organic solvents.[22] The process of delamination will be discussed in more detail in **chapter 3.3.4**.

3.2.3. Modification of layered silicates

Depending on their composition the silicate layers can carry a permanent charge. This layer charge is balanced by counter ions in the interlayer space. By exchanging the interlayer cation, typical cations like Na^+, K^+, or Ca^{2+}, for organic cations the properties of the layered silicate can be modified.[27, 36] The exchange for alkylamines of different

chain lenghts allows for the determination of the layer charge.[37] Depending on the layer charge the alkylamines form mono- or bilayers in the interlayer. Modification with larger organic molecules can lead to unique properties of the layered silicate.[38] For example, the exchange of sodium in synthetic hectorite for diammoniumbutane enables the use as gas separation membrane, as the resulting pores are selective for CO_2.[39] Furthermore, modification with organocations hydrophobizes the layered silicate. This is extremely important for their use in polymer nanocomposites as the interactions between the polymer matrix and the filler highly affect the properties of the nanocomposite. This was already shown in the early stages of polymer nanocomposites by the researchers in the Toyota laboratories.[5] To prepare the nylon composites the layered silicate was first modified by 12-aminolauric acid before the monomer was added. Since then many different organocations were applied to adjust the surface of the layered silicate to the polymer matrix.[14] Often alkylammonium ions are used as the hydrophobic carbon chain allows for better dispersion of the silicate in the polymer matrix. For nanocomposites from *in-situ* polymerization modifiers with a reactive group can be used to form nanocomposites without any small molecules influencing the properties of the nanocomposite.[40-42] In this case the resulting polymer is a polycation, which can be described as a macromolecular modifier. Additionally, this can be achieved by using polyelectrolytes for the modification of the layered silicate. As the conditions of the processing, e.g. high temperatures in melt extrusion, can lead to a decomposition of the modifier the choice of the modifier is important and dependent on several factors like compatibility of modifier and polymer or temperature stability.

3.2.4. Delamination of layered silicates

The swelling of layered materials is a complex process. Layered silicates like the synthetic hectorite from melt synthesis allow for crystalline swelling even with air humidity. For this material, the crystalline swelling from zero water layer (0WL) to one water layer (1WL) and to two water layers (2WL) corresponds to sharp and stepwise transitions (Figure 2).[29, 43] The state of the hectorite depends on the relative humidity of the surrounding atmosphere. In the 1WL state, the Na^+ is coordinated by three water molecules on one side, whereas on the other side, it has direct contact with the basal oxygen atoms. In the 2WL state, the Na^+ is coordinated by six water molecules that form hydrogen bonds to the basal oxygen atoms. For lower charged clays like montmorillonite, a third water layer can be realized.[44] The energy from this hydration process is high enough to enable the separation despite the attractive forces of the clay platelets.

When placed in water repulsive interactions between the platelets dominate once the attractive ion-surface forces are overcome by hydration. When diluted with deionized water the material will reach the Gouy-Chapman regime first.[33] This, so-called Wigner crystal, is a homogeneous, lyotropic lamellar phase. Further dilution with water leads to screening of the lon-range electrostatic interactions between the clay platelets and causes melting of the Wigner crystal.[33] At water levels where the interlayer distance exceeds the Debye length the electrostatic repulsion of adjacent platelets becomes prevailing. Due to the large lateral size of the synthetic hectorite the individual clay sheets cannot rotate freely resulting in a homogeneous nematic liquid crystalline suspension. Only at very low concentrations ($\phi < 1 \cdot 10^{-4}$) isotropic suspensions with freely rotating clay sheets are realized.[33] This process of osmotic swelling depends on the charge density of the layered silicate and can be suppressed by the ionic strength in the solvent.[33, 45] Further, the interlayer cation has a huge influence on the delamination. As a certain interlayer distance has to be surpassed hydration properties and steric demand of the interlayer cation need to be sufficient.[46] For lower-charged hectorite the sodium interlayer cation from the synthesis already allows for osmotic swelling in water. Higher-charged layered silicates need larger interlayer cations.[47]

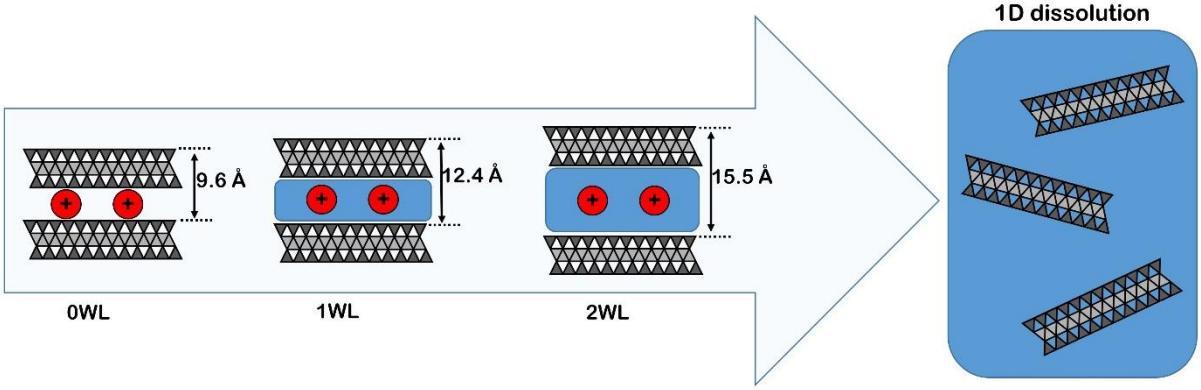

Figure 2: Schematic representation of the 1D dissolution of synthetic sodium hectorite starting from 0WL state with a stepwise transition to 1WL then to 2WL and in the end to individual monolayers.[33]

The delamination into single sheets in water by a thermodynamically driven process is extremely important as large aspect ratio nanosheets have a very large influence on the properties of their composite materials due to their large interface. As many polymer matrices cannot be processed in water, the production of polymer clay nanocomposites for such polymers was restricted to mechanical exfoliation of the filler by shear forces or sonication. The forces during these processes can affect the aspect ratio of the filler thus influencing the interface between the filler and the polymer.[48-52] There-

fore, the delamination of layered silicates in organic solvents and solvent mixtures became extremely important. Over the last years 1D dissolution into 2D nanosheets was reported for several materials in water but also in solvent mixtures and in organic solvents.[15, 53] For synthetic hectorite, delamination in binary solvent mixtures of water and acetonitrile as well as water and dimethylsulfoxide was reported.[34, 54] Further, Mayr et al. showed the delamination in ternary solvent mixtures.[35] By complexing the Na^+ in the interlayer of the hectorite with crown ethers, it is even possible to delaminate the clay in organic solvents without the use of any water.[22] These recent findings open up many opportunities as polymers that could not be processed in water can now be combined with delaminated clays to exploit their potential in polymer clay nanocomposites.

3.3. Application of layered materials

3.3.1. Production and properties of nanocomposites

Nanocomposites are a class of materials that is known for many years. After the discovery of the enhanced material properties of nylon when combined with clay in the Toyota Research Labs at the end of the last century this class of materials got a lot of attention.[5, 6] Over the years, many different synthesis routes were tested and evaluated. Mainly they can be divided into three different methods (Figure 3).[55] First, they can be produced by melt-compounding[55, 56] This industrially used method uses extrusion to combine the polymer and the nanofiller. The shear forces of the extrusion process and the high temperature allow for exfoliation of the filler and for polymer diffusion between the platelets of the clay. The avoidance of large amounts of solvent as well as many commercial polymers can be processed by extrusion makes this first method appealing to companies. Secondly, they can be prepared by *in-situ* polymerization.[55, 56] In this case, the clay is directly dispersed in the monomer. After dispersing and swelling the clay in the monomer, polymerization is started, e.g. by radiation (UV) or heat. For this method, it is important to check the compatibility of the clay and the monomer and eventually the clay has to be modified before adding the monomer. The third method is solvent-based, therefore the polymer or monomer is dissolved in a solvent before the layered silicate is added.[55, 56] This work focuses on the solvent-based synthesis route as the layered silicate can be utilized from its delaminated state. Further, this method allows for several processing technologies, e.g. doctor blading, spray coating, or slot-die coating.[57, 58] On the one hand the solvent-based route is limited to solvents relevant for industrial applications. On the other hand, this route allows for

higher filler content due to the easier handling of the composite dispersion. Additionally, the thermodynamically driven delamination of the layered silicates into single nanosheets enables the use of extremely large aspect ratios.

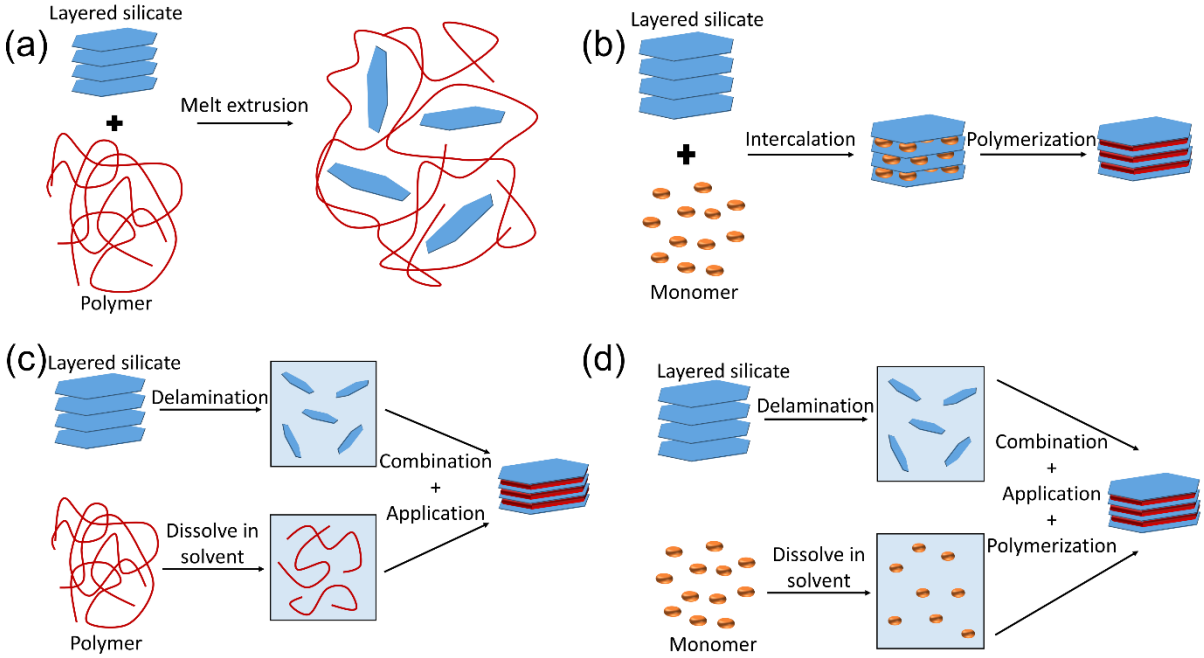

Figure 3: Schematic representation of the different synthesis routes of polymer nanocomposites: (a) melt extrusion, (b) *in-situ* polymerization, (c) solvent-based processing, and (d) solvent-based processing combined with *in-situ* polymerization. [adapted from [55] (RSC Adv., 2014, 4, 29393, 10.1039/C4RA01778A) with permission from the Royal Society of Chemistry.]

As there are various methods for the preparation of polymer clay nanocomposites their structures or morphologies vary as well. Before these morphologies are discussed in detail, a distinction between exfoliation and delamination has to be made. Lagaly and Gardolinky define the breaking of larger stacks into thinner stacks of clay layers as exfoliation, whereas delamination is defined as the separation of the individual layers.[59] As discussed in **chapter 3.2.2** and **chapter 3.2.4** delamination of clay layers needs a high intracrystalline reactivity and homogeneous charge density. Most natural and some synthetic clays do not show a high enough intracrystalline reactivity and thus, they do not delaminate, leading to nanocomposites with stacks of clay layers of different sizes (Figure 4a). At low filler content, the clay platelets can be delaminated and randomly dispersed in the polymer matrix (Figure 4b). The aspect ratio of the clay has a large influence on the properties of the nanocomposite. Therefore, the quality of delamination is crucial and further affects the morphology of the nanocomposites. Starting with a homogeneously swollen dispersion of delaminated clay and using a high clay content two different morphologies of the nanocomposite can be realized. In the first case of phase segregation, the nanocomposite consists of a polymer-rich phase

and an intercalated phase (Figure 4c). In the intercalated phase, a small amount of the total polymer content is intercalated in the interlayer space of the clay. In the second case, the complete amount of polymer is intercalated into the interlayer space of the clay forming 1D crystalline nanocomposites, which are also referred to as hybrid Bragg stacks (Figure 4d).[60] These highly ordered hybrid materials are of great interest as they show highly anisotropic properties and allow for direction depending analysis of the elastic moduli and thermal conductivity.[17, 18]

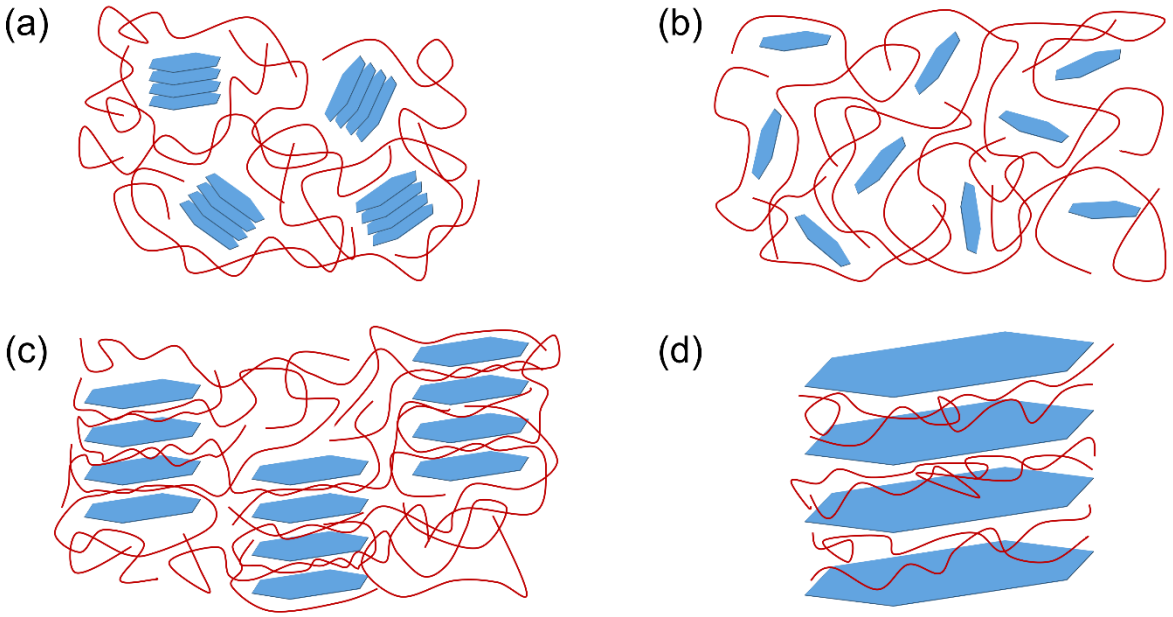

Figure 4: Dispersion of the layered silicate in the polymer matrix. (a) Small stacks of the layered silicate are distributed within the polymer matrix. (b) Full exfoliation of the layered silicate in the polymer matrix. (c) Phase segregation leads to a polymer rich phase and an intercalated phase. (d) Strictly alternating layered silicate and polymer also referred to as hybrid Bragg stack.[60]

Independently from the morphology of the nanocomposite, it is known that the incorporation of the clay leads to enhanced properties compared to the unfilled polymer matrix.[61] Depending on the shape, size, and amount of the clay filler the properties can be varied. Already low filler contents can change the properties, like mechanics, thermal stability, flame retardancy, or gas barrier properties significantly.[62]

For mechanical enhancement, several important mechanical parameters can be considered. Young's modulus, tensile strength, toughness, and elongation at break might be the most important ones when polymers are studied. For understanding the enforcement, the properties of the individual components are extremely important. For a single layer of synthetic sodium hectorite an in-plane modulus of 142 GPa was reported.[63] The in-plane modulus increases to 176 GPa when a double layer of the synthetic hectorite is considered.[64] These in-plane moduli are in accordance to in-plane

moduli reported for micas.[65] Compared to the in-plane modulus the cross-plane modulus of the synthetic sodium hectorite is much smaller.[17] Brillouin light spectroscopy was used to determine the modulus of 25 GPa. Polymers generally exhibit moduli between 0.4 GPa and 4.5 GPa.[66] Therefore, the clay provides the mechanical enhancement in polymer clay nanocomposites as it has the much higher modulus. For example nacre-like Bragg stacks consisting of synthetic hectorite and poly(ethylene glycol) have shown an extremely high Young's modulus of 162 GPa.[18]

Clay fillers can further be incorporated into a polymer matrix to improve flame retardancy. The layered silicate improves the char formation and lowers the flammability. Already low filler content can reduce the heat release rate by 50 – 70 %.[67]

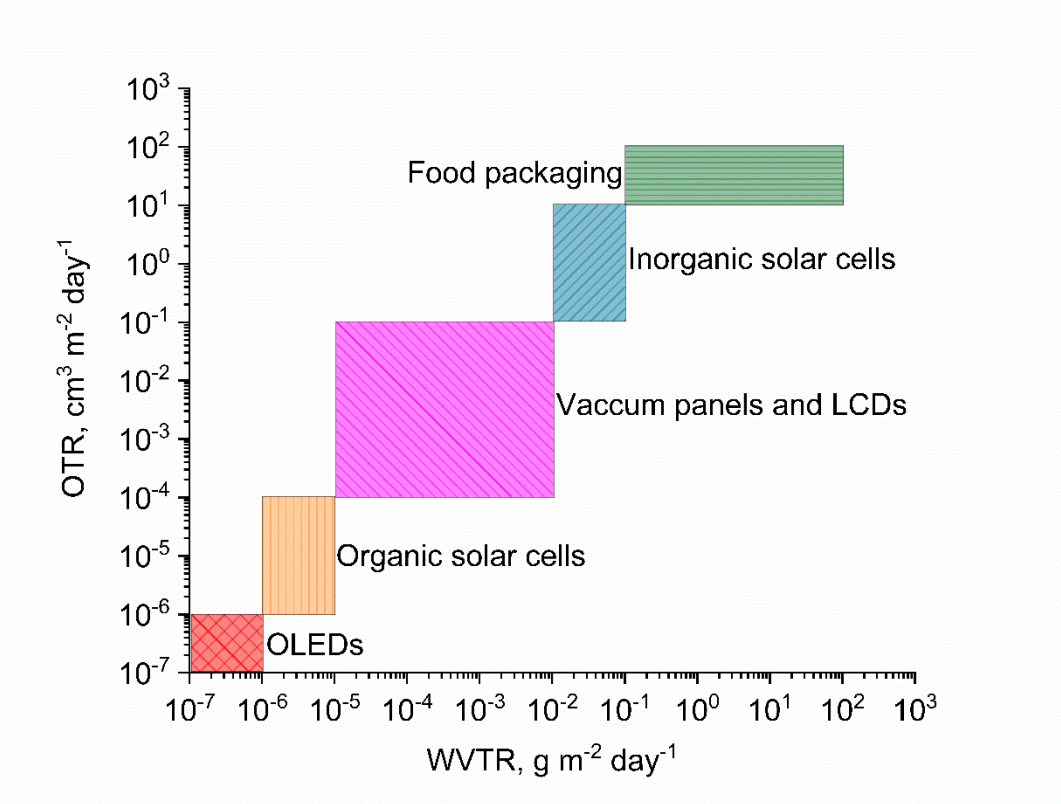

Figure 5: Required oxygen and water vapor transmission rates for a variety of applications.[68]

The enhanced gas barrier that polymer clay nanocomposites demonstrate is one of the major benefits and the property mainly focused on in this work. The incorporation of the layered silicate into the polymer matrix leads to the formation of the so-called "tortuous path" reducing the permeability of the polymer up to several orders of magnitude by extension of the diffusion path of the gas molecules. The theory of gas diffusion through a polymer or nanocomposite film and gas barriers will be discussed in detail in **chapter 3.5**. Gas barriers are used in many everyday applications. This starts

from low-end applications such as food packaging and extends to high-end applications such as the encapsulation of OLEDs (Figure 5).

Polymers like polyethylene, polypropylene, polystyrene, or polyethylene terephthalate are commodity polymers that offer flexibility and sufficient gas barriers for simple packaging applications (Figure 6).

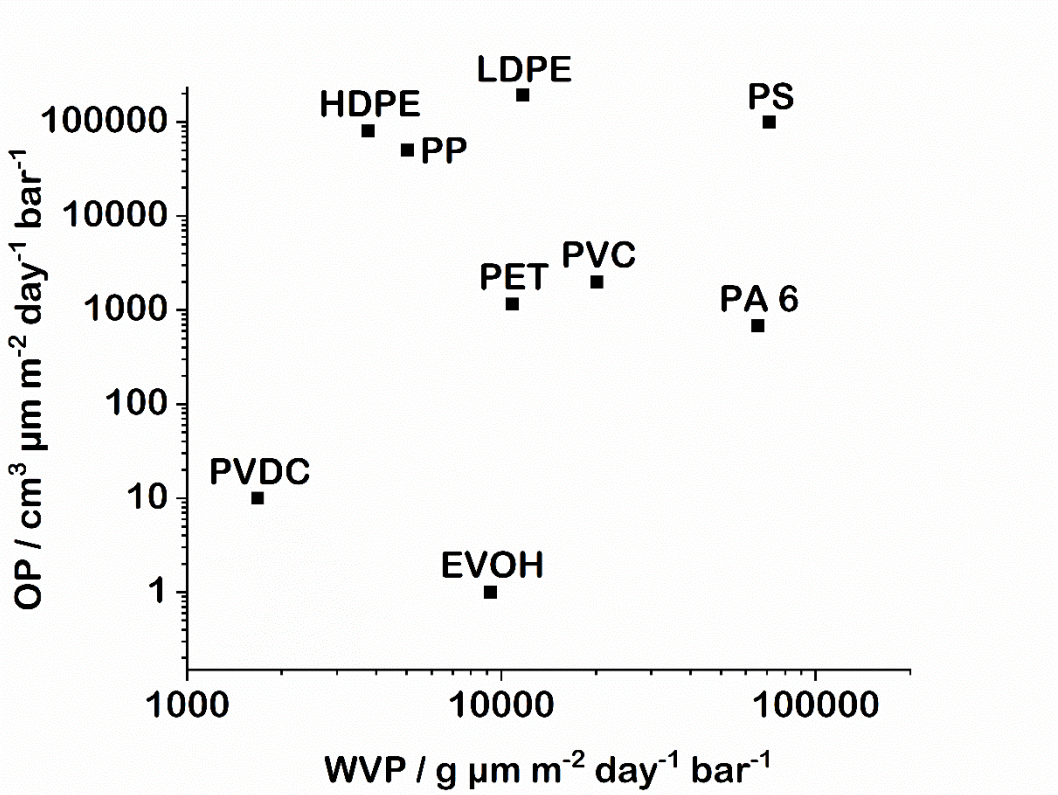

Figure 6: Oxygen (OP, 23 °C and 50 % r.h.) and water vapor permeability (WVP, 38 °C and 90 % r.h) of commercial packaging polymers. EVOH: ethylene vinyl alcohol, HDPE: high density polyethylene, LDPE: low density polyethylene, PA 6: polyamide 6, PET: polyethylene terephthalate, PP: polypropylene, PS: polystyrene, PVC: polyvinyl chloride, PVDC: polyvinylidene dichloride.[23, 69-71]

For more challenging applications, halogen-containing polymers or metalized polymer films are employed. Despite the low cost of those commodity polymers, these packaging solutions need either organic solvents or a lot of energy for processing. Further, they do not show high degradability or easy recycling. Unfortunately, sustainable polymer solutions like polylactic acid (PLA) or water soluble polymers like polyvinyl alcohol show poor gas permeabilities. The incorporation of clay particles can improve the gas barriers of such biopolymers or water-soluble polymers to render the nanocomposites sustainable alternatives to commercial packaging products. The properties of synthetic hectorite render this clay material as the ideal gas barrier additive. The incorporation of such clay can reduce the permeability by several orders of magnitude and can hydrophobize the gas barrier resulting in a lower susceptibility to humidity.[20, 21] Water-

borne nanocomposites from synthetic hectorite and polyvinylpyrrolidone (PVP) or polyvinylalcohol (PVOH) form so called hybrid Bragg stacks. These show excellent oxygen and water vapor permeabilities and can improve the gas barrier even more than predicted by the Cussler equation due to confinement effects.[20, 21] The PVP/hectorite system gives oxygen permeabilities of 0.143 cm^3 µm m^{-2} day^{-1} bar^{-1} at 23 °C and 75 % r.h., whereas the PVOH/hectorite system provides an oxygen permeability of 0.0067 cm^3 µm m^{-2} day^{-1} bar^{-1} at 23 °C and 65 % r.h. and a water vapor permeability of 42.5 g m^{-2} day-1 bar^{-1} at 23 °C and 90 % r.h.[20, 21] The recently reported delamination of hectorite in organic solvents allows for the use of even more kinds of polymers.[22] Self-supporting nanocomposite films derived from PLA and synthetic sodium-hectorite modified by crown ethers demonstrate oxygen permeabilities of 124 cm^3 µm m^{-2} day-^{1} atm^{-1} superior to PVDC.[72]

3.3.2. Application of layered silicates in binder-free coatings and films

Besides all the attention given to layered silicates by their use in polymer nanocomposites, they can also be used without any binders like polymers. A first step in this direction was the preparation of flexible and heat resistant saponite films containing less than 20 wt-% polymer reported by Ebina & Mizukami.[73] But even without a binder, layered silicates like montmorillonite can from textured coatings or self-standing films.[74] Especially, the preparation from delaminated dispersions allows for transparent and flexible films with large overlapping areas of the individual platelets. A self-standing film of synthetic smectite was found to have a water and heat resistance up to 500 °C.[13] Spin-coated hectorite coatings on steel from aqueous paste showed great heat resistance as well as electrical insulation.[75] Nam et al. reported self-standing montmorillonite films with different interlayer cations.[76] As the interlayer cation of the layered silicate plays a key role in the swelling process, it has a significant influence on the formation and formability of the binder-free coatings and films as well as on the actual properties, like gas barrier performance, of such coatings and films.[77, 78] For monovalent interlayer cations the repulsion between the platelets is lower than for polyvalent cations.[79] This results in smooth and flat films for mono- and divalent cations like Na^+, Li^+, Mg^{2+}, or Ca^{2+}, whereas the film with Al^{3+} shrunk significantly and the Fe-montmorillonite film was torn.[76] The films with monovalent interlayer cations showed gas barrier properties similar to polyethylene terephthalate films. For films out of synthetic stevensite Nam et al. could show the influence of the clay particle size on the properties.[80]

Increasing particle size led to improved formability and flexibility, whereas the transparency was lower. Möller et al. reported transparent binder-free films of Li-hectorite with great barrier properties, outperforming polypropylene and other commercial clay materials, like montmorillonite, synthetic hectorite, mica, and vermiculite.[81]

3.4. Fundamentals of polymerization

Polymers are widely used materials in today's society. They can be found in packaging, construction, health care, and many more areas and often they are used in combination with other materials, like layered silicates in the nanocomposites discussed in **chapter 3.3.1**. Many small molecules, called monomers, linked to each other, build up these polymers.[82] As the synthesis can follow different mechanisms, a distinction must be made between chain-growth polymerization and step-growth polymerization (Figure 7).[83] The chain-growth polymerization proceeds by the addition of a monomer to a polymerizable functional group, e.g. a C=C double bond. The active site is transported to the newly added monomer.[84] In addition to the monomer, to start this polymerization reaction an initiator is needed.[82] This can be a radical, a carbocation, or a carbanion. Mainly, the growing polymer chain is reacting with monomers, but termination reactions can also occur. For the chain-growth polymerization, the degree of polymerization is independent of conversion and high molecular weights are reached even at low conversion rates. For example, radical, cationic, anionic, or coordinative polymerizations are chain-growth polymerizations. A special case of the chain-growth polymerization is the living polymerization.[82] The living polymerization is characterized by fast initiation and chain growth without any side reactions or termination reactions. This results in a direct proportionality to the conversion. The life span of the active polymer chain is infinite and the chain growth only stops if the monomers are completely consumed. By adding new monomers, the living polymerization can continue. Typically, anionic polymerizations are living polymerizations. In contrast to chain-growth polymerizations, no initiator is needed for step-growth polymerizations.[82] Thus, the monomers at least need to be bifunctional. As the monomers, oligomers, and polymers react with each other high molecular weights are only achieved with high conversion rates.[83] Polycondensation reactions are a typical example of step-growth polymerizations.

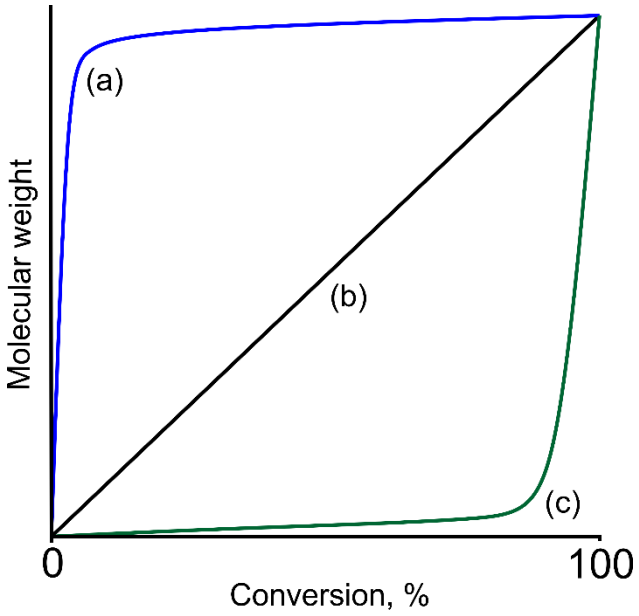

Figure 7: Degree of polymerization as a function of conversion for (a) a chain-growth polymerization, (b) a living polymerization, and (c) a step-growth polymerization.[82]

One of the most investigated polymerization types and the most important one for this work is the radical polymerization. To start this reaction a radical, a reactive species with an unpaired electron, is needed.[83, 84] Such radicals can be generated by heat or ultraviolet light.[84]

$$\mathrm{I} \longrightarrow 2\,\mathrm{R}^{\bullet}$$

The *in-situ* generation of radicals allows the start reaction for radical polymerizations. The conversion of the radicals with monomers is not complete as the radical polymerization is typically performed in a solvent (except for bulk polymerizations) and thus the radicals need to meet a monomer in order to start the polymerization. If the mobility of the radicals is low, e.g. due to high viscosity of the solvent, they might recombine and prevent the start reaction. During the start reaction, a radical of the initiator reacts with a monomer. The radical is then transferred to the monomer resulting in the start radical $\mathrm{RM}^{\bullet}$.[82, 83]

$$\mathrm{R}^{\bullet} + \mathrm{M} \longrightarrow \mathrm{RM}^{\bullet}$$

The start reaction is fast compared to the formation of the radicals from the initiator. Therefore, the formation of the radicals determines the reaction rate v_i of the initiation.[83, 84]

$$v_i = 2 \cdot f \cdot k_d \cdot [I] \qquad (1)$$

With the initiator's efficiency *f*, the constant for initiator dissociation k_d and the initiator concentration [*I*].

The start radical can now react with additional monomers leading to a growing polymer chain P•.[83, 84]

$$\mathrm{RM}^{\bullet} + n\ \mathrm{M} \longrightarrow \mathrm{P}^{\bullet}$$

The constant of chain propagation k_p is independent of the degree of polymerization. Therefore, the reaction rate of the chain propagation v_p is described by **equation 2**: [83, 84]

$$v_p = k_p \cdot [P^{\bullet}][M] \qquad (2)$$

The termination of the chain propagation happens by the reaction of two radicals with each other. Two different reactions can occur. The first reaction is the recombination. In this case, two radicals at the end of propagating polymer chains build up a new bond and the degree of polymerization is doubled.[83, 84]

$$\mathrm{P}_1^{\bullet} + \mathrm{P}_2^{\bullet} \longrightarrow \mathrm{P}_1 - \mathrm{P}_2$$

The second termination reaction is a disproportionation. In this reaction a proton is transferred from one radical to another one. Due to this transfer one polymer chain will have a C=C double bond. The degree of polymerization does not change in the case of a disproportionation.[83, 84]

$$\mathrm{P}_1\mathrm{CH}_2 - \mathrm{CH}_2^{\bullet} + \mathrm{P}_2 - \mathrm{CH}_2^{\bullet} \longrightarrow \mathrm{P}_1\mathrm{CH}_2 = \mathrm{CH}_2 + \mathrm{P}_2 - \mathrm{CH}_3$$

The activation energy of disproportionation is higher, thus, recombination occurs more frequently. Additionally, the reaction between an active polymer radical and a radical from an initiator can lead to a termination of the polymerization. The rate of termination v_t depends on the concentration of active polymer radicals [$P^{\bullet}$] and the constant of termination k_t.[83, 84]

$$v_t = 2 \cdot k_t \cdot [P^{\bullet}]^2 \qquad (3)$$

Besides these three main reactions in radical polymerizations, chain transfer reactions can occur. In this case, the radical is transferred to another molecule most of the time in exchange for a proton. This molecule can be another polymer chain, a monomer, or a solvent molecule and is able to continue the polymerization. [83, 84]

$$\mathrm{PCH}_2 - \mathrm{CH}_2^{\bullet} + \mathrm{HX} \longrightarrow \mathrm{PCH}_2 - \mathrm{CH}_3 + \mathrm{X}^{\bullet}$$

The rate of chain transfer v_c is described by equation 4: [83, 84]

$$v_c = k_c \cdot [P^{\bullet}] \cdot [HX]$$

With the constant of chain transfer k_c and the concentrations of the active polymer chain [$P^{\bullet}$] and the transfer molecule [*HX*].

3.5. Gas barrier

3.5.1. Fundamentals of gas permeability

A pressure difference on either side of a film can cause a gas to move through the film because of a concentration gradient. The process of permeation of a gas through a non-porous film is described in three steps.[85]

1. The permeating gas is absorbed into the film
2. Diffusion of the absorbed gas through the film
3. The permeating gas is desorbed from the film

The solubility and the diffusivity of a gas are important parameters that affect the permeation of the gas. The product of the solubility coefficient *S* and the diffusion coefficient *D* is the permeability *P:*[86]

$$P = D \cdot S \tag{4}$$

Fick's first law can describe the diffusion of a gas molecule from a high concentration to a low concentration. In combination with Henry's law *P* can be described by the product of the diffusion flux of the permeant *J* and the thickness of the barrier film *l* divided by the pressure difference of the permeant *Δp*.[86, 87]

$$P = \frac{J \cdot l}{\Delta p} = TR \cdot l \tag{5}$$

From this *P* can be further described by the product of the transmission rate *TR* and *l*. Measurements of the gas barrier normally give the *TR*. Multiplication with *l* results in *P* as shown by **equation 4**. As the *TR* is highly dependent on *l* the conversion to *P* allows for comparability. The calculation of *P* for water vapor differs as far as *Δp* is dependent on the relative humidity and the temperature of the measurement. For the examination of barrier coatings, it may be necessary to subtract the contribution of the substrate from the measured transmission rate.

3.5.2. Tortuous path theory

In the simple case of a neat polymer, its *P* is described by **equation 4**. The gas molecules can directly diffuse through the polymer (Figure 8a). Now *P* can be affected in

several ways. Permeants like oxygen have a hydrophobic character, thus their solubility in hydrophobic polymer matrices is higher. By choosing the combination of permeant and barrier matrix the permeability can be tuned. Additionally, *P* is affected by temperature, relative humidity and even the partial crystalline part of the polymer matrix, as crystalline domains are considered impermeable.

The incorporation of impermeable platelets is further influencing *S* and *D*. If the impermeable filler is considered to not influence the polymer the solubility is decreased proportionally to the filler content ϕ.[86]

$$S = S_0(1 - \phi) \tag{6}$$

With the solubility coefficient S of the composite and S_0 of the neat polymer matrix.

The incorporation of the impermeable filler further extends the pathway of the permeant through the barrier, creating a so-called “tortuous path” (Figure 8b). The tortuosity τ caused by this affects the diffusion coefficient *D*:[86]

$$D = \frac{D_0}{\tau} \tag{7}$$

With the diffusion coefficient D of the composite and D_0 of the neat polymer matrix.

The tortuosity *f* is described by the pathway *l’* of the permeant through the filled composite divided by the thickness *l* of the barrier film.[86]

$$\tau = \frac{l'}{l} \tag{8}$$

From the **equations 4**, **6**, **7,** and **8** follows **equation 9**:

$$\frac{P}{P_0} = \frac{1-\phi}{\tau} \tag{9}$$

As *l’* can be estimated with **equation 10**:

$$l' = l + < N > \frac{L}{2} \tag{10}$$

With <*N*> being the mean number of fillers and *L* as their length.

<*N*> is estimated by **equation 11** by relating the film thickness *l* and the filler content ϕ to the thickness of the filler *d*.[86]

$$< N > = l\frac{\phi}{d} \tag{11}$$

From that *f* results in **equation 12**:

$$\tau = 1 + \frac{L}{2d}\phi \tag{12}$$

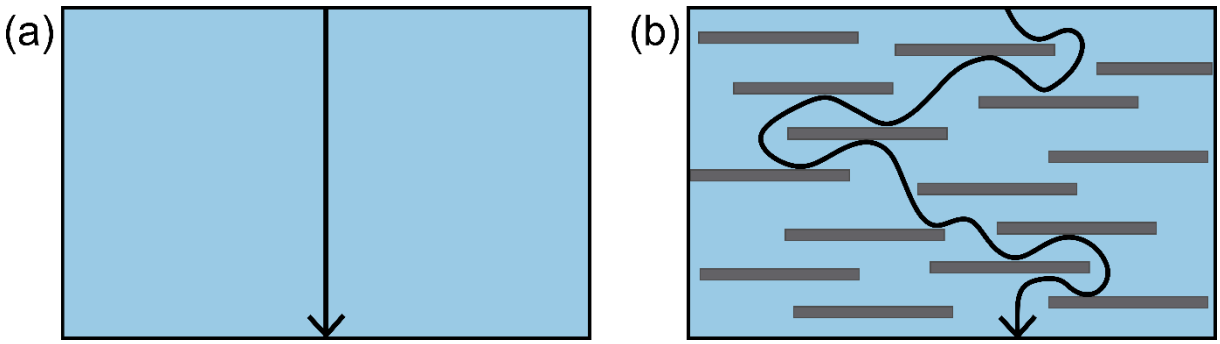

Figure 8: Schematic illustration of the pathway of a gas molecule (a) through a neat polymer matrix and (b) through a tortuous path.

This tortuous path model was first described by Nielsen in 1967.[88] By combining **equations 9** and **12**, he related the permeability to the filler content and aspect ratio as shown by **equation 13**.

$$\frac{P}{P_0} = \frac{1-\phi}{1+\frac{\alpha}{2}\phi} \tag{13}$$

This first model was further developed by many others, as Nielsen's model was simple. Additionally to the filler content and the aspect ratio the permeability is also dependent on the shape of the fillers and their spatial orientation in the barrier film.[89] For semi-dilute systems using fillers with high aspect ratio and a parallel alignment of the fillers to the surface Cussler's model is the most appropriate model to consider (**equation 14**, Figure 9). The geometrical factor μ in this model changes with the shape of the fillers. For synthetic hectorite as used in this work, hexagonal platelets are considered giving μ the value of $\frac{4}{9}$.[90]

$$P_{rel} = \frac{P}{P_0} = \left(1 + \mu\left(\frac{\alpha^2\phi^2}{1-\phi}\right)\right) \tag{14}$$

The inverse of the relative permeability gives the barrier improvement factor (BIF). This is a measure of the improvement in the gas barrier due to the incorporation of the filler. The relation between aspect ratio and filler content shows that very large aspect ratios, e.g. from synthetic hectorite, can lead to extremely high BIFs even at low filler contents. Whereas high filler contents of fillers with low aspect ratios, e.g. natural layered silicates, are not capable of reaching high BIFs.

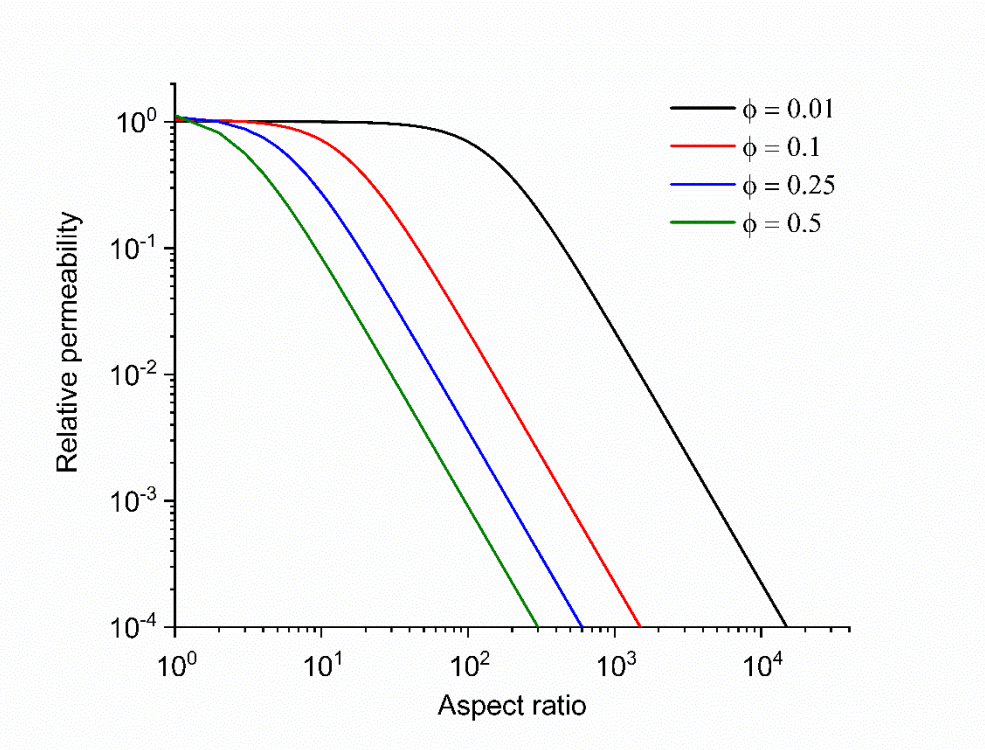

Figure 9: Dependency of the relative permeability on the .aspect ratio of the 2D filler material at various filler contents (ϕ = 0.01, 0.1, 0.25, 0.5) according to Cussler (**equation 14**).

3.6. Scope of this thesis

Due to their 2D character and their large aspect ratio, layered silicates are appropriate filler materials for polymer nanocomposites for gas barrier applications. Synthetic sodium hectorite with superior charge homogeneity realizes an extremely high aspect ratio (≈20000) by osmotic swelling into 1 nm thin nanosheets. The combination with water-soluble polymers can decrease the permeability by several orders of magnitude compared to the unfilled polymers. So far, only three combinations of polymers and hectorite are known that form highly ordered, 1D nanostructured composites. The use of monomers with subsequent polymerization in the delaminated state could provide an alternative route for the preparation of such nanocomposites. Water-soluble monomers allow for easy and eco-friendly processing. Here, hydrogel-forming monomers were combined with the synthetic sodium hectorite. As hydrogels tend to uptake large amounts of water the resulting nanocomposites would not be expected to show a great barrier performance at elevated temperatures and humidities. This work, therefore, investigates if a high clay loading in a hydrogel matrix is sufficient to reduce the water uptake for improving the gas barrier at elevated temperature and humidity and whether the molecular weight of the used monomer influences the barrier performance. In

chapter 6.2 these nanocomposites are evaluated regarding their structure and gas barrier properties.

The fabrication of hybrid Bragg stacks requires delaminated monolayers of synthetic hectorite and a polymer dissolved in the same solvent. As 1D dissolution of the synthetic hectorite was extended to organic solvents more hydrophobic polymer matrices can be used to decrease the sensitivity to water vapor.[15, 22] Exchanging the hygroscopic Na^+ for a more hydrophobic functional organocation enables the co-polymerization of the modifier with a monomer in the interlayer space. The enthalpic gain of this polycationic polymer will eventually overcome the entropic loss yielding hybrid Bragg stacks. Further, the electrostatic interaction between the polyanionic clay surface and the polycationic polymer matrix in combination with the use of a more hydrophobic interlayer cation could shift the onset of swelling, which causes a breakdown of the barrier, to higher humidities. In **chapter 6.3**, it is investigated if the preparation of 1D crystalline hybrid Bragg stacks from organically modified hectorite after delamination in organic solvents is possible. Further, this work explores if the ion exchange of Na^+ for a more hydrophobic organocation and the use of a more hydrophobic polymer matrix shifts the onset of swelling, which causes a breakdown of the gas barrier, to higher humidities.

For high-end gas barrier packaging often an alternative approach of blocking diffusion by dense inorganic layers like Al_2O_3 or SiO_x is chosen.[23] Such inorganic layers, however, need sophisticated vapor deposition or sol-gel processes and suffer when mechanical stress is applied as they tend to be brittle.[24, 91] The layered silicate, as an impermeable filler, is the component mainly contributing to the barrier properties of polymer nanocomposites by creation of the “tortuous path”. Binder-free clay coatings could potentially combine the best features of both approaches. The delamination of the hectorite allows for spray coating of dilute suspensions and the formation of textured binder-free, flexible coatings of clay nanosheets that overlap by large areas. As the hydrophilicity causes swelling of neat sodium hectorite, the gas barrier is probably highly affected by additional diffusion pathways along the interlayer space. Therefore, **chapter 6.4** investigates the gas barrier of binder-free, all-clay coatings and explores if suppressing the swelling by ion exchange and fixing the interlayer height to a smaller distance than the kinetic diameter of oxygen can block the diffusion of gases along the interlayer space.

4. Synopsis

This dissertation consists of three manuscripts (Figure 10). The first two manuscripts deal with the development and application of polymer nanocomposites from nematically swollen dispersions of synthetic hectorite *via* polymerization of monomers within the interlayer space. The third manuscript investigates the potential of binder-free hectorite films as glass-like barrier coatings by suppressing swelling through ion exchange of hygroscopic Na^+ for more hydrophobic organocation to block diffusion along the interlayer space.

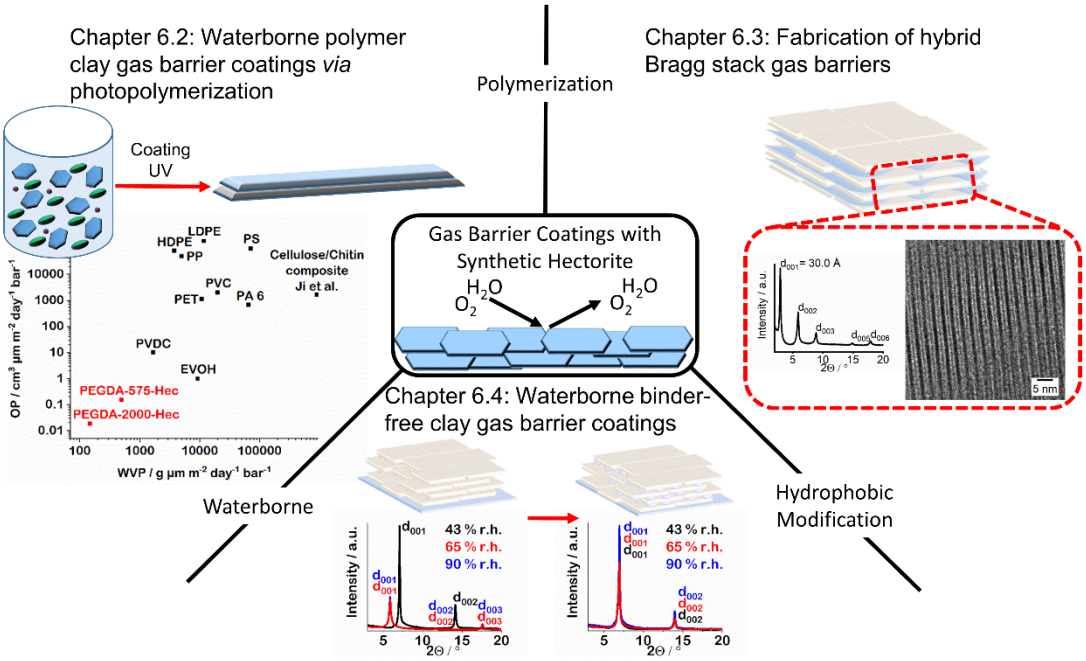

Figure 10: Schematic overview of the featured publications of this thesis and their general relation. [Adopted with permission from *ACS Appl. Polym. Mater.* **2023**, 5, 576-582. Copyright 2023 American Chemical Society. Adopted from *Nanoscale* **2023**, 15, 7044-7050 with permission from the Royal Society of Chemistry. Adopted with permission form *ACS Appl. Nano Mater.* (submitted). Copyright 2023 American Chemical Society.]

4.1. Waterborne polymer clay gas barrier coatings *via* photopolymerization

For gas barrier applications, a high aspect ratio of the filler is crucial. Synthetic sodium hectorite allows for delamination into single nanosheets by osmotic swelling in water. In combination with water-soluble polymers, improvements by several orders of magnitude could be realized.[20, 21, 57] However, the number of water-soluble polymers is limited and the addition of monomers to the dispersion of hectorite with a subsequent *in-situ* polymerization enables the preparation of even more water-based polymer nanocomposites. Previous studies showed that this *in-situ* polymerization method can lead to photoresponsive hydrogel nanocomposites with sodium hectorite.[92, 93] But so far it was not tested what happens if such a hydrogel nanocomposite is dried.

Here synthetic sodium hectorite was osmotically swollen in solutions of poly(ethylene glycol) diacrylate (PEGDA) of two different molecular weights (575 g mol^{-1} and 2000 g mol^{-1}). SAXS measurements proved that neither the monomer nor the initiator prevented the delamination of the hectorite into single nanosheets. By doctor blading wet coats of the nematic dispersions could be applied to a one-sided corona-treated polyethylene terephthalate (PET) substrate. Subsequently, these wet coats were photopolymerized by UV light. Infrared spectroscopy of the dried coatings confirmed a successful polymerization. Due to the higher number of ethylene glycol units in the higher molecular PEGDA, the nanocomposite with PEGDA of 2000 g mol^{-1} was expected to be more sensitive to water vapor.

X-ray diffraction (XRD) and cross-sectional transmission electron microscopy (TEM) images of both nanocomposites indicated partial phase segregation having polymer-rich domains with a thickness < 10 nm. Upon equilibration at 38 °C and 90 % r.h. the XRD pattern showed that the various domains of PEGDA and intercalated PEGDA had different sensitivities towards water vapor. However, the nanocomposite with the lower molecular PEGDA displayed significant water uptake, while the XRD pattern indicated much lower water uptake for the nanocomposite with a higher molecular weight PEGDA (Figure 11). These findings were counterintuitive as the longer PEG segments were expected to result in higher hydrophilicity.

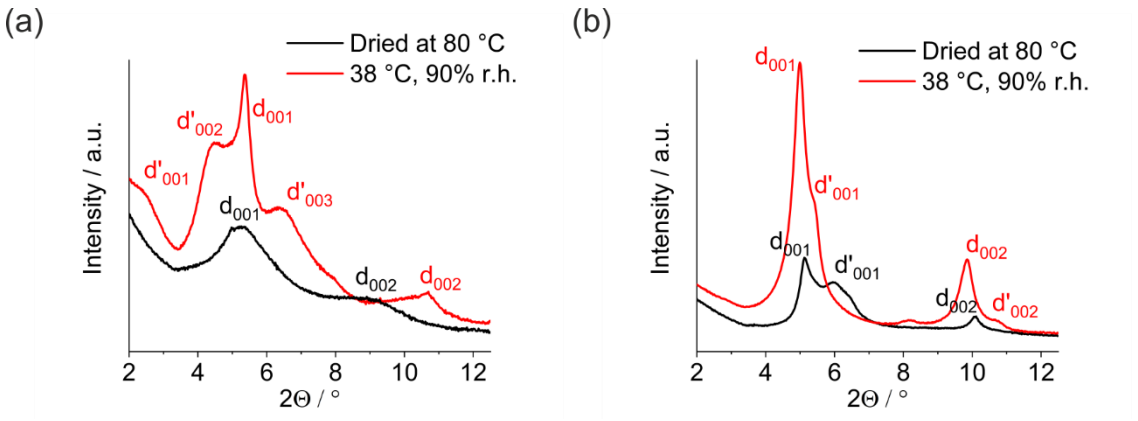

Figure 11: XRD pattern at dried conditions (black) and at 38 °C and 90 % r.h. of (a) the nanocomposite of synthetic sodium hectorite with lower molecular weight PEGDA (575 g mol^{-1}) and (b) the nanocomposite of synthetic sodium hectorite with higher molecular weight PEGDA (2000 g mol^{-1}). [Adopted with permission from *ACS Appl. Polym. Mater.* **2023**, 5, 576-582. Copyright 2023 American Chemical Society.]

At dry conditions, a rather high oxygen permeability of 4277 cm^3 µm m^{-2} day^{-1} bar^{-1} was reported by Chen et al. for neat PEGDA films,[94] thus, the waterborne nanocomposite coatings were expected to potentially have a collapse in barrier with increasing relative humidity as the XRD suggested substantial water uptake. At 23 °C and 65 % r.h. the nanocomposite containing PEGDA with 575 g mol^{-1} showed an OTR of 0.0354 cm^{-1} m^{-2} day^{-1} bar^{-1} and the nanocomposite containing PEGDA with 2000 g mol^{-1} had an OTR of 0.0042 cm^{-1} m^{-2} day^{-1} bar^{-1}. Increasing the temperature and the r.h. to 38 °C and 90 % led to a surprisingly low breakdown of the OTR to 1.864 cm^{-1} m^{-2} day^{-1} bar^{-1} and 0.662 cm^{-1} m^{-2} day^{-1} bar^{-1}, for the nanocomposite with lower molecular PEGDA and higher molecular PEGDA, respectively. For water vapor transmission the barrier properties behaved similarly to that for oxygen transmission. Even at harsh conditions of 38 °C and 90 % r.h. the material containing PEGDA with a molecular weight of 2000 g mol^{-1} is superior by a factor of 2.8 with a WVTR of 1.805 g m^{-2} day^{-1}. Due to the dependency of the OTR and WVTR on the thickness of the samples, those were converted to oxygen (OP) and water vapor permeabilities (WVP) to allow for better comparison with common packaging polymers. Thus, both nanocomposites outperform even high-performance materials like PVDC.

Despite the gas barrier properties, the optical appearance of the nanocomposites is essential for their application in packaging, e.g. of foods or pharmaceuticals. Measurements of optical transparency, haze, and clarity indicate increased haze for both nanocomposite coatings compared to the uncoated PET, while the optical properties of the nanocomposite with higher molecular weight PEGDA are superior to the lower molecular weight material. After a clear coat of PVOH was applied the optical properties of

both nanocomposites did not differ significantly from the uncoated PET. Thus, the increased haze was caused by scattering due to surface roughness.

These results rendered the PEGDA hectorite nanocomposites a waterborne, halogen-free, and biocompatible alternative to commercially used, chloride-containing, or poorly degradable polymer films.

4.2. Fabrication of hybrid Bragg stack gas barriers

One-dimensional crystalline polymer clay nanocomposites are a rare phenomenon and only three such systems are known. Due to the strictly alternating order of an inorganic layer and a polymer layer, these materials can be seen as translational uniform single phase, also referred to as hybrid Bragg stack. This 1D order is reflected by high anisotropy in the elastic moduli or thermal conductivity.[17, 18] The confinement of the polymer results in an increased T_g and further influences the gas barrier as the ordered Bragg stacks show improved transmission rates compared to disordered nanocomposites.[19, 20] The fabrication of hybrid Bragg stacks requires dispersions with only monolayers of the hectorite as well as a polymer matrix that is soluble in the same solvent that is used for the 1D dissolution of the hectorite.[15] So far, only water-soluble polymers (polyvinylpyrrolidone, polyethylene glycol, and polyvinylalcohol) could be combined with synthetic hectorite to form hybrid Bragg stacks. One major issue with these waterborne nanocomposites is their hygroscopic nature. At a certain humidity threshold swelling starts and causes the gas barrier to deteriorate. On one hand a replacement of hydrophilic counter cations by more hydrophobic organocations could help to shift the onset of swelling to higher humidities. On the other hand a more hydrophobic polymer matrix could also enable a lower sensitivity of the gas barrier towards high humidities. As selected organocations allow the synthetic hectorite to delaminate in organic solvents hybrid Bragg stack barriers can potentially be made with more hydrophobic polymer matrices that were not accessible from water. The use of a polycationic polymer could even hamper swelling even more due to the strong electrostatic interactions with the anionic clay sheets. The use of polycations, however, is not an option for the fabrication of 1D crystalline nanocomposites as mixing of the polycation and the clay would cause heterocoagulation and disordered composite materials. As shown in **chapter 4.1**, acrylate-based monomers can be polymerized between the hectorite nanosheets by UV light. The nanocomposites discussed in **chapter 4.1** have not shown a 1D periodicity despite polymerization of a homogeneous mixture indicating insufficient interactions and too little enthalpic gain. To fabricate hybrid Bragg stacks with improved water sensitivity by polymerization of monomers is still a valid route and co-polymerization of a functional organocation and a monomer could enable their fabrication due to the polycationic character of the resulting polymer.

In this work, synthetic sodium hectorite was organically modified with vinylbenzyltrimethylammonium. Energy dispersive X-ray spectroscopy (EDX) showed no residual sodium indicating complete exchange of the hectorite. This modifier allowed for 1D dissolution of the layered silicate in *N*-methylformamide (NMF), as shown by SAXS measurements.

When being mixed with bisphenol A glycerolate diacrylate, a monomer soluble in NMF, homogeneous mixtures of delaminated clay nanosheets and monomer were obtained. SAXS measurements indicated no influence of the monomer or the photoinitiator on the delamination of the modified hectorite. Doctor blading was used to produce a coating on a corona treated PET substrate. Subsequently the coating was polymerized by UV light before the solvent was removed. FTIR could indicate a successful polymerization in the interlayer space. The XRD pattern of the dried nanocomposite showed a d-spacing of 30.0 Å (Figure 12a). The according *00l*-series had a coefficient of variation of 0.44 % indicating a single-phase material (hybrid Bragg stack) with a rational *00l*-series. Cross-sectional TEM images (Figure 12b) confirm the 1D nanostructure of the nanocomposite, while a greyscale analysis results in a d-spacing of 29.85 Å. These results indicate a filler content of 32 vol% which is expected for complete incorporation of the monomer in the interlayer space. Further, the filler content was confirmed by thermal gravimetric analysis. The coating was a little turbid compared to the uncoated PET substrate, which was quantified by measuring optical transmittance, haze, and clarity. Therefore, a clear coat of PVOH was applied resulting in optical properties similar to the PET substrate. Thus, the increased haze was caused by the surface roughness of the coating.

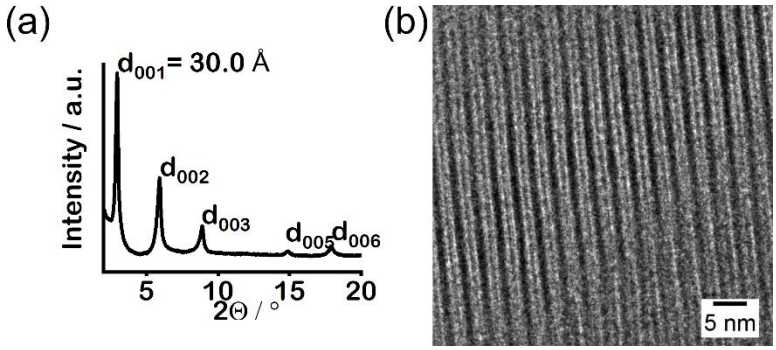

Figure 12: (a) XRD pattern of the hybrid Bragg stack film. (b)TEM image of the cross-section of the hybrid Bragg stack. [Adopted from *Nanoscale* **2023**, 15, 7044-7050 with permission from the Royal Society of Chemistry.]

As the incorporation of clay nanosheets into a polymer matrix can improve the gas barrier properties significantly the coatings were investigated regarding their OTR and

WVTR. At 23 °C and 50 % r.h. the coating showed an OTR of 0.21 cm^3 m^{-2} day^{-1} bar^{-1}. Due to swelling the transmission rate increases to 1.19 cm^3 m^{-2} day^{-1} bar^{-1} at 23 °C and 90 % r.h. For water vapor, a WVTR as low as 0.05 g m^{-2} day^{-1} was achieved. At 23 °C and 90 % r.h. the WVTR rises to 0.78 g m^{-2} day^{-1}. Unfortunately, this indicated no improvement of the water vapor sensitivity compared to waterborne hybrid Bragg stack gas barriers. For comparison with the unfilled polymer and commonly used barrier polymers for packaging the transmission rates were converted to permeabilities. Compared to the unfilled polymer matrix a barrier improvement factor (BIF) of 4.89×10^3 was found for oxygen at 23 °C and 50 % r.h. For water vapor a BIF of 2.78×10^3 could be calculated, showing the improvement due to the incorporation of the clay nanosheets. In addition, it was demonstrated that the nanocomposite outperforms commercial packaging polymers like PVDC, PE, PP, or PS.

These results show that in-situ polymerization of monomers in a homogeneous, nematic dispersion of osmotically swollen hectorite nanosheets enables a new synthesis route for hybrid Bragg stacks. Further, this method allows for perfectly structured nanocomposites of anionic clay and polycationic polymers that were not accessible by solution mixing.

4.3. Waterborne binder-free clay gas barrier coatings

Polymer clay nanocomposites are known for their improved gas barrier properties compared to unfilled polymers. This is caused by the incorporation of impermeable clay sheets with high aspect ratio and is demonstrated in **chapter 4.1** and **chapter 4.2**. For challenging packaging applications that require high gas barriers and transparency inorganic layers of Al_2O_3 or SiO_x are used.[23] These inorganic coatings are applied by sophisticated vapor deposition or sol-gel processes and exhibit brittleness to some extent, which can lead to pinholes upon mechanical stress.[24, 91] In the past multiple approaches preparing binder-free clay coatings without the use of any polymer binder were reported, indicating very large impact of the aspect ratio and interlayer cations on the formability and properties of the resulting films.[13, 74, 76, 81] Such all-clay gas barriers could combine the approaches of the tortuous path of polymer nanocomposites and the dense inorganic gas barriers by fixing the interlayer height to values smaller than the kinetic diameter of the permeates to block diffusion along the interlayer space. Here, synthetic sodium hectorite was delaminated in water into individual nanosheets of 1 nm thickness with an extremely high aspect ratio of 20000. This is extremely important because even a few multilayer stacks would create severe defects in the band-like structure formed by the overlapping of the large aspect ratio nanosheets. The successful delamination was proven by SAXS measurements of a concentrated gel (8 wt%) indicating a consistent layer distance of 29.3 nm between each nanosheet. Spray-coating of dilute dispersions (0.5 wt%) led to glass-like coatings of the nanosheets with large overlapping areas.

The swelling properties and the delamination of the sodium hectorite on the one hand enable easy and water-based processing, on the other hand, its susceptibility to water is expected to prevent the use of binder-free sodium hectorite coatings as gas barrier at elevated humidities. Intercalation compounds of guanidinium and clay minerals are known to not swell with humidity. Additionally, the reported basal spacing of 12.5 Å indicates a flat-lying orientation between the clay nanosheets resulting in an interlayer height (2.9 Å) smaller than the kinetic diameter of oxygen (3.5 Å).[95] Therefore, the exchanged coatings are expected to block diffusion along the interlayer. For the exchange the coating was soaked in a 1 M solution of guanidinium hydrochloride for ion exchange and to hydrophobize the hectorite coating. The high ion concentration prevented the delamination of the clay and ensured that the coating stayed intact. EDX

measurements of the coating confirmed a complete exchange of the sodium for guanidinium. XRD patterns of both materials at 43 % r.h., 65 % r.h., and 90 % r.h. indicated significant swelling of the sodium hectorite to the 2WL state, whereas the d-spacing of the guanidinium hectorite did not change upon exposure to more severe conditions (Figure 13).

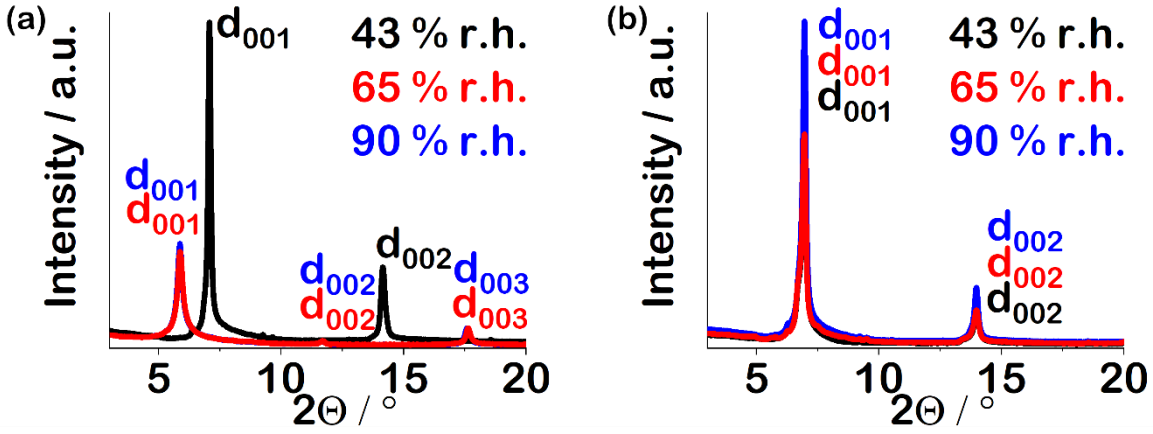

Figure 13: XRD pattern of (a) sodium hectorite and (b) guanidinium hectorite at relative humidities of 43 % (black), 65 % (red), and 90 % (blue). [Adopted with permission form *ACS Appl. Nano Mater.* (submitted). Copyright 2023 American Chemical Society.]

TEM images of the cross-section revealed a perfectly 1D crystalline monodomain film for the restacked sodium hectorite. Whereas the guanidinium hectorite showed additional lenses between defect-free monodomain guanidinium hectorite films. The sodium hectorite and the guanidinium hectorite coatings, both, appeared transparent (Figure 14). Measurements of optical transmittance, haze, and clarity revealed a slightly increased haze due to a rougher surface of the coatings compared to an uncoated PET foil.

Surprisingly, the sodium hectorite coating showed good OTR even at harsh conditions of 38 °C and a relative humidity of 90 % (0.42 $cm^3\ m^{-2}\ day^{-1}\ atm^{-1}$). Despite the suppressed swelling and despite an interlayer height smaller than the kinetic diameter of oxygen the OTR of 0.32 $cm^3\ m^{-2}\ day^{-1}\ atm^{-1}$ shows that the guanidinium hectorite fails to block diffusion completely. Nevertheless, the coating can compete with methyl-Si-O-Si coatings made by vacuum-UV decomposition of perhydrosilazanes and outperforms published binder-free clay films of Na-montmorillonite, Li-montmorillonite, or Mg-montmorillonite.

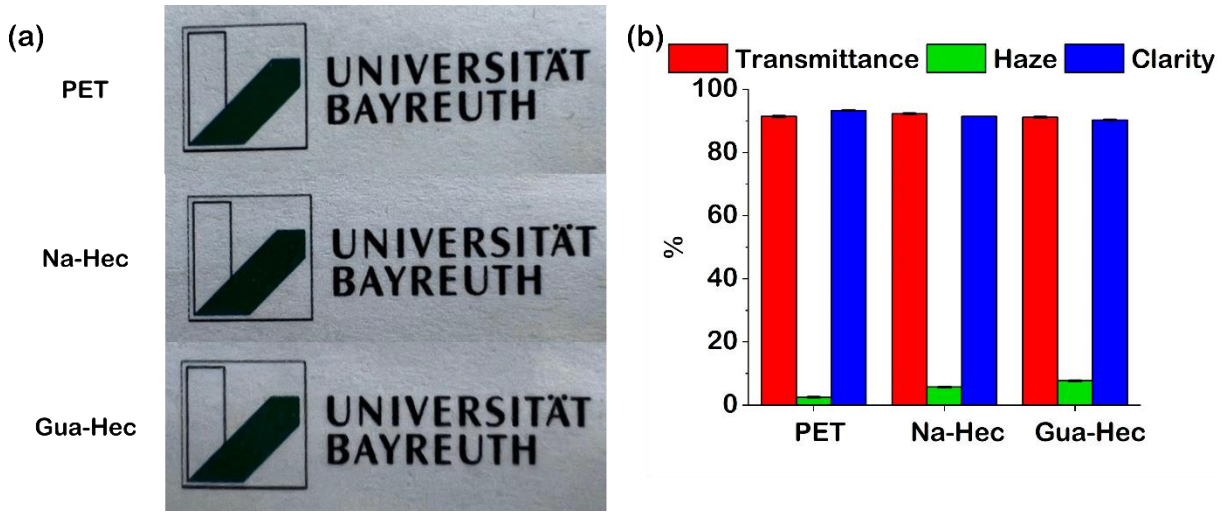

Figure 14: (a) Photographs of uncoated PET, sodium hectorite coated PET, and guanidinium hectorite coated PET. (b) Optical transmittance, haze, and clarity measurements of uncoated PET, sodium hectorite coated PET, and guanidinium hectorite coated PET. [Adopted with permission form *ACS Appl. Nano Mater.* (submitted). Copyright 2023 American Chemical Society.]

For water vapor the guanidinium exchanged coating showed substantially lower transmission rates (0.93 g m^{-2} day^{-1} at 23 °C/65 % r.h. and 3.74 g m^{-2} day^{-1} at 38 °C/90 % r.h.) than the sodium hectorite (3.90 g m^{-2} day^{-1} at 23 °C/65 % r.h. and 12.31 g m^{-2} day^{-1} at 38 °C/90 % r.h.). Despite the different hydrophilicity of both coatings, the WVTR increased by a similar factor upon increasing the r.h. to 90 %. As several factors like swelling of the coatings, solubility of the permeate as well as concentration of the permeate might change upon increasing humidity the WVTR was converted to WVP. For the guanidinium hectorite the WVP increases only slightly from 100.2 g µm m^{-2} day^{-1} atm^{-1} to 126.7 g µm m^{-2} day^{-1} atm^{-1}. As indicated by XRD this material does not swell at high humidities, thus the increase can be attributed to a higher solubility of water vapor in the film. For sodium hectorite, the WVP even decreases from 1291.3 g µm m^{-2} day^{-1} atm^{-1} to 912.7 g µm m^{-2} day^{-1} atm^{-1}. At first sight, this seems counterintuitive but can be attributed to the higher concentration of the permeate as no swelling between 65 % r.h. and 90 % r.h. takes place and in the 2WL state the structure is completely packed with water molecules so the solubility can only change marginally. The difference between both coatings, therefore, can be attributed to additional diffusion pathways in the swollen sodium hectorite.

The combination of transparency and barrier performance renders these waterborne coatings competitive with other inorganic barrier materials.

5. Literature

1. Novoselov, K. S.; Geim, A. K.; Morozov, S. V.; Jiang, D.; Zhang, Y.; Dubonos, S. V.; Grigorieva, I. V.; Firsov, A. A., Electric field effect in atomically thin carbon films. *Science* **2004,** *306* (5696), 666-9.
2. Novoselov, K. S.; Jiang, D.; Schedin, F.; Booth, T. J.; Khotkevich, V. V.; Morozov, S. V.; Geim, A. K., Two-dimensional atomic crystals. *Proc Natl Acad Sci U S A* **2005,** *102* (30), 10451-3.
3. Khan, K.; Tareen, A. K.; Aslam, M.; Wang, R.; Zhang, Y.; Mahmood, A.; Ouyang, Z.; Zhang, H.; Guo, Z., Recent developments in emerging two-dimensional materials and their applications. *Journal of Materials Chemistry C* **2020,** *8* (2), 387-440.
4. Usuki, A.; Kawasumi, M.; Kojima, Y.; Okada, A.; Kurauchi, T.; Kamigaito, O., Swelling behavior of montmorillonite cation exchanged for ω-amino acids by ∈-caprolactam. *J. Mater. Res.* **1993,** *8* (5), 1174-1178.
5. Usuki, A.; Kojima, Y.; Kawasumi, M.; Okada, A.; Fukushima, Y.; Kurauchi, T.; Kamigaito, O., Synthesis of nylon 6-clay hybrid. *J. Mater. Res.* **1993,** *8* (5), 1179-1184.
6. Kojima, Y.; Usuki, A.; Kawasumi, M.; Okada, A.; Fukushima, Y.; Kurauchi, T.; Kamigaito, O., Mechanical properties of nylon 6-clay hybrid. *J. Mater. Res.* **1993,** *8* (5), 1185-1189.
7. Podsiadlo, P.; Kaushik, A. K.; Arruda, E. M.; Waas, A. M.; Shim, B. S.; Xu, J.; Nandivada, H.; Pumplin, B. G.; Lahann, J.; Ramamoorthy, A.; Kotov, N. A., Ultrastrong and stiff layered polymer nanocomposites. *Science* **2007,** *318* (5847), 80-3.
8. Walther, A.; Bjurhager, I.; Malho, J. M.; Pere, J.; Ruokolainen, J.; Berglund, L. A.; Ikkala, O., Large-area, lightweight and thick biomimetic composites with superior material properties via fast, economic, and green pathways. *Nano Lett.* **2010,** *10* (8), 2742-8.
9. Zhang, J.; Jiang, D. D.; Wilkie, C. A., Thermal and flame properties of polyethylene and polypropylene nanocomposites based on an oligomerically-modified clay. *Polym. Degrad. Stab.* **2006,** *91* (2), 298-304.
10. Sargolzaei, J.; Tavakol, M.; Akbarabady, Effect of MMT Clay Content on Thermal Behaviour of MDPE/MMT Nanocomposite. *Adv. Compos. Lett.* **2010,** *19* (5).
11. Li, Y. C.; Schulz, J.; Mannen, S.; Delhom, C.; Condon, B.; Chang, S.; Zammarano, M.; Grunlan, J. C., Flame retardant behavior of polyelectrolyte-clay thin film assemblies on cotton fabric. *ACS Nano* **2010,** *4* (6), 3325-37.
12. Kiliaris, P.; Papaspyrides, C. D., Polymer/layered silicate (clay) nanocomposites: An overview of flame retardancy. *Prog. Polym. Sci.* **2010,** *35* (7), 902-958.
13. Ebina, T., Development of Clay-Based Films. *Chem. Rec.* **2018,** *18* (7-8), 1020-1032.
14. Mittal, V., Polymer Layered Silicate Nanocomposites: A Review. *Materials* **2009,** *2* (3), 992-1057.
15. Dudko, V.; Khoruzhenko, O.; Weiß, S.; Daab, M.; Loch, P.; Schwieger, W.; Breu, J., Repulsive Osmotic Delamination: 1D Dissolution of 2D Materials. *Adv. Mater. Technol.* **2022**.
16. Detzel, A.; Bodrogi, F.; Kauertz, B.; Carola, B.; Welle, F.; Schmid, M.; Schmitz, K.; Müller, K.; Käb, H. *Biobasierte Kunststoffe als Verpackung von Lebensmitteln*; Bundesministerium für Ernährung und Landwirtschaft, Fachagentur für Nachwachsende Rohstoffe: 2018.
17. Wang, Z.; Rolle, K.; Schilling, T.; Hummel, P.; Philipp, A.; Kopera, B. A. F.; Lechner, A. M.; Retsch, M.; Breu, J.; Fytas, G., Tunable Thermoelastic Anisotropy in Hybrid Bragg Stacks with Extreme Polymer Confinement. *Angew. Chem. Int. Ed. Engl.* **2020,** *59* (3), 1286-1294.

18. Dörres, T.; Bartkiewicz, M.; Herrmann, K.; Schöttle, M.; Wagner, D.; Wang, Z.; Ikkala, O.; Retsch, M.; Fytas, G.; Breu, J., Nanoscale-Structured Hybrid Bragg Stacks with Orientation- and Composition-Dependent Mechanical and Thermal Transport Properties: Implications for Nacre Mimetics and Heat Management Applications. *ACS Appl. Nano Mater.* **2022,** *5* (3), 4119-4129.
19. Rolle, K.; Schilling, T.; Westermeier, F.; Das, S.; Breu, J.; Fytas, G., Large T (g) Shift in Hybrid Bragg Stacks through Interfacial Slowdown. *Macromolecules* **2021,** *54* (5), 2551-2560.
20. Schilling, T.; Habel, C.; Rosenfeldt, S.; Röhrl, M.; Breu, J., Impact of Ultraconfinement on Composite Barriers. *ACS Appl. Polym. Mater.* **2020,** *2* (7), 3010-3015.
21. Röhrl, M.; Federer, L. K. S.; Timmins, R. L.; Rosenfeldt, S.; Dörres, T.; Habel, C.; Breu, J., Disorder-Order Transition-Improving the Moisture Sensitivity of Waterborne Nanocomposite Barriers. *ACS Appl. Mater. Interfaces* **2021,** *13* (40), 48101-48109.
22. Dudko, V.; Ottermann, K.; Rosenfeldt, S.; Papastavrou, G.; Breu, J., Osmotic Delamination: A Forceless Alternative for the Production of Nanosheets Now in Highly Polar and Aprotic Solvents. *Langmuir* **2021,** *37* (1), 461-468.
23. Lange, J.; Wyser, Y., Recent innovations in barrier technologies for plastic packaging?a review. *Packag. Technol. Sci.* **2003,** *16* (4), 149-158.
24. Wu, F.; Misra, M.; Mohanty, A. K., Challenges and new opportunities on barrier performance of biodegradable polymers for sustainable packaging. *Prog. Polym. Sci.* **2021,** *117*, 101395.
25. *Tonminerale und Tone*. Steinkopff Heidelberg: 1993.
26. *Handbook of Clay Science*. 2006.
27. Guida-Pietrasanta, F.; Boutevin, B.; Nuyken, O.; Becker, O.; Simon, G. P.; Dusek, K.; Rusanov, A. L.; Likhatchev, D.; Kostoglodov, P. V.; Müllen, K.; Klapper, M.; Schmidt, M.; Usuki, A.; Hasegawa, N.; Kato, M.; Kobayashi, S., *Inorganic Polymeric Nanocomposites and Membranes*. Springer Berlin, Heidelberg: 2005.
28. Utracki, L. A., *Clay-Containig Polymeric Nanocomposites*. Rapra Technology Limited: 2004.
29. Breu, J.; Seidl, W.; Stoll, A. J.; Lange, K. G.; Probst, T. U., Charge homogeneity in synthetic fluorohectorite. *Chem. Mater.* **2001,** *13* (11), 4213-4220.
30. Kalo, H.; Möller, M. W.; Ziadeh, M.; Dolejš, D.; Breu, J., Large scale melt synthesis in an open crucible of Na-fluorohectorite with superb charge homogeneity and particle size. *Appl. Clay Sci.* **2010,** *48* (1-2), 39-45.
31. Stöter, M.; Kunz, D. A.; Schmidt, M.; Hirsemann, D.; Kalo, H.; Putz, B.; Senker, J.; Breu, J., Nanoplatelets of sodium hectorite showing aspect ratios of approximately 20,000 and superior purity. *Langmuir* **2013,** *29* (4), 1280-5.
32. Bailey, S. W., Nomenclature for regular interstratifications. *Clay Minerals* **2018,** *17* (2), 243-248.
33. Rosenfeldt, S.; Stöter, M.; Schlenk, M.; Martin, T.; Albuquerque, R. Q.; Förster, S.; Breu, J., In-Depth Insights into the Key Steps of Delamination of Charged 2D Nanomaterials. *Langmuir* **2016,** *32* (41), 10582-10588.
34. Kunz, R.; Amschler, S.; Edenharter, A.; Mayr, L.; Herlitz, S.; Rosenfeldt, S.; Breu, J., Giant Multistep Crystalline Vs. Osmotic Swelling of Synthetic Hectorite in Aqueous Acetonitrile. *Clays Clay Miner.* **2020,** *67* (6), 481-487.
35. Mayr, L.; Amschler, S.; Edenharter, A.; Dudko, V.; Kunz, R.; Rosenfeldt, S.; Breu, J., Osmotic Swelling of Sodium Hectorite in Ternary Solvent Mixtures: Nematic Liquid Crystals in Hydrophobic Media. *Langmuir* **2020,** *36* (14), 3814-3820.
36. de Paiva, L. B.; Morales, A. R.; Valenzuela Díaz, F. R., Organoclays: Properties, preparation and applications. *Appl. Clay Sci.* **2008,** *42* (1-2), 8-24.

37. Lagaly, G., Interaction of alkylamines with different types of layered compounds. *Solid State Ionics* **1986,** *22* (1), 43-51.
38. Rieß, M.; Senker, J.; Schobert, R.; Breu, J., Microporous Organically Pillared Layered Silicates (MOPS): A Versatile Class of Functional Porous Materials. *Chemistry* **2019,** *25* (9), 2103-2111.
39. Rieß, M.; Siegel, R.; Senker, J.; Breu, J., Diammonium-Pillared MOPS with Dynamic CO2 Selectivity. *Cell Reports Physical Science* **2020,** *1* (10).
40. Şen, S.; Gündem, H. B.; Ortaç, B., Property enhancement in unsaturated polyester nanocomposites by using a reactive intercalant for clay modification. *J. Appl. Polym. Sci.* **2013,** *129* (6), 3247-3254.
41. Ahmadian-Alam, L.; Haddadi-Asl, V.; Roghani-Mamaqani, H.; Hatami, L.; Salami-Kalajahi, M., Use of clay-anchored reactive modifier for the synthesis of poly (styrene-co-butyl acrylate)/clay nanocomposite via in situ AGET ATRP. *Journal of Polymer Research* **2011,** *19* (1).
42. Kim, S.-K.; Kwen, H.-D.; Choi, S.-H., Radiation-induced synthesis of vinyl copolymer based nanocomposites filled with reactive organic montmorillonite clay. *Radiat. Phys. Chem.* **2012,** *81* (5), 519-523.
43. Dazas, B.; Lanson, B.; Breu, J.; Robert, J.-L.; Pelletier, M.; Ferrage, E., Smectite fluorination and its impact on interlayer water content and structure: A way to fine tune the hydrophilicity of clay surfaces? *Microporous Mesoporous Mater.* **2013,** *181*, 233-247.
44. Skipper, N. T.; Lock, P. A.; Titiloye, J. O.; Swenson, J.; Mirza, Z. A.; Howells, W. S.; Fernandez-Alonso, F., The structure and dynamics of 2-dimensional fluids in swelling clays. *Chem. Geol.* **2006,** *230* (3-4), 182-196.
45. Kalo, H.; Moller, M. W.; Kunz, D. A.; Breu, J., How to maximize the aspect ratio of clay nanoplatelets. *Nanoscale* **2012,** *4* (18), 5633-9.
46. Daab, M.; Eichstaedt, N. J.; Habel, C.; Rosenfeldt, S.; Kalo, H.; Schiessling, H.; Förster, S.; Breu, J., Onset of Osmotic Swelling in Highly Charged Clay Minerals. *Langmuir* **2018,** *34* (28), 8215-8222.
47. Daab, M.; Eichstaedt, N. J.; Edenharter, A.; Rosenfeldt, S.; Breu, J., Layer charge robust delamination of organo-clays. *RSC Adv* **2018,** *8* (50), 28797-28803.
48. Sangermano, M.; Lak, N.; Malucelli, G.; Samakande, A.; Sanderson, R. D., UV-curing and characterization of polymer–clay nanocoatings by dispersion of acrylate-funtionalized organoclays. *Prog. Org. Coat.* **2008,** *61* (1), 89-94.
49. Decker, C.; Keller, L.; Zahouily, K.; Benfarhi, S., Synthesis of nanocomposite polymers by UV-radiation curing. *Polymer* **2005,** *46* (17), 6640-6648.
50. Spadaro, G.; Dispenza, C.; Alessi, S.; Tartaglione, G.; Camino, G., Radiation curing of diacrylate glycerolate of bisphenol-A in the presence of an organically modified montmorillonite for the production of flame-resistant polymer–clay composites. *Adv. Polym. Technol.* **2006,** *25* (2), 109-120.
51. Vijayan, P. P.; Puglia, D.; Pionteck, J.; Kenny, J. M.; Thomas, S., Liquid-rubber-modified epoxy/clay nanocomposites: effect of dispersion methods on morphology and ultimate properties. *Polym. Bull.* **2015,** *72* (7), 1703-1722.
52. Perez-Rodriguez, J. L.; Wiewiora, A.; Drapala, J.; Perez-Maqueda, L. A., The effect of sonication on dioctahedral and trioctahedral micas. *Ultrason. Sonochem.* **2006,** *13* (1), 61-7.
53. Loch, P.; Schuchardt, D.; Algara-Siller, G.; Markus, P.; Ottermann, K.; Rosenfeldt, S.; Lunkenbein, T.; Schwieger, W.; Papastavrou, G.; Breu, J., Nematic suspension of a microporous layered silicate obtained by forceless spontaneous delamination via repulsive osmotic swelling for casting high-barrier all-inorganic films. *Sci Adv* **2022,** *8* (20), eabn9084.
54. Dudko, V.; Rosenfeldt, S.; Siegel, R.; Senker, J.; Matejdes, M.; Breu, J., Delamination by Repulsive Osmotic Swelling of Synthetic Na-Hectorite with Variable Charge in Binary Dimethyl Sulfoxide-Water Mixtures. *Langmuir* **2022,** *38* (35), 10781-10790.

55. Unalan, I. U.; Cerri, G.; Marcuzzo, E.; Cozzolino, C. A.; Farris, S., Nanocomposite films and coatings using inorganic nanobuilding blocks (NBB): current applications and future opportunities in the food packaging sector. *RSC Adv.* **2014,** *4* (56), 29393-29428.
56. Vasile, C., Polymeric Nanocomposites and Nanocoatings for Food Packaging: A Review. *Materials (Basel)* **2018,** *11* (10).
57. Tsurko, E. S.; Feicht, P.; Nehm, F.; Ament, K.; Rosenfeldt, S.; Pietsch, I.; Roschmann, K.; Kalo, H.; Breu, J., Large Scale Self-Assembly of Smectic Nanocomposite Films by Doctor Blading versus Spray Coating: Impact of Crystal Quality on Barrier Properties. *Macromolecules* **2017,** *50* (11), 4344-4350.
58. Röhrl, M.; Mettke, J. H.; Rosenfeldt, S.; Schmalz, H.; Mansfeld, U.; Timmins, R. L.; Habel, C.; Breu, J.; Durst, F., Shear orientation of nematic phases of clay nanosheets: processing of barrier coatings. *J. Coat. Technol. Res.* **2021,** *19* (2), 487-495.
59. Gardolinski, J. E. F. C.; Lagaly, G., Grafted organic derivatives of kaolinite: II. Intercalation of primary n-alkylamines and delamination. *Clay Minerals* **2018,** *40* (4), 547-556.
60. Dörres, T. S. Hybrid Bragg stacks - polymer-clay nanocomposites defined by ultraconfinement. University of Bayreuth, 2020.
61. *Polymer-Clay Nanocomposites*. Wiley: 2001.
62. Beall, G. W.; Powell, C., *Fundamentals of Polymer-Clay Nanocomposites*. Cambridge University Press: 2011.
63. Kunz, D. A.; Erath, J.; Kluge, D.; Thurn, H.; Putz, B.; Fery, A.; Breu, J., In-plane modulus of singular 2:1 clay lamellae applying a simple wrinkling technique. *ACS Appl Mater Interfaces* **2013,** *5* (12), 5851-5.
64. Stöter, M.; Godrich, S.; Feicht, P.; Rosenfeldt, S.; Thurn, H.; Neubauer, J. W.; Seuss, M.; Lindner, P.; Kalo, H.; Möller, M.; Fery, A.; Förster, S.; Papastavrou, G.; Breu, J., Controlled Exfoliation of Layered Silicate Heterostructures into Bilayers and Their Conversion into Giant Janus Platelets. *Angew. Chem. Int. Ed. Engl.* **2016,** *55* (26), 7398-402.
65. McNeil, L. E.; Grimsditch, M., Elastic moduli of muscovite mica. *J. Phys.: Condens. Matter* **1993,** *5*, 1681-1690.
66. Brostow, W., Mechanical Properties. In *Physical Properties of Polymers Handbook*, Mark, J. E., Ed. Springer, New York: 2007.
67. Gilman, J., Flammability and thermal stability studies of polymer layered-silicate (clay) nanocomposites. *Appl. Clay Sci.* **1999,** *15* (1-2), 31-49.
68. Chen, T. N.; Wuu, D. S.; Wu, C. C.; Chiang, C. C.; Chen, Y. P.; Horng, R. H., High-Performance Transparent Barrier Films of SiO[sub x]/SiN[sub x] Stacks on Flexible Polymer Substrates. *J. Electrochem. Soc.* **2006,** *153* (10).
69. Oxygen and Walter Vapour Barrier Properties of Flex Pack Films. https://usa.dupontteijinfilms.com/wp-content/uploads/2017/01/Oxygen_And_Walter_Vapour_Barrier_Properties_of_Flex_Pack_Films.pdf (accessed 15 May 2023).
70. Aulin, C.; Gällstedt, M.; Lindström, T., Oxygen and oil barrier properties of microfibrillated cellulose films and coatings. *Cellulose* **2010,** *17* (3), 559-574.
71. Schmid, M.; Dallmann, K.; Bugnicourt, E.; Cordoni, D.; Wild, F.; Lazzeri, A.; Noller, K., Properties of Whey-Protein-Coated Films and Laminates as Novel Recyclable Food Packaging Materials with Excellent Barrier Properties. *International Journal of Polymer Science* **2012,** *2012*, 1-7.
72. Timmins, R. L.; Kumar, A.; Röhrl, M.; Havlíček, K.; Agarwal, S.; Breu, J., High Barrier Nanocomposite Film with Accelerated Biodegradation by Clay Swelling Induced Fragmentation. *Macromolecular Materials and Engineering* **2021,** *307* (6).
73. Ebina, T.; Mizukami, F., Flexible Transparent Clay Films with Heat-Resistant and High Gas-Barrier Properties. *Adv. Mater.* **2007,** *19* (18), 2450-2453.

74. Nam, H.-J.; Ebina, T.; Ishii, R.; Nanzyo, H.; Mizukami, F., Self-Standing Film Formability of Various Clays. *Clay Sci.* **2007,** *13* (4-5), 159-165.
75. Noguchi, Y.; Hayashi, S.; Sugai, I.; Tanaike, O.; Iijima, T.; Ebina, T., Ceramic Coating On Stainless Steel Surface using Aqueous Clay Paste. *Clay Sci.* **2017,** *21* (3), 59-61.
76. Nam, H.-J.; Ebina, T.; Mizukami, F., Formability and properties of self-standing clay film by montmorillonite with different interlayer cations. *Colloids Surf. A Physicochem. Eng. Asp.* **2009,** *346* (1-3), 158-163.
77. Tamura, K.; Yamada, H.; Nakazawa, H., Stepwise Hydration of High-Quality Synthetic Smectite with Various Cations. *Clays Clay Miner.* **2000,** *48* (3), 400-404.
78. Montes-H, G.; Duplay, J.; Martinez, L.; Geraud, Y.; Rousset-Tournier, B., Influence of interlayer cations on the water sorption and swelling–shrinkage of MX80 bentonite. *Appl. Clay Sci.* **2003,** *23* (5-6), 309-321.
79. Luckham, P. F.; Rossi, S., The colloidal and rheological properties of bentonite suspensions. *Adv. Colloid Interface Sci.* **1999,** *82* (1-3), 43-92.
80. Nam, H.-J.; Ishii, R.; Ebina, T.; Mizukami, F., Flexible transparent self-standing binderless clay film prepared by hydrothermally-treated synthetic clay. *Mater. Lett.* **2009,** *63* (1), 54-57.
81. Möller, M. W.; Lunkenbein, T.; Kalo, H.; Schieder, M.; Kunz, D. A.; Breu, J., Barrier properties of synthetic clay with a kilo-aspect ratio. *Adv. Mater.* **2010,** *22* (46), 5245-9.
82. Tieke, B., *Makromolekulare Chemie*. WILEY-VCH Verlag GmbH & Co. KGaA: 2014.
83. Seiffert, S.; Kummerlöwe, C.; Vennemann, N., *Lechner, Gehrke, Nordmeier - Makromolekulare Chemie*. 2020.
84. Koltzenburg, S.; Maskos, M.; Nuyken, O., *Polymere: Synthese, Eigenschaften und Anwendungen*. 2014.
85. Ismail, A. F.; Khulbe, K. C.; Matsuura, T., *Gas Separation Membranes*. Springer: 2015.
86. Choudalakis, G.; Gotsis, A. D., Permeability of polymer/clay nanocomposites: A review. *Eur. Polym. J.* **2009,** *45* (4), 967-984.
87. Stannett, V., The transport of gases in synthetic polymeric membranes — an historic perspective. *J. Membr. Sci.* **1978,** *3* (2), 97-115.
88. Nielsen, L. E., Models for the Permeability of Filled Polymer Systems. *Journal of Macromolecular Science: Part A - Chemistry* **1967,** *1* (5), 929-942.
89. Cussler, E. L.; Hughes, S. E.; Ward, W. J.; Aris, R., Barrier membranes. *J. Membr. Sci.* **1988,** *38* (2), 161-174.
90. Moggridge, G. D.; Lape, N. K.; Yang, C.; Cussler, E. L., Barrier films using flakes and reactive additives. *Prog. Org. Coat.* **2003,** *46* (4), 231-240.
91. With, P. C.; Helmstedt, U.; Prager, L., Flexible Transparent Barrier Applications of Oxide Thin Films Prepared by Photochemical Conversion at Low Temperature and Ambient Pressure. *Front. Mater.* **2020,** *7*.
92. Zhu, Q. L.; Dai, C. F.; Wagner, D.; Daab, M.; Hong, W.; Breu, J.; Zheng, Q.; Wu, Z. L., Distributed Electric Field Induces Orientations of Nanosheets to Prepare Hydrogels with Elaborate Ordered Structures and Programmed Deformations. *Adv. Mater.* **2020,** *32* (47), e2005567.
93. Zhu, Q. L.; Du, C.; Dai, Y.; Daab, M.; Matejdes, M.; Breu, J.; Hong, W.; Zheng, Q.; Wu, Z. L., Light-steered locomotion of muscle-like hydrogel by self-coordinated shape change and friction modulation. *Nat Commun* **2020,** *11* (1), 5166.
94. Chen, Y.; Ye, Y.; Chen, Z.-R., Vapor-based synthesis of bilayer anti-corrosion polymer coatings with excellent barrier property and superhydrophobicity. *J. Mater. Sci.* **2018,** *54* (7), 5907-5917.
95. Mehio, N.; Dai, S.; Jiang, D. E., Quantum mechanical basis for kinetic diameters of small gaseous molecules. *J. Phys. Chem. A* **2014,** *118* (6), 1150-4.

6. Results

6.1. Author's individual contributions

Gas Barriers from In Situ Polymerized Poly(ethylene glycol) Diacrylate Clay Nanocomposites for Food Packaging

Dominik Schuchardt, Maximilian Röhrl, Sabine Rosenfeldt, and Josef Breu

J. Breu and I developed the concept and wrote the manuscript. M. Röhrl and S. Rosenfeldt commented on the manuscript. I did the synthesis and most of the characterization. M. Röhrl supported the gas barrier measurements. S. Rosenfeldt helped with SAXS measurements and fitted the SAXS data. All authors contributed to the scientific discussion.
My contribution to this publication is 80 %.

Fabrication of Bragg Stack Films of Clay Nanosheets and Polycations via Co-polymerization of Intercalated Monomers and Functional Interlayer Cations

Dominik Schuchardt, Sabine Rosenfeldt, Hussein Kalo, and Josef Breu

The concept of the manuscript was developed by J. Breu and me. J. Breu and I wrote the manuscript. S. Rosenfeldt and H. Kalo commented on the manuscript. I did the synthesis and most of the characterization. S. Rosenfeldt helped with the SAXS measurements and fitted the SAXS data. All authors contributed to the scientific discussion.
My contribution to this publication is 80 %.

Spraying Transparent Nanoglass Coatings

Dominik Schuchardt, Maximilian Röhrl, Lukas Federer, Sabine Rosenfeldt, Hussein Kalo, and Josef Breu

The manuscript was conceptualized and written by J. Breu and me. M. Röhrl, L. Federer, S. Rosenfeldt and H. Kalo commented on the manuscript. I performed most of the synthesis and most of the characterization. L. Federer helped with the synthesis. M. Röhrl conducted the contact angle measurements. S. Rosenfeldt supported the SAXS measurements and fitted the SAXS data. All authors contributed to the scientific discussion.
My contribution to this publication is 75 %.

6.2. Gas barriers from in situ polymerized poly(ethylene glycol) diacrylate clay nanocomposites for food packaging

Dominik Schuchardt†, Maximilian Röhrl†, Sabine Rosenfeldt†, Josef Breu†*

Published in: *ACS Applied Polymer Materials* **2023**, 5, 1, 576-582.

† Bavarian Polymer Institute, Department of Chemistry, University of Bayreuth, Universitätsstraße 30, 95447 Bayreuth, Germany

* Corresponding author: josef.breu@uni-bayreuth.de

ACS APPLIED POLYMER MATERIALS

pubs.acs.org/acsapm Article

Gas Barriers from In Situ Polymerized Poly(ethylene glycol) Diacrylate Clay Nanocomposites for Food Packaging

Dominik Schuchardt, Maximilian Röhrl, Sabine Rosenfeldt, and Josef Breu*

Cite This: *ACS Appl. Polym. Mater.* 2023, 5, 576−582 Read Online

ACCESS | Metrics & More | Article Recommendations | Supporting Information

ABSTRACT: Hydrogel nanocomposites of poly(ethylene glycol) diacrylate (PEGDA) and clay are commonly known for their good biocompatibility and high oxygen permeability while offering sufficient mechanical stability. Dry nanocomposite coatings of this class of polymers would thus not be expected to show appreciable gas barrier performance against oxygen and, even more unlikely for a waterborne system, against water vapor. Here, we applied a wet coat of a homogeneous, nematic mixture of PEGDA of two different molecular weights (575 and 2000 g mol^{-1}) and a large aspect ratio synthetic clay (hectorite, 75 wt %) onto a polyethylene terephthalate (PET) substrate. The wet coat was then photopolymerized quantitatively, as evidenced by infrared spectroscopy, and then dried. Thin coatings of <5 μm obtained via this in situ polymerization showed excellent barrier performance with the higher molecular weight material outperforming the lower molecular weight material. The nanocomposite with PEGDA of the molecular weight of 2000 g mol^{-1} had an oxygen transmission rate as low as 0.0042 cm^3 m^{-2} day^{-1} bar^{-1} at 23 °C and 65% relative humidity (r.h.) and a water vapor transmission rate of 0.035 g m^{-2} day^{-1}. The coated PET thus outperforms many high-performance polymers such as polyvinylidene chloride used in the packaging of foods or pharmaceuticals. Even more surprising for a waterborne coating, the nanocomposite barriers proved rather insensitive to swelling by water vapor as evidenced by the oxygen transmission rate of 0.662 cm^3 μm m^{-2} day^{-1} bar^{-1} and water vapor transmission rate of 1.805 g μm m^{-2} day^{-1} bar^{-1} under harsh conditions of 38 °C and 90% r.h. Clearly, these nanocomposites provide a halogen-free, waterborne, biocompatible, and degradable alternative to commonly used high-performance packaging materials.

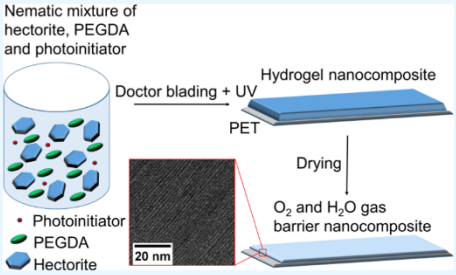

KEYWORDS: *clay, nanocomposite, gas barrier, in situ polymerization, food packaging*

INTRODUCTION

Poly(ethylene glycol) diacrylate (PEGDA) monomers or oligomers are widely used to prepare hydrogels. These gels offer good biocompatibility, while properties may be adjusted in a modular way by applying various molecular structures and molecular weights.[1,2] Moreover, the gels are regarded as degradable.[3,4] The polymer matrix has been compounded with inorganic fillers such as clay or graphene oxide to improve the mechanical strength of the hydrogels.[5−7] For a three-dimensionally printed nanocomposite (≈5−12 vol %) of PEGDA hydrogels, the clay filler was shown not to hamper good oxygen diffusion as needed in biomedical applications.[8,9] The combination of sufficient mechanical properties and biocompatibility renders these nanocomposite materials highly interesting for biomedical applications.[9−11]

As such, waterborne precursors are expected to swell with water vapor and because this in turn will act as a softener, this polymer matrix was so far only investigated for oxygen barriers under dry conditions [0% relative humidity (r.h.)] and even under these favorable conditions, the permeability was found to be rather high (4277 cm^3 μm m^{-2} day^{-1} bar^{-1}).[12] Impermeable clay fillers are known to decrease the permeability by several orders of magnitude with other polymer matrices due to the fabrication of a tortuous path.[13−16] Waterborne polymer coatings, however, tend to swell at higher r.h., causing a collapse in the barrier and consequently, such matrices were disregarded for barrier applications. We have, however, previously reported that the incorporation of large aspect ratio clay nanosheets at high filler levels retarded swelling substantially, mimicking a kind of hydrophobization. As a consequence, the onset of swelling and thus the breakdown of the barrier of such nanocomposites is shifted to substantially higher r.h.[17−19] Based on this observation, PEGDA reappeared on the stage as a potentially attractive matrix for nanocomposite barrier coatings because of its smooth water-based processability, biocompatibility, and degradability.[3,4]

Here, we prepare homogeneous, nematic dispersions of sodium−hectorite mixed with PEGDA of different molecular

Received: September 22, 2022
Accepted: December 1, 2022
Published: December 13, 2022

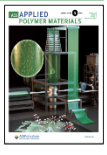

https://doi.org/10.1021/acsapm.2c01672
ACS Appl. Polym. Mater. 2023, 5, 576−582

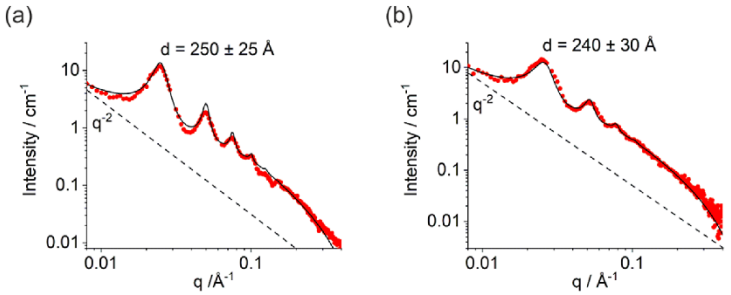

Figure 1. One-dimensional SAXS curves (red dots: measurement, black line: fit) of aqueous (a) Na-Hec and PEGDA 575 and (b) Na-Hec and PEGDA 2000 dispersions indicating a homogeneous, liquid crystalline phase made of hectorite and the monomer. The q^{-2} scaling displays the two-dimensional character of the layered silicates.[23]

weights. Wet coats of these dispersions were first photopolymerized followed by drying. Surprisingly, the dried nanocomposite coatings showed excellent gas barrier properties against oxygen and water vapor even at elevated r.h. and temperature, rendering them appropriate for challenging packaging applications such as pharmaceutical products.

RESULTS AND DISCUSSION

For gas barrier applications, it is important to maximize the aspect ratio α of the layered silicates. This is indicated by the highly nonlinear dependency of the permeability on aspect ratio as given by the Cussler equation.

$$P_{rel} = \frac{P}{P_0} = \left(1 + \mu \cdot \left(\frac{\alpha^2 \cdot \phi^2}{1 - \phi}\right)\right)^{-1} \quad (1)$$

where P is the permeability of the nanocomposite, P_0 is the permeability of the neat polymer, ϕ is the filler content, and μ is a geometrical factor referring to the shape of the filler.[20] Therefore, synthetic sodium fluorohectorite is the ideal filler material for waterborne barrier coatings as its delamination in water is thermodynamically driven by a gentle, forceless process resembling the dissolution of ionic crystals.[21] While melt synthesis yields large crystal diameters, this delamination process preserves this diameter with the nanosheets produced. Immersed in water, the hectorite spontaneously delaminates exclusively into single clay nanosheets of 1 nm thickness while the full lateral extension is preserved, yielding an extremely high $\alpha \approx 20{,}000$.[22] As indicated by the small-angle X-ray scattering (SAXS) measurements (Figure 1), the delamination of the clay is not affected by the presence of PEGDA nor the initiator. At the given concentration (10 wt %), the uniform separation of clay nanosheets remains too small to yield an isotropic dispersion. Rather rotation of individual nanosheets is hampered, and homogeneous, liquid crystalline (nematic) dispersions of clay and monomer are obtained and applied for wet coating.

With the large diameter of hectorite nanosheets given, even the mediocre shear forces during doctor blading are fully sufficient to orient them parallel to the surface of the substrate producing a single domain film.

During successive photopolymerization of the wet coat, a hydrogel is formed, which is then dried into a dense nanocomposite film. The filler content was not varied in order to optimize the barrier. Rather the same filler content was chosen for the different types of PEGDA to determine the influence of the molecular weight on permeability and its dependence on r.h. A rather high filler content of 75% was chosen for this comparison as the Cussler equation suggests permeability to decrease in a highly nonlinear fashion with filler content. The high filler content of 75 wt % in the nanocomposite was confirmed by thermogravimetric analysis (Figure S1). On storing the film under ambient conditions, broad Fourier-transform infrared spectroscopy (FTIR) bands at 3410 cm^{-1} corresponding to O−H stretching of water (Figure S2) indicate a certain degree of swelling with water vapor. The signals at 2920 and 2874 cm^{-1} are assigned to C−H stretching of the polyethyleneglycol (PEG) chains.[24] At 1720 cm^{-1}, the C═O stretching is observed (Figure 2).[25] The

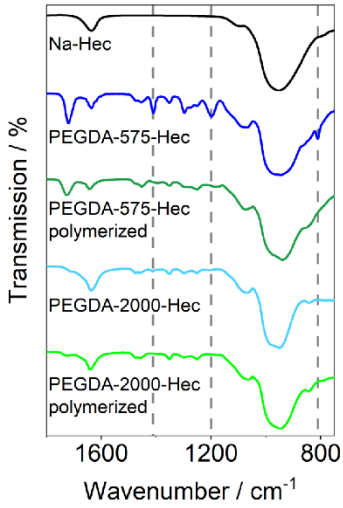

Figure 2. FTIR spectra from 1800 to 750 cm^{-1} of Na−Hec and the nanocomposites PEGDA-575-Hec and PEGDA-2000-Hec before (blue) and after photopolymerization (green). Vertical dashed lines show the position of the characteristic bands of the acrylic group at 1410, 1208, and 810 cm^{-1} that disappear during the photopolymerization.

signal at 1640 cm^{-1} originates from O−H deformation of water.[26] The band at 952 cm^{-1} is assigned to Si−O stretching.[24,26] The characteristic peaks at 1410 cm^{-1} (C═O), 1208 cm^{-1} (−CH═CH_2), and 810 cm^{-1} (−CH═CH_2) for the acrylic group disappear after photopolymerization indicating a high degree of polymerization for both samples.[27−29]

https://doi.org/10.1021/acsapm.2c01672
ACS Appl. Polym. Mater. 2023, 5, 576−582

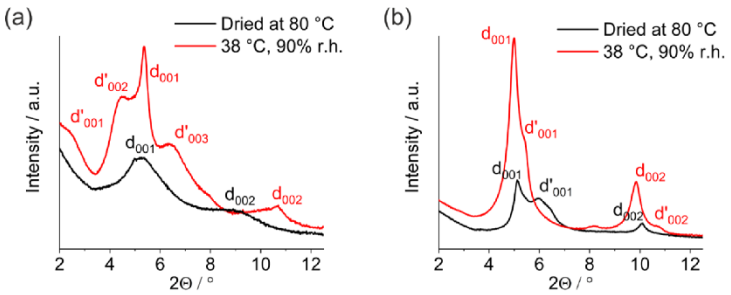

Figure 3. XRD patterns of (a) PEGDA-575-Hec and (b) PEGDA-2000-Hec dried (black) and equilibrated at 38 °C and 90% r.h. (red).

The molecular weight of PEGDA differs with the length of the PEG segments with ≈10 and ≈43 ethyleneglycol (EG) units for PEGDA 575 and 2000, respectively. With the increasing length of PEG segments, the polymer matrix is expected to become more hydrophilic and thus PEGDA-2000-Hec was expected to be more prone to swelling with water vapor. The PEG segments, moreover, are expected to coordinate to the Na^+ interlayer cations, and this attractive interaction favors intercalation of polymer chains between the clay nanosheets in the nanocomposites. For instance, for pure PEG two well-defined, one-dimensionally crystalline intercalation compounds have been reported with 18 and 14 Å periodicities, corresponding to 73 and 84 wt % of PEG,[30] respectively.

X-ray diffraction (XRD) pattern (Figure 3) and transmission electron microscopy (TEM) images of cross-sections of the PEGDA-575-Hec (Figure 4) both indicate partial phase

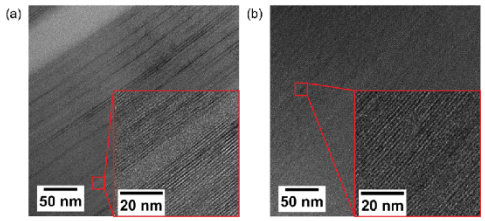

Figure 4. Cross-sectional TEM images of (a) PEGDA-575-Hec and (b) PEGDA-2000-Hec coatings. Dark lines correspond to 1 nm thick clay nanosheets; thin and thick grey domains indicate intercalated PEGDA and phase-segregated PEGDA domains.

segregation. A certain volume fraction of the PEGDA matrix is intercalated, while the remaining polymer segregates into pure PEGDA domains. Most of these segregated domains have thicknesses <10 nm (Figure 4a). This on one hand represents still a severe confinement that will directly alter properties such as swelling of these pure PEGDA domains in comparison to bulk PEGDA. On the other hand, the length scale of segregation implies that the diffraction experiment gives virtual basal spacings that correspond to a volume-weighted average taken over the coherence length of the X-ray beam (typically 500 nm). The averaging, moreover, might lead to more than one peak. A Fourier transformation of the TEM image focused on ordered intercalated domains gives 13.9 Å as the real basal spacing of the intercalated domains, while the X-ray pattern gives a broad hump at 16.7 Å.

During equilibration at 90% r.h. and 38 °C, the various domains will be differently sensitive to swelling, meaning that the water vapor uptake is modulated by the domain structure. Reflections with a *d*-spacing of 37.0, 19.3, and 13.7 Å in any case indicate substantial water uptake of the nanocomposite. They are most likely related to a superstructure. This would imply that the consecutive layers in the intercalated domains adopt strictly alternating distinct hydration states. Ordered interstratifications are a frequent phenomenon with these synthetic hectorites.[31−33] The increase of ≈3 Å from 16.7 to ≈20 Å would indicate the incorporation of a complete layer of water into these domains. The superstructure of this hydrated layer and a non-hydrated layer would then result in a new d_{001}'-reflection at 37 Å, while the original reflections would vanish. The original d_{001}-reflection is still observed as some domains seem to be insensitive to water vapor exposure.

XRD pattern and TEM images of cross-sections of PEGDA-2000-Hec confirm partial phase segregation also for this material. A Fourier transform of the TEM image focused on ordered intercalated domains gives a slightly higher *d*-spacing of 15.3 Å compared to PEGDA-575-Hec. In the XRD, basal reflections are observed at 17.2 and 14.8 Å. Shifts observed upon equilibration at 38 °C and 90% r.h. to 17.6 and 16.3 Å, respectively, are much smaller for this higher molecular weight as compared to those for the PEGDA-575-Hec nanocomposite. The significantly lower water vapor sensitivity is counter-intuitive, as the longer PEG segments were actually expected to render the material more hydrophilic.

Cross-sectional scanning electron microscopy (SEM) images of the nanocomposite coatings on polyethylene terephthalate (PET) show the lamellar, perfectly textured, monodomain structure and indicate a similar nanocomposite coating thickness of both samples of 4.2 and 4.4 μm (Figure S4) for PEGDA-575-Hec and PEGDA-2000-Hec, respectively.

Both nanocomposite coatings appear transparent after drying (Figure S5). Apparently, segregated PEGDA domains are limited in size (<10 nm) as discussed above because of kinetics being hindered by the tortuous path building up on drying the films. Thus, little to no scattering is observed as indicated by the rather low haze values (Figure 5).

Measuring optical transmittance, haze, and clarity indicates, however, superior optical properties with a higher molecular weight of the PEGDA-2000-Hec as compared to the coating with PEGDA-575-Hec (Figure 5). The neat PET substrate and both coatings show high transmittance. Clarity and haze are, however, affected by coating whereby PEGDA-2000-Hec is less affected. This is attributed to clay nanosheets sticking out of the coating and thus increasing the roughness of the nanocomposites. By applying a clear coat of polyvinyl alcohol (PVOH), the surface can be smoothened, and all optical

https://doi.org/10.1021/acsapm.2c01672
ACS Appl. Polym. Mater. 2023, 5, 576−582

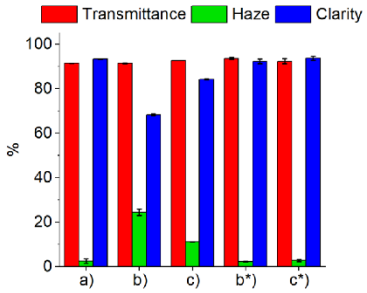

Figure 5. Optical transmittance, haze, and clarity of (a) PET substrate, (b) PEGDA-575-Hec, (c) PEGDA-2000-Hec, (b*) PEGDA-575-Hec with an additional clear coat, and (c*) PEGDA-2000-Hec with an additional clear coat.

performance parameters are brought back to the values of the uncoated PET substrate.

Swelling of waterborne polymer coatings and nanocomposites has a major impact on their barrier properties, causing a breakdown of the barrier. According to the XRD results, the PEGDA-575-Hec coating is expected to be more prone to water vapor uptake than PEGDA-2000-Hec. In line with this, the oxygen transmission rates (OTRs) at 23 °C and 65% r.h. PEGDA-575-Hec were found to be an order of magnitude higher than the OTRs of PEGDA-2000-Hec (Table 1).

Table 1. Oxygen and Water Vapor Transmission Rates of the PEGDA Nanocomposites[a]

		PEGDA-575-Hec	PEGDA-2000-Hec
coating thickness, μm		4.2	4.4
OTR, $cm^3\ m^{-2}\ day^{-1}\ bar^{-1}$	23 °C, 65% r.h.	0.0354	0.0042
	38 °C, 90% r.h.	1.864	0.662
WVTR, $g\ m^{-2}\ day^{-1}$	23 °C, 65% r.h.	0.355	0.035
	38 °C, 90% r.h.	5.085	1.805

[a]The contribution of the PET substrate was corrected according to Roberts et al.[35]

Nevertheless, for a waterborne formulation, both coatings performed surprisingly well. PEGDA-575-Hec had an OTR of 0.0354 $cm^3\ m^{-2}\ day^{-1}\ bar^{-1}$ at 23 °C and 65% r.h., whereas the OTR of PEGDA-2000-Hec was 0.0042 $cm^3\ m^{-2}\ day^{-1}\ bar^{-1}$. For comparison, the published OTR values at these conditions for coatings of comparable thickness made of hectorite clay and PVOH were 0.0018 $cm^3\ m^{-2}\ day^{-1}\ bar^{-1}$.[13] For coatings made of hectorite and polyvinylpyrrolidone, an OTR of 0.01 $cm^3\ m^{-2}\ day^{-1}\ bar^{-1}$ at 23 °C and 60% r.h. was reported.[34] Compared to neat PEGDA films, this corresponds to improvement factors for permeability of 1.34×10^6 and 4.23×10^7 for PEGDA-575-Hec and PEGDA-2000-Hec, respectively (Table S1). Even at more severe environmental settings at 38 °C and 90% r.h., where XRD suggests substantial swelling with water vapor, the permeability increase was surprisingly low. The OTR rose only to 1.864 and 0.662 $cm^3\ m^{-2}\ day^{-1}\ bar^{-1}$ for PEGDA-575-Hec and PEGDA-2000-Hec, respectively.

With water vapor, the nanocomposite coatings swell to a certain equilibrium value. Swelling does not continue with time but is limited. Please note that vapor transmission rates were in any case measured after achieving these equilibria as permeabilities will be significantly affected by swelling. Even at 38 °C and 90% r.h., the coatings were not gel-like but solid. With respect to the influence of the molecular weight of the polymer matrix, water vapor transmission rates (WVTRs) showed the same trend as the OTR performance. At 23 °C and 65% r.h., the WVTR for PEGDA-575-Hec was 0.355 $g\ m^{-2}\ day^{-1}$. The WVTR of PEGDA-2000-Hec was 1 order of magnitude lower (0.035 $g\ m^{-2}\ day^{-1}$) than that of PEGDA-575-Hec at 23 °C and 65% r.h., while at 38 °C and 90% r.h., they differed by a factor of 2.8 (5.085 and 1.805 $g\ m^{-2}\ day^{-1}$ for PEGDA-575-Hec and PEGDA-2000-Hec, respectively). For comparable coatings made of hectorite and PVOH, a WVTR of 0.05 $g\ m^{-2}\ day^{-1}$ at 23 °C and 65% r.h. was reported.[13]

The WVTR and OTR measured for PET coated with PEGDA-2000-Hec at 38 °C and 90% r.h. render this packaging material a high-performance alternative to chloride-containing or poorly degradable polymer films, while being waterborne and biocompatible. For better comparability with commonly used packaging materials, the OTR and WVTR are converted to oxygen permeability (OP) and water vapor permeability (WVP, Figure 6, Table S2).

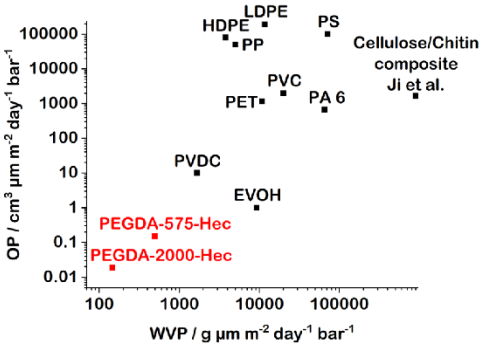

Figure 6. OPs and WVPs of PEGDA-575-Hec and PEGDA-2000-Hec (red) as compared to common packaging polymer materials (black). Most OP values have been recorded at 23 °C and 50% r.h. and WPV at 38 °C and 90% r.h., while for PEGDA-Hec nanocomposites, OP was recorded at harsher conditions (23 °C and 65% r.h.) and the values for cellulose/chitin composite were taken from Ji et al. WPV was measured at milder conditions (23 °C and 50% r.h). EVOH: ethylene vinyl alcohol; HDPE: high-density polyethylene; LDPE: low-density polyethylene; PA 6: polyamide 6; PET: polyethylene terephthalate; PP: polypropylene; PVDC: polyvinylidene dichloride; PVC: polyvinyl chloride.[36−40]

PEGDA-575-Hec showed an OP of 0.149 $cm^3\ \mu m\ m^{-2}\ day^{-1}\ bar^{-1}$ (23 °C and 65% r.h.) and a WVP of 496.4 $g\ \mu m\ m^{-2}\ day^{-1}\ bar^{-1}$ (38 °C and 90% r.h). For PEGDA-2000-Hec, an OP of 0.019 $cm^3\ \mu m\ m^{-2}\ day^{-1}\ bar^{-1}$ (23 °C and 65% r.h.) and a WVP of 147 $g\ \mu m\ m^{-2}\ day^{-1}\ bar^{-1}$ (38 °C and 90% r.h.) could be determined. Therefore, both composites outperform previously published eco-friendly barrier materials such as cellulose/chitin composites that showed an OP of 1670 $cm^3\ \mu m\ m^{-2}\ day^{-1}\ bar^{-1}$ at 23 °C and 65% r.h. and a WVP of 900,000 $g\ \mu m\ m^{-2}\ day^{-1}\ bar^{-1}$ at 23 °C and 50% r.h.[40,41] Furthermore, they even outperformed commercial high-performance packaging materials such as PVDC (OP: 10 $cm^3\ \mu m\ m^{-2}\ day^{-1}\ bar^{-1}$ at 23 °C and 65% r.h.; WVP: 1675 $g\ \mu m\ m^{-2}\ day^{-1}\ bar^{-1}$ at 38 °C and 90% r.h.) or EVOH (OP: 1

https://doi.org/10.1021/acsapm.2c01672
ACS Appl. Polym. Mater. 2023, 5, 576−582

cm^3 μm m^{-2} day^{-1} bar^{-1} at 23 °C and 65% r.h.; WVP: 9237 g μm m^{-2} day^{-1} bar^{-1} at 38 °C and 90% r.h).[36−39]

CONCLUSIONS

In conclusion, we were able to prepare PEGDA/hectorite nanocomposite coatings by in situ photopolymerization of wet coats. Despite the longer, more hydrophilic PEG segments, the higher molecular weight PEGDA was less sensitive to water vapor and showed impressive barrier performance even at severe environmental conditions of 38 °C and 90% r.h. The combination of the excellent optical and barrier properties renders the biocompatible and degradable PEGDA-Hec nanocomposites, especially the one with higher molecular weight of PEGDA, most interesting in challenging packaging applications. Furthermore, as the molecular weight of PEGDA, the curing condition, the filler content, as well as the segregation pattern are expected to substantially affect the degradation kinetics of the nanocomposite barrier films,[42] detailed degradation studies will be addressed in future research.

EXPERIMENTAL SECTION

Materials and Methods. The synthetic sodium fluorohectorite $[Na_{0.5}]^{inter}[Mg_{2.5}Li_{0.5}]^{oct}[Si_4]^{tet}O_{10}F_2$ (Na-Hec) was produced by melt synthesis followed by longtime annealing.[43] The clay has a cation exchange capacity of 1.27 mequiv g^{-1}. PEGDA (molecular weight 575 and 2000 g mol^{-1}) and the photoinitiator 2-hydroxy-4′-(2-hydroxyethoxy)-2-methylpropiophenone were purchased from Sigma Aldrich and used as supplied. A PET foil (36 μm, Bleher KG, Germany) with a one-sided corona treatment was used as the substrate.

Composite Preparation. Na-Hec was immersed in a solution of PEGDA (PEGDA-575 and PEGDA-2000) in double distilled water. The dispersion was placed in an overhead shaker for 7 days to ensure complete delamination of the clay, yielding dispersions with a total solid content of 7%. A high filler content of 75 wt % Na-Hec was added. Dispersions with this filler content are honey viscous, allowing for easy processing by doctor blading. The dispersions were first deoxygenated by bubbling Ar gas through it for 1 h followed by degassing with a SpeedMixer (DAC 400.2 VAC-P, Hauschild GmbH & Co. KG, Germany). Then, 1 mol % photoinitiator based on the monomer was added. Coatings were applied onto PET substrates by automated doctor blading (ZAA 2300, Zehntner GmbH Testing Instruments, Switzerland). The speed of the blade was set to 10 mm s^{-1}, and the blade height was 100 μm. Polymerization of the wet coats was initiated by irradiation with a UV lamp (λ = 365 nm, Herolab GmbH Laborgeräte, Germany) for 15 min. Finally, the coatings (PEGDA-575-Hec and PEGDA-2000-Hec) were dried first under ambient conditions for 12 h before being put in an oven at 80 °C for another 12 h.

Characterization Methods. *Powder XRD.* XRD measurements were done in Bragg−Brentano-geometry using Cu K_α radiation (λ = 1.541878 Å). Panalytical's Highscore Plus software was used to analyze the XRD patterns.

SAXS. SAXS intensities were recorded with a "Double Ganesha AIR" system (SAXSLAB, XENOCS). This laboratory-based system uses a rotating copper anode (MicroMax 007HF, Rigaku Corporation, Japan) as the X-ray source. The data are recorded by a position-sensitive detector (PILATUS 300 K, Dectris). For an improved signal-to-noise ratio, dispersions of Na-Hec/PEGDA with a higher total solid content of ∼10% were prepared. After equilibration, the gels were filled into 1 mm glass capillaries (Hildenberg). SAXS curves were fitted by applying a model described in the Supporting Information (Figure S6) using the software Scatter (version 2.5).[44]

FTIR. For FTIR measurements, a Jasco FTIR 6100 spectrometer was employed.

OTR. OTRs were measured on a Mocon OX-TRAN 2/21 M10x (Minneapolis, USA) with a lower detection limit of 0.0005 cm^3 m^{-2} day^{-1} bar^{-1}. The samples were tested at 23 °C and 65% r.h. and at 38 °C and 90% r.h. Forming gas (Linde Formiergas 95/5) was used as carrier gas and 100% oxygen (Linde Sauerstoff 3.5) as the permeant. Measurements were not started before a steady state was achieved in a lengthy conditioning period.

WVTR. WVTRs were determined using a HiBarSens HBS 2.0 HT (Sempa Systems GmbH, Germany) with a lower detection limit of 1 × 10^{-6} g m^{-2} day^{-1}. The samples were tested at 23 °C and 65% r.h. and at 38 °C and 90% r.h.

TEM. Cross-sectional TEM images were taken employing a JEOL-JEM-2200FS (JEOL GmbH, Germany) microscope. Cross sections of the nanocomposite films were prepared using a JEOL EM-09100IS Cryo Ion Slicer (JEOL GmbH, Germany).

SEM. Cross-sectional SEM images were recorded on a Zeiss 1530. For sample preparation, the coatings were cut with a razor blade. The images were then used to determine the coating thickness.

Optical Properties. Transmittance, haze, and clarity were determined using a BYK-Gardner Haze-Gard Plus (BYK-Gardner GmbH, Germany). An average of five measurements for each sample was taken. The clear coat was applied by casting a PVOH solution (5 wt %) onto the coating.

ASSOCIATED CONTENT

Supporting Information

The Supporting Information is available free of charge at https://pubs.acs.org/doi/10.1021/acsapm.2c01672.

Thermogravimetric Analysis and FTIR spectra of the nanocomposite coatings; XRD patterns of neat, unfilled PEGDA films; cross-sectional SEM images of the nanocomposite coatings; pictures of the nanocomposite coatings; preparation and OTR values of neat PEGDA films; conversion of OTR values to OP values and WVTR values to WVP values; and simplified disc model applied for fitting the SAXS measurements (PDF)

AUTHOR INFORMATION

Corresponding Author

Josef Breu − *Bavarian Polymer Institute and Department of Chemistry, University of Bayreuth, Bayreuth 95447, Germany*; orcid.org/0000-0002-2547-3950; Email: josef.breu@uni-bayreuth.de

Authors

Dominik Schuchardt − *Bavarian Polymer Institute and Department of Chemistry, University of Bayreuth, Bayreuth 95447, Germany*

Maximilian Röhrl − *Bavarian Polymer Institute and Department of Chemistry, University of Bayreuth, Bayreuth 95447, Germany*

Sabine Rosenfeldt − *Bavarian Polymer Institute and Department of Chemistry, University of Bayreuth, Bayreuth 95447, Germany*

Complete contact information is available at: https://pubs.acs.org/10.1021/acsapm.2c01672

Author Contributions

The manuscript was written through the contributions of all authors. All authors have given approval to the final version of the manuscript.

Funding

This work was funded by the ALTANA Institute.

Notes

The authors declare no competing financial interest.

■ ACKNOWLEDGMENTS

The authors acknowledge the support of the Keylab "Mesoscale Characterization: Scattering Techniques", the Keylab "Polymer Additives and Fillers", and the Keylab "Optical and Electron Microscopy" of the Bavarian Polymer Institute. The authors thank Florian Puchtler for the synthesis of the synthetic sodium hectorite and Marco Schwarzmann for the SEM measurements as well as for the preparation of the TEM samples by cryo-ion-slicer and their measurement. We appreciate multiple stimulating discussions with people involved in the ALTANA Institute (Christian Schaumberg, Hubert Schießling, Ralf Hoffmann, Udo Krappe, and Hussein Kalo).

■ REFERENCES

(1) Warr, C.; Valdoz, J. C.; Bickham, B. P.; Knight, C. J.; Franks, N. A.; Chartrand, N.; Van Ry, P. M.; Christensen, K. A.; Nordin, G. P.; Cook, A. D. Biocompatible PEGDA Resin for 3D Printing. *ACS Appl. Bio Mater.* **2020**, *3*, 2239−2244.

(2) Jamadi, M.; Shokrollahi, P.; Houshmand, B.; Joupari, M. D.; Mashhadiabbas, F.; Khademhosseini, A.; Annabi, N. Poly (Ethylene Glycol)-Based Hydrogels as Self-Inflating Tissue Expanders with Tunable Mechanical and Swelling Properties. *Macromol. Biosci.* **2017**, *17*, 1600479.

(3) Browning, M. B.; Cereceres, S. N.; Luong, P. T.; Cosgriff-Hernandez, E. M. Determination of the in vivo degradation mechanism of PEGDA hydrogels. *J. Biomed. Mater. Res., Part A* **2014**, *102*, 4244−4251.

(4) Reid, B.; Gibson, M.; Singh, A.; Taube, J.; Furlong, C.; Murcia, M.; Elisseeff, J. PEG hydrogel degradation and the role of the surrounding tissue environment. *J. Tissue Eng. Regener. Med.* **2015**, *9*, 315−318.

(5) Owusu-Adom, K.; Guymon, C. A. Chemical Compatibility and Reaction-Induced Exfoliation in Photopolymerizable Clay Nanocomposites. *Macromolecules* **2008**, *42*, 180−187.

(6) Sangermano, M.; Marchi, S.; Valentini, L.; Bon, S. B.; Fabbri, P. Transparent and Conductive Graphene Oxide/Poly(ethylene glycol) diacrylate Coatings Obtained by Photopolymerization. *Macromol. Mater. Eng.* **2011**, *296*, 401−407.

(7) Cho, M. S.; Shin, B.; Nam, J. D.; Lee, Y.; Song, K. Nanocomposites of polymer gel electrolyte based on poly(ethylene glycol diacrylate) and Mg-Al layered double hydroxides. *Polym. Int.* **2004**, *53*, 1523−1528.

(8) Kadilak, A. L.; Rehaag, J. C.; Harrington, C. A.; Shor, L. M. A 3D-printed microbial cell culture platform with in situ PEGDA hydrogel barriers for differential substrate delivery. *Biomicrofluidics* **2017**, *11*, 054109.

(9) Zhai, X.; Ruan, C.; Ma, Y.; Cheng, D.; Wu, M.; Liu, W.; Zhao, X.; Pan, H.; Lu, W. W. 3D-Bioprinted Osteoblast-Laden Nanocomposite Hydrogel Constructs with Induced Microenvironments Promote Cell Viability, Differentiation, and Osteogenesis both In Vitro and In Vivo. *Adv. Sci.* **2018**, *5*, 1700550.

(10) Chang, C.-W.; van Spreeuwel, A.; Zhang, C.; Varghese, S. PEG/clay nanocomposite hydrogel: a mechanically robust tissue engineering scaffold. *Soft Matter* **2010**, *6*, 5157.

(11) Kim, Y. H.; Sohn, J.-W.; Woo, Y.; Hong, J.-H.; Kim, G. M.; Kang, B. K.; Park, J. Preparation of Microstructure Molds of Montmorillonite/Polyethylene Glycol Diacrylate and Multi-Walled Carbon Nanotube/Polyethylene Glycol Diacrylate Nanocomposites for Miniaturized Device Applications. *J. Nanosci. Nanotechnol.* **2015**, *15*, 7860−7865.

(12) Chen, Y.; Ye, Y.; Chen, Z.-R. Vapor-based synthesis of bilayer anti-corrosion polymer coatings with excellent barrier property and superhydrophobicity. *J. Mater. Sci.* **2018**, *54*, 5907−5917.

(13) Röhrl, M.; Federer, L. K. S.; Timmins, R. L.; Rosenfeldt, S.; Dörres, T.; Habel, C.; Breu, J. Disorder-Order Transition-Improving the Moisture Sensitivity of Waterborne Nanocomposite Barriers. *ACS Appl. Mater. Interfaces* **2021**, *13*, 48101−48109.

(14) Ebina, T. Development of Clay-Based Films. *Chem. Rec.* **2018**, *18*, 1020−1032.

(15) Doblhofer, E.; Schmid, J.; Rieß, M.; Daab, M.; Suntinger, M.; Habel, C.; Bargel, H.; Hugenschmidt, C.; Rosenfeldt, S.; Breu, J.; Scheibel, T. Structural Insights into Water-Based Spider Silk Protein-Nanoclay Composites with Excellent Gas and Water Vapor Barrier Properties. *ACS Appl. Mater. Interfaces* **2016**, *8*, 25535−25543.

(16) Cussler, E. L.; Hughes, S. E.; Ward, W. J.; Aris, R. Barrier membranes. *J. Membr. Sci.* **1988**, *38*, 161−174.

(17) Grunlan, J. C.; Grigorian, A.; Hamilton, C. B.; Mehrabi, A. R. Effect of clay concentration on the oxygen permeability and optical properties of a modified poly(vinyl alcohol). *J. Appl. Polym. Sci.* **2004**, *93*, 1102−1109.

(18) Song, Y.; Gerringer, J.; Qin, S.; Grunlan, J. C. High Oxygen Barrier Thin Film from Aqueous Polymer/Clay Slurry. *Ind. Eng. Chem. Res.* **2018**, *57*, 6904−6909.

(19) Ding, F.; Liu, J.; Zeng, S.; Xia, Y.; Wells, K. M.; Nieh, M. P.; Sun, L. Biomimetic nanocoatings with exceptional mechanical, barrier, and flame-retardant properties from large-scale one-step coassembly. *Sci. Adv.* **2017**, *3*, No. e1701212.

(20) Falla, W. R.; Mulski, M.; Cussler, E. L. Estimating diffusion through flake-filled membranes. *J. Membr. Sci.* **1996**, *119*, 129−138.

(21) Rosenfeldt, S.; Stöter, M.; Schlenk, M.; Martin, T.; Albuquerque, R. Q.; Förster, S.; Breu, J. In-Depth Insights into the Key Steps of Delamination of Charged 2D Nanomaterials. *Langmuir* **2016**, *32*, 10582−10588.

(22) Stöter, M.; Kunz, D. A.; Schmidt, M.; Hirsemann, D.; Kalo, H.; Putz, B.; Senker, J.; Breu, J. Nanoplatelets of sodium hectorite showing aspect ratios of ≈20,000 and superior purity. *Langmuir* **2013**, *29*, 1280−1285.

(23) Boldon, L.; Laliberte, F.; Liu, L. Review of the fundamental theories behind small angle X-ray scattering, molecular dynamics simulations, and relevant integrated application. *Nano Rev.* **2015**, *6*, 25661.

(24) Zhai, X.; Hou, C.; Pan, H.; Lu, W. W.; Liu, W.; Ruan, C. Nanoclay Incorporated Polyethylene-Glycol Nanocomposite Hydrogels for Stimulating In Vitro and In Vivo Osteogenesis. *J. Biomed. Nanotechnol.* **2018**, *14*, 662−674.

(25) Jain, E.; Hill, L.; Canning, E.; Sell, S. A.; Zustiak, S. P. Control of gelation, degradation and physical properties of polyethylene glycol hydrogels through the chemical and physical identity of the crosslinker. *J. Mater. Chem. B* **2017**, *5*, 2679−2691.

(26) Jaynes, W. F.; Traina, S. J.; Bigham, J. M.; Johnston, C. T. Preparation and Characterization of Reduced-Charge Hectorites. *Clays Clay Miner.* **1992**, *40*, 397−404.

(27) Decker, C.; Moussa, K. Photopolymerization of multifunctional monomers in condensed phase. *J. Appl. Polym. Sci.* **1987**, *34*, 1603−1618.

(28) Ravi, N.; Mitra, A.; Hamilton, P.; Horkay, F. Characterization of the network properties of poly(ethylene glycol)-acrylate hydrogels prepared by variations in the ethanol-water solvent composition during crosslinking copolymerization. *J. Polym. Sci., Part B: Polym. Phys.* **2002**, *40*, 2677−2684.

(29) Colthup, N. B.; Daly, L. H.; Wiberley, S. E.*Introduction to Infrared and Raman Spectroscopy*, 3rd ed.; Academic Press, 1990.

(30) Dörres, T.; Bartkiewicz, M.; Herrmann, K.; Schöttle, M.; Wagner, D.; Wang, Z.; Ikkala, O.; Retsch, M.; Fytas, G.; Breu, J. Nanoscale-Structured Hybrid Bragg Stacks with Orientation- and Composition-Dependent Mechanical and Thermal Transport Properties: Implications for Nacre Mimetics and Heat Management Applications. *ACS Appl. Nano Mater.* **2022**, *5*, 4119−4129.

(31) Möller, M. W.; Hirsemann, D.; Haarmann, F.; Senker, J.; Breu, J. Facile Scalable Synthesis of Rectorites. *Chem. Mater.* **2010**, *22*, 186−196.

https://doi.org/10.1021/acsapm.2c01672
ACS Appl. Polym. Mater. 2023, 5, 576−582

(32) Stöter, M.; Biersack, B.; Reimer, N.; Herling, M.; Stock, N.; Schobert, R.; Breu, J. Ordered Heterostructures of Two Strictly Alternating Types of Nanoreactors. *Chem. Mater.* **2014**, *26*, 5412−5419.
(33) Stöter, M.; Biersack, B.; Rosenfeldt, S.; Leitl, M. J.; Kalo, H.; Schobert, R.; Yersin, H.; Ozin, G. A.; Förster, S.; Breu, J. Encapsulation of functional organic compounds in nanoglass for optically anisotropic coatings. *Angew. Chem., Int. Ed.* **2015**, *54*, 4963−4967.
(34) Schilling, T.; Habel, C.; Rosenfeldt, S.; Röhrl, M.; Breu, J. Impact of Ultraconfinement on Composite Barriers. *ACS Appl. Polym. Mater.* **2020**, *2*, 3010−3015.
(35) Roberts, A. P.; Henry, B. M.; Sutton, A. P.; Grovenor, C. R. M.; Briggs, G. A. D.; Miyamoto, T.; Kano, M.; Tsukahara, Y.; Yanaka, M. Gas permeation in silicon-oxide/polymer (SiOx/PET) barrier films: role of the oxide lattice, nano-defects and macro-defects. *J. Membr. Sci.* **2002**, *208*, 75−88.
(36) Oxygen and Walter Vapour Barrier Properties of Flex Pack Films. https://usa.dupontteijinfilms.com/wp-content/uploads/2017/01/Oxygen_And_Walter_Vapour_Barrier_Properties_of_Flex_Pack_Films.pdf (accessed 21 July, 2022).
(37) Lange, J.; Wyser, Y. Recent innovations in barrier technologies for plastic packaging?a review. *Packag. Technol. Sci.* **2003**, *16*, 149−158.
(38) Aulin, C.; Gällstedt, M.; Lindström, T. Oxygen and oil barrier properties of microfibrillated cellulose films and coatings. *Cellulose* **2010**, *17*, 559−574.
(39) Schmid, M.; Dallmann, K.; Bugnicourt, E.; Cordoni, D.; Wild, F.; Lazzeri, A.; Noller, K. Properties of Whey-Protein-Coated Films and Laminates as Novel Recyclable Food Packaging Materials with Excellent Barrier Properties. *Int. J. Polym. Sci.* **2012**, *2012*, 1−7.
(40) Ji, Y.; Waters, S.; Lim, E.; Lang, A. W.; Ciesielski, P. N.; Shofner, M. L.; Reynolds, J. R.; Meredith, J. C. Minimizing Oxygen Permeability in Chitin/Cellulose Nanomaterial Coatings by Tuning Chitin Deacetylation. *ACS Sustainable Chem. Eng.* **2021**, *10*, 124−133.
(41) Kim, T.; Tran, T. H.; Hwang, S. Y.; Park, J.; Oh, D. X.; Kim, B. S. Crab-on-a-Tree: All Biorenewable, Optical and Radio Frequency Transparent Barrier Nanocoating for Food Packaging. *ACS Nano* **2019**, *13*, 3796−3805.
(42) Timmins, R. L.; Kumar, A.; Röhrl, M.; Havlíček, K.; Agarwal, S.; Breu, J. High Barrier Nanocomposite Film with Accelerated Biodegradation by Clay Swelling Induced Fragmentation. *Macromol. Mater. Eng.* **2021**, *307*, 2100727.
(43) Breu, J.; Seidl, W.; Stoll, A. J.; Lange, K. G.; Probst, T. U. Charge homogeneity in synthetic fluorohectorite. *Chem. Mater.* **2001**, *13*, 4213−4220.
(44) Förster, S.; Fischer, S.; Zielske, K.; Schellbach, C.; Sztucki, M.; Lindner, P.; Perlich, J. Calculation of scattering-patterns of ordered nano- and mesoscale materials. *Adv. Colloid Interface Sci.* **2011**, *163*, 53−83.

https://doi.org/10.1021/acsapm.2c01672
ACS Appl. Polym. Mater. 2023, 5, 576−582

Supporting Information

Gas Barriers from In Situ Polymerized Poly(ethylene glycol) Diacrylate Clay Nanocomposites for Food Packaging

*Dominik Schuchardt, Maximilian Röhrl, Sabine Rosenfeldt, and Josef Breu**

Bavarian Polymer Institute and Department of Chemistry, University of Bayreuth, Bayreuth 95447, Germany

*: corresponding author: josef.breu@uni-bayreuth.de

KEYWORDS: clay, nanocomposite, gas barrier, *in situ* polymerization, food packaging

Thermogravimetric anylsis (TGA). A Linseis STA PT 1600 (Linseis Messgeräte GmbH, Germany) was used to perform TGA. The PEGDA-Hec nanocomposites were stripped off from the substrate and milled to a powder applying a cryogenic mill prior to the measurement. A heating rate of 10 °C min^{-1} was used to heat the samples up to 1000 °C in synthetic air.

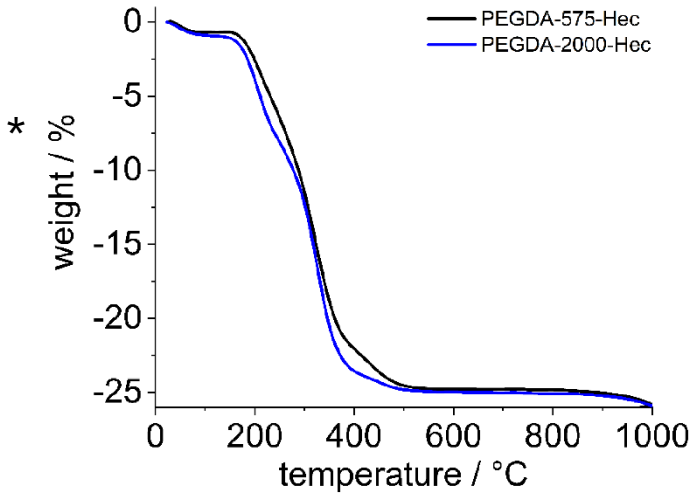

Figure S1: TGA curves of PEGDA-575-Hec (black) and PEGDA-2000-Hec (blue).

*Correction: instead of “weigth / %“ please read “weight loss / %”

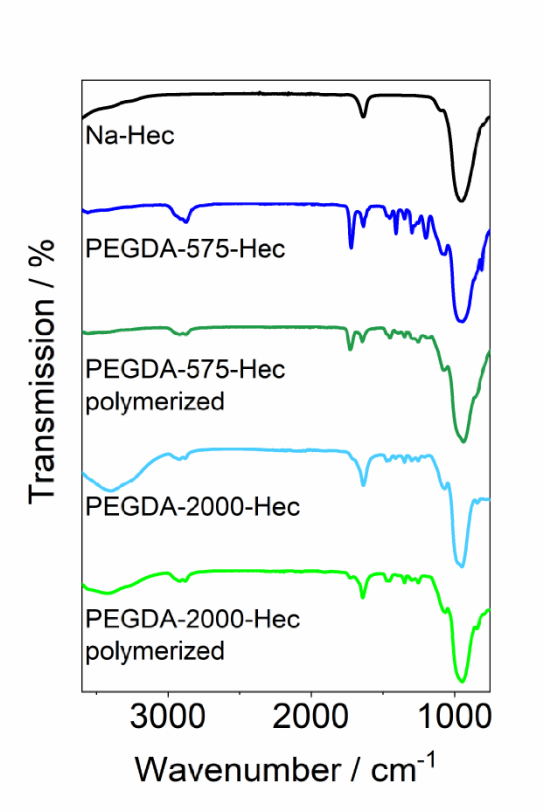

Figure S2: FTIR spectra from 3600 cm^{-1} to 750 cm^{-1} of Na-Hec, PEGDA-575-Hec and PEGDA-2000-Hec before (blue) and after photopolymerization (green).

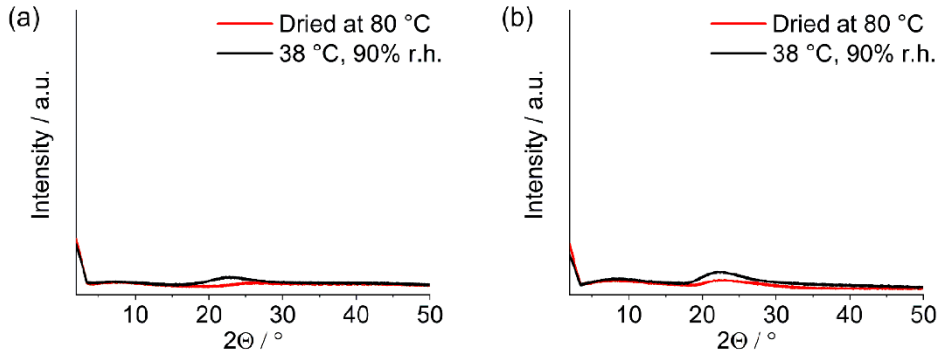

Figure S3. XRD pattern of (a) PEGDA-575 and (b) PEGDA-2000 dried at 80 °C (red) and equilibrated at 38 °C and 90 % r.h.

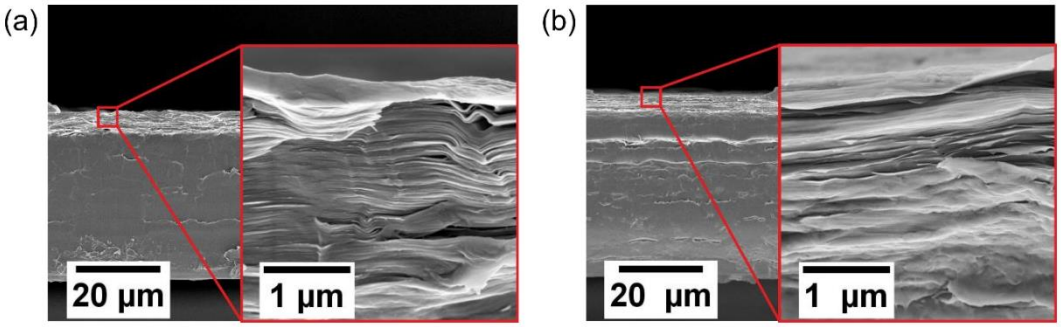

Figure S4. (a) Cross-sectional SEM image of PEGDA-575-Hec and (b) cross-sectional SEM image of PEGDA-2000-Hec.

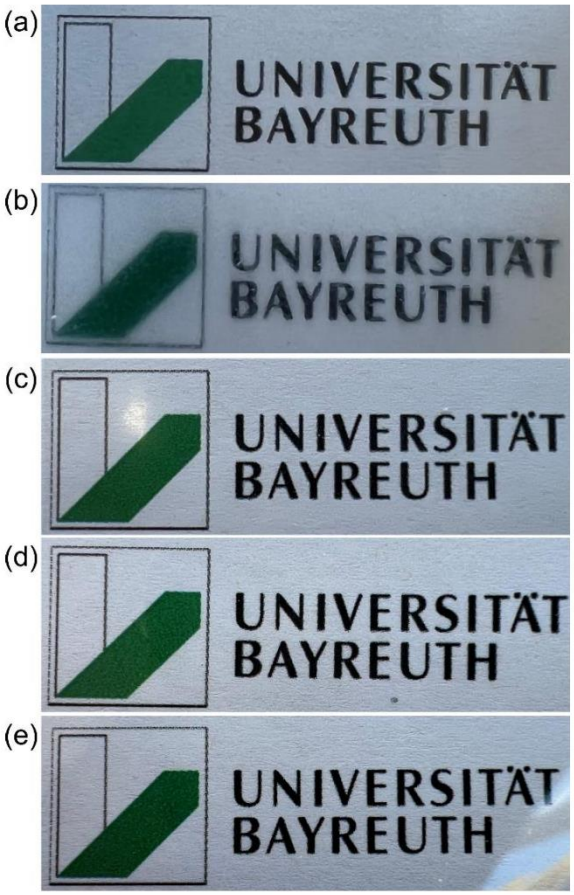

Figure S5. Pictures of (a) uncoated PET, (b) PEGDA-575-Hec, (c) PEGDA-575-Hec with an additional clear coat, (d) PEGDA-2000-Hec, and (e) PEGDA-2000-Hec with an additional clear coat.

Preparation of neat PEGDA films. For PEGDA-575 2.7 g and for PEGDA-2000 0.64 g were dissolved in 5 ml double distilled water each. The solutions were de-oxygenated by bubbling with Ar gas for 1 h and then degassed using a SpeedMixer (DAC 400.2 VAC-P, Hauschild GmbH & Co. KG, Germany). 1 mol% photoinitiator was added to each solution and both were casted into a petri dish. The mixtures were then photopolymerized with a UV lamp (λ = 365 nm, Herolab GmbH

Laborgeräte, Germany) and subsequently dried at ambient conditions for 12 h before being put in an oven at 60 °C for another 24 h.

The thickness of the neat PEGDA films was measured with a High-Accuracy Digimatic Micrometer (Mitutoyo, Japan) with a measuring range of 0 – 25 mm and a resolution of 0.1 µm. An average of 10 measurements for each film was used.

Table S1: Oxygen transmission rates of the neat PEGDA films.

		PEGDA-575	PEGDA-2000
Coating/ film thickness, µm		571.2	133.8
OTR,	**23 °C, 65 % r.h.**	349	3660
$cm^3\ m^{-2}\ day^{-1}\ bar^{-1}$	**38 °C, 90 % r.h.**	907	6010

Conversion of transmission rates to permeabilities. The OTR is dependent on the thickness of the sample. For better comparability, the OTR is converted into oxygen permeability by multiplication with the thickness for better comparability (Table S2). For the conversion of the water vapor transmission rate the results are multiplied by the thickness and as the transmission rate is dependent on the relative humidity transmission rate needs to be divided by the product of the vapor pressure and the relative humidity. Additionally, during this process, the influence of the substrate is removed according to Roberts et al.[1]

Table S2: Oxygen and water vapor permeablilities of the PEGDA-Hec nanocomposites..

		PEGDA-575	PEGDA-2000
OP, cm^3 µm m^{-2} day^{-1} bar^{-1}	**23 °C, 65 % r.h.**	0.149	0.019
	38 °C, 90 % r.h.	8.108	2.950
WVP, g µm m^{-2} day^{-1} bar^{-1}	**23 °C, 65 % r.h.**	88.08	8.52
	38 °C, 90 % r.h.	496.36	147.09

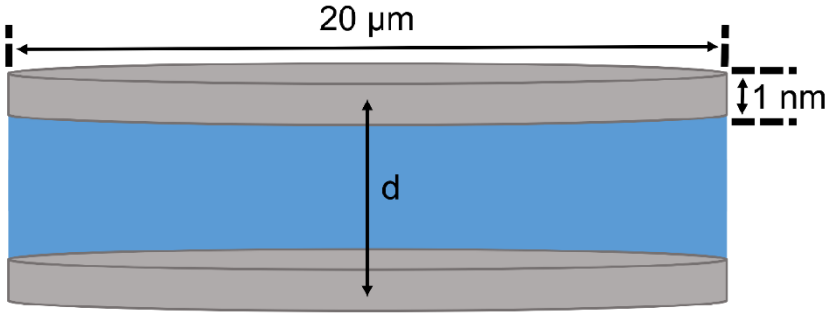

Figure S6: A simplified disc model was applied as fitting model to calculate the layer distance d from SAXS measurements, assuming a layer width of 20 µm and a layer thickness of 1 nm

1. Roberts, A. P.; Henry, B. M.; Sutton, A. P.; Grovenor, C. R. M.; Briggs, G. A. D.; Miyamoto, T.; Kano, M.; Tsukahara, Y.; Yanaka, M., Gas permeation in silicon-oxide/polymer (SiOx/PET) barrier films: role of the oxide lattice, nano-defects and macro-defects. *J. Membr. Sci.* **2002,** *208* (1-2), 75-88.

6.3. Fabrication of Bragg stack films of clay nanosheets and polycations *via* co-polymerization of intercalated monomers and functional interlayer cations

Dominik Schuchardt[†], Sabine Rosenfeldt[†], Hussein Kalo[‡], and Josef Breu[†]*

Published in: *Nanoscale* **2023**, 15, 7044-7050.

[†] Bavarian Polymer Institute, Department of Chemistry, University of Bayreuth, Universitätsstraße 30, 95447 Bayreuth, Germany

[‡] BYK-Chemie GmbH, Plant Moosburg, Stadtwaldstrasse 44, 85368 Moosburg, Germany

* Corresponding author: josef.breu@uni-bayreuth.de

Nanoscale

PAPER

Cite this: *Nanoscale*, 2023, **15**, 7044

Fabrication of Bragg stack films of clay nanosheets and polycations *via* co-polymerization of intercalated monomers and functional interlayer cations†

Dominik Schuchardt,[a] Sabine Rosenfeldt,[a] Hussein Kalo[b] and Josef Breu *[a]

Received 30th January 2023,
Accepted 8th March 2023

DOI: 10.1039/d3nr00438d

rsc.li/nanoscale

The fabrication of one-dimensional (1D) crystalline, monodomain nanocomposite films (hybrid Bragg stacks) is still limited to a few combinations of polymers and clay. The main reason is the segregation of clay and polymers driven by the entropic loss faced by the polymer confined in a narrow slit between the nanosheets. By exchanging synthetic sodium-fluorohectorite with vinylbenzyltrimethylammonium chloride, we succeeded in delaminating clay *via* 1D dissolution in *N*-methylformamide to obtain a liquid crystalline suspension. By combining this with bisphenol A glycerolate diacrylate, 1D crystalline nanocomposites could be obtained *via* photopolymerization of doctor bladed wet coatings. Infrared spectroscopy confirmed the co-polymerization of monomers and the organic modifier between the hectorite platelets. This single-phase hybrid material shows very low oxygen and water vapor transmission rates. The incorporation of the modified clay into the polymer leads to an oxygen transmission rate of 0.21 cm^3 m^{-2} day^{-1} atm^{-1} at 50% r.h. and 23 °C and a water vapor transmission rate of 0.05 g m^{-2} day^{-1} for a coating of 3.7 μm, making this material appropriate for challenging packaging applications.

Introduction

Composite materials of polymers and layered silicates (*e.g.* 2 : 1 clays) are of great interest because of their performance with respect to gas barrier properties,[1] mechanics,[2–5] thermal conductivity,[6,7] or flame retardancy.[8,9] Most of these nanocomposites represent phase segregated composites with clay only and polymer only domains compounded at length scales that are controlled by kinetics. Only a few combinations of polymers and clay are known to form one-dimensional (1D) crystalline hybrid phases (Bragg stacks) representing translational uniform single phases. These ordered phases allow for thorough characterization by determining the direction dependent elastic moduli by Brillouin light scattering and thermal conductivity analysis.[10,11] They show profound anisotropic properties and much increased T_g values compared to neat polymers due to confinement.[12] 1D crystalline Bragg stack barrier films have shown substantially better barrier performance compared to disordered composite materials.[13,14] Moreover, such ordered barrier films are not only superior with respect to the absolute transmission rate but also the onset of swelling with water vapor is significantly retarded.[15] Water incorporated into the polymer matrix in turn acts as a plasticizer and triggers a breakdown of barrier performance. As many barrier applications, in particular, packaging of optoelectronic devices like organic photovoltaic or organic light emitting devices, require excellent performance at elevated humidity levels, the sensitivity of the barrier performance to elevated humidity is a crucial factor.

The formation of such ordered Bragg stack phases requires delamination into monolayers and a polymer matrix that is soluble in the same dispersion medium (in most cases water), allowing for homogeneous mixing of the two. As clay nanosheets carry a permanent negative charge at the basal surface that is counterbalanced by interlayer cations residing in the diffuse double layer, homogenous mixtures are only obtained with neutral polymers. The mixture is then cast as a wet film and upon solvent evaporation a thermodynamically

[a]*Bavarian Polymer Institute and Department of Chemistry, University of Bayreuth, Universitätsstr. 30, 95447 Bayreuth, Germany.*
E-mail: dominik.schuchardt@uni-bayreuth.de, sabine.rosenfeldt@uni-bayreuth.de, josef.breu@uni-bayreuth.de
[b]*BYK-Chemie GmbH, Plant Moosburg, Stadtwaldstrasse 44, 85368 Moosburg, Germany. E-mail: Hussein.Kalo@altana.com*

†Electronic supplementary information (ESI) available: Fig. S1: EDX measurement points; Fig. S2: FTIR spectra of the Bis-GDA-VBTMA-Hec composite, VBTMA-Hec, and Bis-GDA; Fig. S3: XRD pattern of Na-Hec; Fig. S4: TGA curve of Bis-GDA-VBTMA-Hec Fig. S5: 2D XRD pattern, inverse FT, and histogram of Bis-GDA-VBTMA-Hec for grey scale analysis; Fig. S6: model used to fit the SAXS measurements and calculate the basal spacing *d*; Table S1: EDX analysis of the ion exchanged hectorite to confirm exchange of Na^+, Table S2: oxygen and water vapor transmission rates of a neat polymer film from Bis-GDA. See DOI: https://doi.org/10.1039/d3nr00438d

favoured Bragg stack film is obtained, where a defined amount of polymer is intercalated between nanosheets. Entropy loss due to the confinement of high molecular weight polymers disfavours the formation of Bragg stacks. Only for polymers capable of some kind of bonding, *e.g.* hydrogen bonding or complexation with interlayer cations, will the enthalpic gain drive the intercalation despite the confinement effects.

For instance, synthetic sodium-fluorohectorite spontaneously delaminates into strict monolayers when immersed in water.[16,17] When mixed with water soluble polyvinylpyrrolidone (PVP),[15] polyethylene glycol (PEG)[11] or polyvinylalcohol (PVOH),[14] 1D crystalline Bragg stack hybrid films are obtained upon solution casting the suspensions.

One unresolved issue with delaminated sodium-fluorohectorite nanosheets applied as barrier pigments is the presence of hygroscopic inorganic cations needed to balance the anionic charge of the clay. In order to shift the threshold humidity when swelling with water vapor sets in, it would be highly desirable to replace the counter-cations by more hydrophobic organo-cations while not hampering spontaneous delamination. Moreover, a polycationic polymer matrix is expected to bind more strongly to the barrier pigment. In particular in a periodic arrangement of the polyanionic barrier pigment and polycationic matrix, where the Coulombic interaction will be boosted by the Madelung factor by 39%, the strong interaction is expected to hamper swelling even more. Recently we have shown that selected organocations allow for spontaneous delamination, allowing the extension of Bragg type barrier films to more hydrophobic matrices.[18,19] Please note that crystalline films of polycationic polymers with polyanionic clay nanosheets are not directly accessible *via* mixing them in solution as heterocoagulation will be triggered leading to a disordered precipitate.

As photopolymerization of liquid epoxy acrylates mixed with organically modified montmorillonites was shown to be feasible,[20,21] casting wet films followed by polymerization of monomers or prepolymers in confinement between the clay nanosheets appears an attractive alternative route for the synthesis of Bragg stack hybrid films. On one hand, the entropy loss provoked by the confinement may be mitigated by applying monomers or prepolymers of lower molecular weight when casting the wet film. On the other hand, the enthalpy gain may be maximized by covalent bonding to the interlayer cation carrying a functional group, allowing for co-polymerization or crosslinking.

In this publication, we fabricate 1D crystalline Bragg stack films by delaminating synthetic sodium fluorohectorite clay (Na-Hec) that has been ion exchanged with vinylbenzyltrimethylammonium (VBTMA) to allow for spontaneous delamination in *N*-methylformamide (NMF). The organo-suspension was mixed with bisphenol A glycerolate diacrylate (Bis-GDA) and then doctor bladed into a wet film on a polyethylene terephthalate foil (Fig. 1). Photopolymerization yielded a well crystalline, transparent hybrid film showing excellent barrier properties.

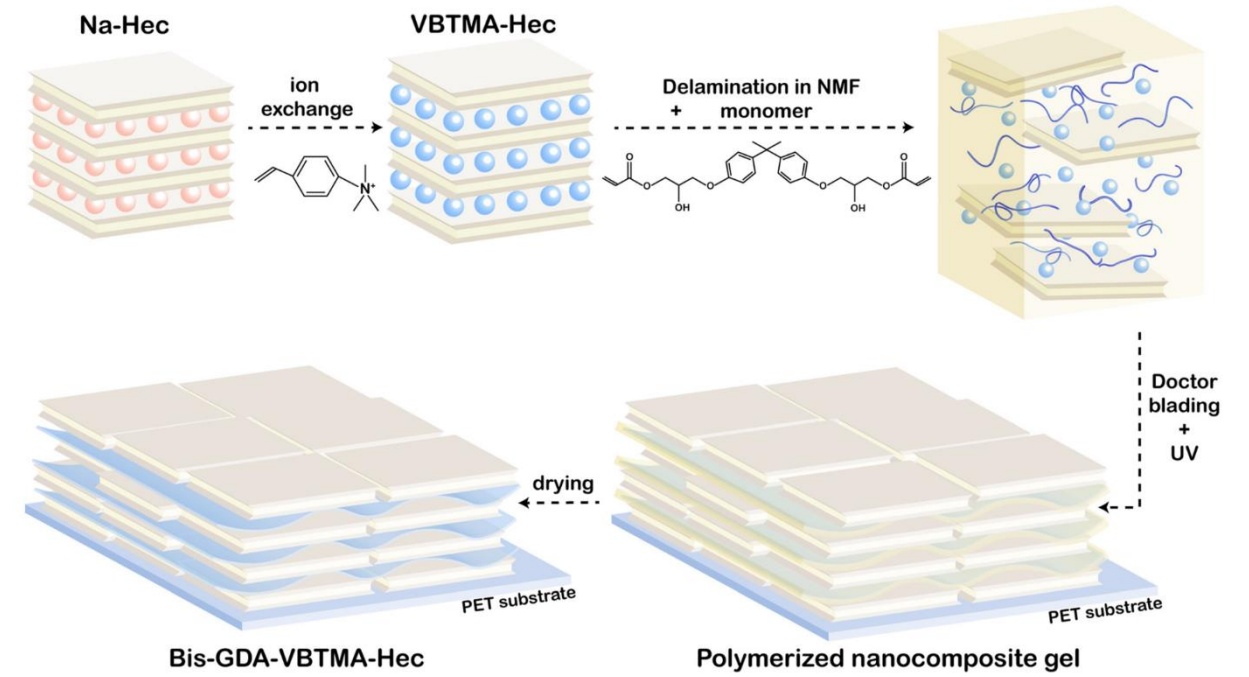

Fig. 1 Schematic illustration of the fabrication of 1D crystalline hybrid Bragg stacks. After ion exchange of Na-Hec for vinylbenzyltrimethylammonium (VBTMA), the hectorite is delaminated in *N*-methylformamide (NMF) together with the monomer. This dispersion is then doctor-bladed and the wet film is photopolymerized and dried.

Results and discussion

An established synthesis procedure using melt synthesis followed by long-term annealing results in synthetic Na-fluorohectorite of superior purity with a nominal composition of $[Na_{0.5}]^{inter}[Mg_{2.5}Li_{0.5}]^{oct}[Si4]^{tet}O_{10}F_2$ (Na-Hec). Both experimentally determined composition ($[Na_{0.48}]^{inter}[Mg_{2.57}Li_{0.47}]^{oct}[Si4]^{tet}O_{10}F_2$) and cation exchange capacity (CEC measured and nominal, 1.26 meq g^{-1} and 1.30 meq g^{-1} respectively) were in good agreement with the expected values.[17,22] This material may be utterly delaminated by 1D dissolution,[23] which represents a spontaneous, thermodynamically driven process and thus produces strictly monolayers. The solvation enthalpy of interlayer cations and the entropy of solvent molecules introduced into the interlayer space *via* swelling are crucial factors for 1D dissolution to be observed. Most successful examples were therefore reported for aqueous dispersions.[24–27] Dudko *et al.* were able to transfer 1D dissolution of synthetic fluorohectorite into different organic solvents. This required hydrophobization of the interlayer Na^+ cation, which was achieved by complexing the sodium cation in the interlayer space with crown ethers.[18] Here we chose to completely replace interlayer Na^+, as evidenced by energy dispersive X-ray spectroscopy (EDX) and powder X-ray diffraction (XRD), by an appropriate organocation (vinylbenzyltrimethylammonium, VBTMA) in order to render the synthetic clay more hydrophobic. EDX showed no residual Na^+ (Table S1, Fig. S1†). In the XRD pattern of the freeze-dried VBTMA-Hec, a rational *d*-spacing of 1.46 nm (Fig. 2a) with a low coefficient of variation (CV) of 0.68% was observed, while no reflections of dry Na-Hec (0.96 nm) were observed. In line with the previously discussed EDX analysis, this indicated complete exchange. VBTMA was identified in a laborious screening as an organocation capable of triggering 1D dissolution in *N*-methylformamide (NMF) while carrying a double bond, allowing it to be co-polymerized.

As synthetic hectorite shows a median diameter of 20 μm, upon delamination nanosheets of 1 nm thickness are obtained with an aspect ratio of 20 000.[17] These nanosheets are held in coplanar orientation at uniform separations by electrostatic repulsion. Given the huge aspect ratio even in dilute suspensions, the separation is much too small to allow for free rotation as isotropic suspensions would need volume fractions as small as 0.000056. For composite fabrication, we applied rather liquid crystalline, nematic suspensions of VBTMA-Hec nanosheets in NMF as obtained by 1D dissolution.[16] The uniformity of the suspension was checked by small-angle X-ray scattering (SAXS) of a concentrated, viscous gel (10 wt%). As expected for nanosheets, the SAXS intensity scales with q^{-2} (Fig. 2b).[28] Furthermore, at this concentration, a platelet separation of 31.3 ± 2.5 nm was observed as indicated by a rational series of interference peaks on the q^{-2} background. Most importantly, there is no peak at higher *q*-values indicating the complete delamination of VBTMA-Hec.

Delamination by 1D dissolution works also when adding bisphenol A glycerolate diacrylate (Bis-GDA) and a photoinitiator to the VBTMA-Hec powder before suspending the mixture in NMF as evidenced by SAXS (Fig. 3a). The minute amounts of the monomer and the photoinitiator do not change the SAXS pattern significantly (compare Fig. 3a with Fig. 2b), but at a closer look some slight deviations in the intensity and the form of the peaks are noticeable. A dilute suspension of such a mixture (total solid content 3 wt%) was doctor bladed onto a polyethylene terephthalate (PET) substrate. The wet coating (100 μm thickness) was then polymerized by UV light. The film was irradiated for 20 minutes, while the viscosity of the wet coating increased. The supported film was then dried in an oven at 100 °C for 24 h before being stored under ambient conditions.

Successful polymerization was checked by Fourier transform infrared spectroscopy (FTIR). Broad bands at 3384 cm^{-1} and 1656 cm^{-1} were attributed to absorbed water molecules (Fig. S2†).[29,30] The absence of a band at 1632 cm^{-1} for the

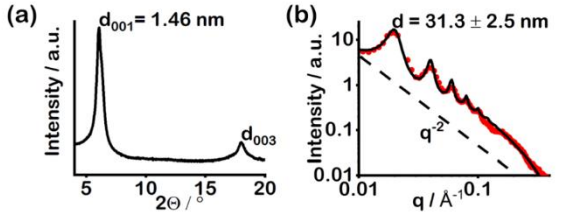

Fig. 2 (a) XRD pattern of VBTMA-Hec and (b) one-dimensional SAXS curve (red dots: measurement, black line: fit) indicating a homogeneous, liquid crystalline dispersion of VBTMA-Hec.

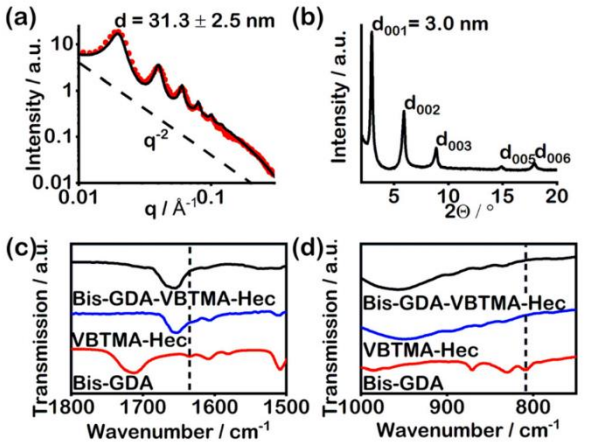

Fig. 3 (a) One-dimensional SAXS curve (red dots: measurement, black line: fit) indicates a homogeneous, liquid crystalline dispersion of the hectorite, monomer and photoinitiator. (b) XRD pattern of the polymerized Bis-GDA-VBTMA-Hec nanocomposite, (c) FTIR spectra of the monomer Bis-GDA (red), VBTMA-Hec and the polymerized Bis-GDA-VBTMA-Hec from 1800 cm^{-1} to 1500 $cm^{-1}$and (d) FTIR spectra of the monomer Bis-GDA (red), VBTMA-Hec and polymerized Bis-GDA-VBTMA-Hec from 1000 cm^{-1} to 750 cm^{-1}. The absence of bands at 1632 cm^{-1} and at 810 cm^{-1} (dashed lines) indicates a successful polymerization.

C=C stretching of the vinyl group of VBTMA and the monomer, as well as the absence of a band at 810 cm^{-1} for the C=C–H stretching of the acrylate group, indicates a high degree of polymerization (Fig. 3c and d).[31–33]

As evidenced by a rational *00l*-series with a small CV of 0.44% (Fig. 3b), a 1D crystalline hybrid Bragg stack was obtained after polymerization and drying. As the thickness of the clay nanosheet is 1 nm (Fig. S3†), the *d*-spacing of 3 nm corresponds to an interlayer height of around 2 nm. The suspension applied contained 123 mg of the monomer and 200 mg of VBTMA-Hec, which in turn comprises 163 mg of silicate and 37 mg of the organocation. Assuming a density of the polymer, made up of the monomer and the organocation, to be 1.15 g cm^{-3}, the nominal polymer : Hec ratio by weight of the Bragg stack is expected to be 46 : 54, while the ratio by volume is expected to be 67 : 33. The former corresponds well to 47% weight loss found in the thermogravimetric analysis (Fig. S4†). The rational *00l*-series with a low CV indicates a high quality of the 1D crystalline order of the nanocomposite.

The cross-sectional transmission electron microscopy (TEM) images of the nanocomposite confirm the perfect periodic homogeneity (Fig. 4). A Fourier transformation of the image gave a *d*-spacing of 30 Å (Fig. S5†), which is in accordance with the XRD results. From these results, the nanocomposite can be considered a single-phase 1D crystalline hybrid material (Bragg stack). As Hec nanosheets are impermeable to gas molecules, the large aspect ratio filler generates a huge tortuous path for diffusion, making the Bragg stack film a promising barrier coating.

The oxygen transmission rate (OTR) and the water vapor transmission rate (WVTR) were measured at two different relative humidities (Table 1). At 50% r.h. and 23 °C, the Bragg stack coating (3.7 μm) yielded an OTR of 0.21 $cm^3\ m^{-2}\ day^{-1}\ atm^{-1}$. Compared to uncoated PET, the OTR is reduced by a factor of 160. Increasing the r.h. to 90% led to an OTR of 1.19 $cm^3\ m^{-2}\ day^{-1}\ atm^{-1}$. For comparison, a polylactic acid coating with a lower content (16 wt%) of crown ether modified Na-Hec also cast from NMF suspension showed an OTR of 2.1 $cm^3\ m^{-2}\ day^{-1}\ atm^{-1}$ (59 μm thickness, 23 °C and 65% r.h.).

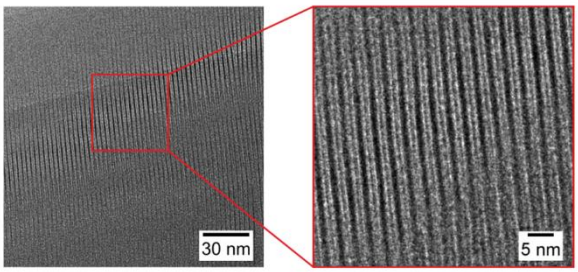

Fig. 4 Cross-sectional TEM image of the Bis-GDA-VBTMA-Hec Bragg stack coating. Dark lines correspond to 1 nm thick clay nanosheets; grey lines correspond to polymerized Bis-GDA in between the clay nanosheets.

Table 1 Oxygen (OTR) and water vapor (WVTR) transmission rates of the Bis-GDA-VBTMA-Hec nanocomposite at 23 °C

	r.h., %	PET (36 μm)	Bis-GDA-VBTMA-Hec
Coating thickness, μm		0	3.7
OTR, $cm^3\ m^{-2}\ day^{-1}\ atm^{-1}$	50	33.69	0.21
	90	31.5	1.19
WVTR, $g\ m^{-2}\ day^{-1}$	50	3.79	0.05
	90	7.39	0.78

Taking the coating thickness and the contribution of the PET substrate into account, transmission rates may be transformed into permeabilities (Table S3†). This allows for calculating the improvement as compared to the permeability of the neat polymer (Table S3†) derived from its transmission rates (Table S2†). In this way, barrier improvement factors (BIFs) of 4.89×10^3 and 1.66×10^3 were found at 50% and 90% r.h.

As expected for a nanocomposite of a high aspect ratio filler at high filler content, the Bragg stack composite outperforms various neat polymers used in commercial packaging applications both with respect to OP and WVP (Fig. 5).[34]

Polymers and their nanocomposites tend to be susceptible to swelling with water vapor that then acts as a plasticizer that increases the segment mobility and thus increases the permeability. We were therefore hoping that replacing the inorganic interlayer cation by a more hydrophobic organocation that moreover becomes covalently linked to the polymer matrix might yield a barrier coating, which is less prone to

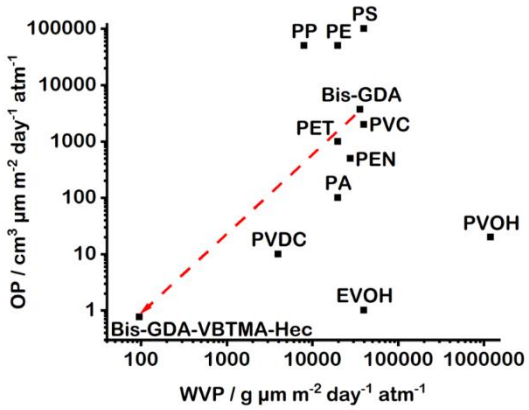

Fig. 5 Oxygen permeability (OP) and water vapor permeability (WVP) of the hybrid Bragg stack film and various polymers commonly used for packaging. Most OP values were recorded at 23 °C and 50% r.h., while for EVOH, PVOH and PA, OP values were recorded at 0% r.h. For WVPs most values were recorded at 23 °C and 85% r.h., while WVP values for the hybrid Bragg stack film and the neat polymer matrix of Bis-GDA were recorded under harsher conditions of 90% r.h. EVOH: polyethylene vinyl alcohol, PVOH: polyvinyl alcohol, PA: polyamide, PEN: polyethylene naphthalate, PET: polyethylene terephthalate, PE: polyethylene, PP: polypropylene, PS: polystyrene, PVC: polyvinyl chloride, PVDC: polyvinylidene dichloride.[34]

swelling and thus is less sensitive to barrier loss at elevated temperatures and r.h.

Moreover, it had been shown that 1D crystallinity also reduces sensitivity to swelling as compared to non-periodic nanosomposites.[14] Unfortunately, this hope did not materialize. At 50% r.h. and 23 °C, the fabricated Bragg stack film with 3.7 μm thickness shows a WVTR of 0.05 g m^{-2} day^{-1}. This is a decrease by a factor of 76 compared to that of the uncoated PET substrate. With rising r.h. the WVTR increases up to 0.78 g m^{-2} day^{-1} at 90% r.h. Compared to the neat polymer, these values correspond to substantial BIFs of 2.78 × 10^3 and 3.74 × 10^2 at 50% r.h. and 90% r.h., respectively. Comparing this performance with that of a Bragg stack type barrier film of the same thickness and a similar polymer : Hec ratio (60 : 40) fabricated with Na-Hec and water soluble PVOH unfortunately indicates no improvement with respect to water vapor sensitivity. The polymer content in the Na-Hec/PVOH coating is not exactly the same, but in a similar range. We chose this system for comparison because it is one of only three materials where formation of hybrid Bragg stack films was previously reported.[11,14,15] Unfortunately, these Bragg stacks come only in well-defined polymer : clay ratios, as the polymer confinement is in the range of molecular dimensions. Therefore, for a given polymer, the stoichiometry is fixed and one cannot vary the polymer content freely without scarifying the periodicity. The chosen comparison is the Bragg stack material that with respect to composition is the closest to Bis-GDA-VBTMA-Hec. Neither replacing hydroscopic Na^+ by VBTMA nor by improving the interaction with the barrier pigment when converting the interlayer cation into a polycation reduces the sensitivity of the barrier performance to high humidity. The PVOH/Na-Hec film shows comparable water vapor barrier performance both at 50% r.h. (WVTR = 0.03 g m^{-2} day^{-1}) and 90%r.h. (WVTR = 0.69 g m^{-2} day^{-1}).

Apparently neither the more hydrophobic organocation nor the co-polymerization with the monomer hampers swelling with water vapor. Although the applied monomer, Bis-GDA, is not water soluble, it nevertheless contains hydrophilic OH groups. Potentially these will render the polymer matrix hydrophilic enough to trigger swelling with water vapor at 90% r.h., causing the deterioration of the barrier. The use of an even more hydrophobic monomer in future studies could enable lower sensitivity to swelling. As both the filler content and hydrophobicity of the polymer are crucial in determining the permeability at elevated humidity, retarding the increase of segment mobility upon incorporation of water molecules acting as plasticizers has great potential.

Conclusion

Mixing polycationic polymers with polyanionic clay nanosheets leads to heterocoagulation of a disordered precipitate. 1D crystalline hybrid Bragg stack films of a synthetic fluorohectorite and a polycationic polymer can, however, be fabricated by first delaminating hectorite modified with a functional organocation *via* 1D dissolution. This suspension can next be homogenously mixed with monomers or prepolymers. Casting wet films followed by photopolymerization and drying finally yields 1D crystalline nanocomposites comprising anionic barrier pigments and a polycationic matrix.

While the nanocomposite films obtained showed excellent barrier properties due to their periodicity, the high filler content and the huge aspect ratio of the filler, the sensitivity of the barrier to water vapor could not be reduced as compared to that of Bragg type barrier films made of water soluble polymers and Na-fluorohectorite. This is disappointing as the method allowed fabricating ordered nanocomposites made with hydrophobic polymer matrices that bind to the filler *via* strong electrostatic interactions of the polycationic matrix produced in the polymerization.

Experimental

Materials

In this study a synthetic sodium fluorohectorite $[Na_{0.48}]^{inter}[Mg_{2.57}Li_{0.47}]^{oct}[Si_4]^{tet}O_{10}F_2$ (Na-Hec) with a cation exchange capacity of 1.26 meq g^{-1} was used.[17] It is produced by melt synthesis followed by a long-time annealing.[22]

N-Methylformamide (NMF), bisphenol A glycerolate diacrylate (Bis-GDA), vinylbenzyltrimethylammonium chloride, and 2-hydroxy-2-methylpropiophenone (HMP, photoinitiator) were purchased from Sigma Aldrich and used as received. A 36 μm thick PET foil (Bleher KG, Germany) was used as the substrate.

Cation exchange

200 mg of Na-Hec were suspended in 10 mL of a 1 M aqueous solution of vinylbenzyltrimethylammonium chloride and the suspension was placed in an overhead shaker overnight. This was repeated 5 times. Subsequently, the modified clay was washed with water until it was free of chloride ions, which was verified by an $AgNO_3$-test. Finally, the clay was freeze-dried.

Bragg stack film fabrication

110 mg of Bis-GDA were dissolved in 6.5 mL of NMF. The solution was then added to 200 mg of modified hectorite. After 1 day of swelling the clay dispersion was deoxygenated by bubbling with Ar gas and subsequently degassed by using a SpeedMixer (DAC 400.2 VAC-P, Hauschild GmbH & Co. KG, Germany). Then 1 mol% HMP based on the monomer was added to the suspension. A wet coating was applied to a PET substrate by doctor blading using an automated device (ZAA 2300, Zehntner GmbH Testing Instruments, Switzerland). The speed of the blade was 10 mm s^{-1} and the blade height was 100 μm. The coating was then polymerized for 20 minutes using a UV lamp with λ = 365 nm (Herolab GmbH Laborgeräte, Germany). Finally, the coating was placed in an oven at 100 °C for 24 h.

Characterization

Powder X-ray diffraction (XRD) patterns were recorded in a Bragg–Brentano-geometry using Cu K_α radiation (λ = 1.541878 Å). For analysis of the XRD patterns, Malvern Panalytical's Highscore Plus software was used.

Small-angle X-ray scattering (SAXS) measurements were performed with a "Double Ganesha AIR" system (SAXSLAB, XENOCS). A rotating copper anode (MicoMax 007HF, Rigaku Corporation, Japan) is the X-ray source of this laboratory-based system. For recording data a position sensitive detector (PILATUS 300 K, Dectris) was used. The samples were measured in 1 mm capillaries (Hilgenberg). The separation in the nematic suspensions was obtained by fitting the SAXS curves applying a model described in the ESI (Fig. S6†) using the software Scatter (version 2.5).[35]

Oxygen transmission rates (OTR) were measured using a Mocon OX-TRAN 2/21 (Minneapolis, USA). The samples were tested at 23 °C and a relative humidity (r.h.) of 50% and 90%. The carrier gas was forming gas (Linde Formiergas 95/5) and 100% oxygen (Linde Sauerstoff 3.5) as the permeant was used. All measurements were performed after conditioning of the samples at the relevant relative humidity until reaching a steady state.

Oxygen transmission rates of the neat PET substrate were measured with a gas transmission tester of Brugger Feinmechanik GmbH[1] at 23 °C and a r.h. of 50% and 90%.

Water vapor transmission rates (WVTR) were measured on a Mocon PERMATRAN-W 3/33 (Minneapolis, USA). The samples were tested at 23 °C and 50% r.h. and at 23 °C and 90% r.h.

The cross-sectional transmission electron microscopy (TEM) images were recorded on a JEOL-JEM-2200FS (JEOL GmbH, Germany) microscope. Preparation of the cross sections of the nanocomposite coatings was done using a JEOL EM-09100IS Cryo Ion Slicer (JEOL GmbH, Germany).

To check for a complete ion exchange, energy dispersive X-ray spectroscopy (EDX) was performed on a Zeiss 1530 equipped with an EDX INCA 357 400 unit (Oxford) with a detection limit of 1 atom%.

The coating thickness was measured with a High-Accuracy Digimatic Micrometer (Mitutoyo, Japan) with a measuring range of 0–25 mm and a resolution of 0.1 μm. The average of 10 measurement points of the film was taken and the thickness of the substrate was subtracted afterwards.

Author contributions

Conceptualization, D. S. and J. B.; methodology, D. S. and S. R.; validation, D. S. and S. R.; formal analysis, D. S, and S. R.; investigation, D. S.; resources, J. B.; data curation, D. S. and S. R.; writing—original draft preparation, D. S., S. R., H. K., and J. B.; writing—review and editing, D. S., S. R., H. K., and J. B.; visualization, D. S.; supervision, J. B.; project administration, J. B.; funding acquisition, J. B. All authors have read and agreed to the published version of the manuscript.

Conflicts of interest

There are no conflicts to declare.

Acknowledgements

The authors acknowledge the support of the Keylab "Mesoscale Characterization: Scattering Techniques", of the Keylab "Polymer Additives and Fillers" and of the Keylab for "Optical and Electron Microscopy" of the Bavarian Polymer Institute. The authors thank Florian Puchtler for the synthesis of the synthetic sodium hectorite and Marco Schwarzmann for the EDX measurements as well as for preparation of the TEM samples using the Cryo Ion Slicer and their measurement. This work was financed by the ALTANA Institute. We appreciate multiple stimulating discussions with people involved in the ALTANA Institute (Christian Schaumberg, Hubert Schießling, Ralf Hoffmann, and Udo Krappe). We thank Olena Khoruzhenko for graphical design.

References

1 T. Ebina, *Chem. Rec.*, 2018, **18**, 1020–1032.
2 Y. Kojima, A. Usuki, M. Kawasumi, A. Okada, Y. Fukushima, T. Kurauchi and O. Kamigaito, *J. Mater. Res.*, 1993, **8**, 1185–1189.
3 P. Podsiadlo, A. K. Kaushik, E. M. Arruda, A. M. Waas, B. S. Shim, J. Xu, H. Nandivada, B. G. Pumplin, J. Lahann, A. Ramamoorthy and N. A. Kotov, *Science*, 2007, **318**, 80–83.
4 P. Podsiadlo, M. Michel, K. Critchley, S. Srivastava, M. Qin, J. W. Lee, E. Verploegen, A. J. Hart, Y. Qi and N. A. Kotov, *Angew. Chem., Int. Ed.*, 2009, **48**, 7073–7077.
5 A. Walther, I. Bjurhager, J. M. Malho, J. Pere, J. Ruokolainen, L. A. Berglund and O. Ikkala, *Nano Lett.*, 2010, **10**, 2742–2748.
6 J. Zhang, D. D. Jiang and C. A. Wilkie, *Polym. Degrad. Stab.*, 2006, **91**, 298–304.
7 J. Sargolzaei and M. Tavakol Akbarabady, *Adv. Compos. Lett.*, 2010, **19**, 164–173.
8 Y. C. Li, J. Schulz, S. Mannen, C. Delhom, B. Condon, S. Chang, M. Zammarano and J. C. Grunlan, *ACS Nano*, 2010, **4**, 3325–3337.
9 P. Kiliaris and C. D. Papaspyrides, *Prog. Polym. Sci.*, 2010, **35**, 902–958.
10 Z. Wang, K. Rolle, T. Schilling, P. Hummel, A. Philipp, B. A. F. Kopera, A. M. Lechner, M. Retsch, J. Breu and G. Fytas, *Angew. Chem., Int. Ed.*, 2020, **59**, 1286–1294.
11 T. Dörres, M. Bartkiewicz, K. Herrmann, M. Schöttle, D. Wagner, Z. Wang, O. Ikkala, M. Retsch, G. Fytas and J. Breu, *ACS Appl. Nano Mater.*, 2022, **5**, 4119–4129.
12 K. Rolle, T. Schilling, F. Westermeier, S. Das, J. Breu and G. Fytas, *Macromolecules*, 2021, **54**, 2551–2560.

13 E. S. Tsurko, P. Feicht, F. Nehm, K. Ament, S. Rosenfeldt, I. Pietsch, K. Roschmann, H. Kalo and J. Breu, *Macromolecules*, 2017, **50**, 4344–4350.
14 M. Röhrl, L. K. S. Federer, R. L. Timmins, S. Rosenfeldt, T. Dörres, C. Habel and J. Breu, *ACS Appl. Mater. Interfaces*, 2021, **13**, 48101–48109.
15 T. Schilling, C. Habel, S. Rosenfeldt, M. Röhrl and J. Breu, *ACS Appl. Polym. Mater.*, 2020, **2**, 3010–3015.
16 S. Rosenfeldt, M. Stöter, M. Schlenk, T. Martin, R. Q. Albuquerque, S. Förster and J. Breu, *Langmuir*, 2016, **32**, 10582–10588.
17 M. Stöter, D. A. Kunz, M. Schmidt, D. Hirsemann, H. Kalo, B. Putz, J. Senker and J. Breu, *Langmuir*, 2013, **29**, 1280–1285.
18 V. Dudko, K. Ottermann, S. Rosenfeldt, G. Papastavrou and J. Breu, *Langmuir*, 2021, **37**, 461–468.
19 V. Dudko, R. L. Timmins, O. Khoruzhenko, M. Röhrl, C. Greve, S. Rosenfeldt, T. Tammelin, S. Agarwal, E. M. Herzig and J. Breu, *Adv. Mater.*, 2022, **3**, 9052–9062.
20 C. Decker, K. Zahouily, L. Keller, S. Benfarhi, T. Bendaikha and J. Baron, *J. Mater. Sci.*, 2002, **37**, 4831–4838.
21 F. M. Uhl, D. C. Webster, S. P. Davuluri and S.-C. Wong, *Eur. Polym. J.*, 2006, **42**, 2596–2605.
22 J. Breu, W. Seidl, A. J. Stoll, K. G. Lange and T. U. Probst, *Chem. Mater.*, 2001, **13**, 4213–4220.
23 V. Dudko, O. Khoruzhenko, S. Weiß, M. Daab, P. Loch, W. Schwieger and J. Breu, *Adv. Mater. Technol.*, 2023, **8**, 2200553.
24 P. Loch, D. Schuchardt, G. Algara-Siller, P. Markus, K. Ottermann, S. Rosenfeldt, T. Lunkenbein, W. Schwieger, G. Papastavrou and J. Breu, *Sci. Adv.*, 2022, **8**, eabn9084.
25 T. Sasaki, M. Watanabe, H. Hashizume, H. Yamada and H. Nakazawa, *J. Am. Chem. Soc.*, 1996, **118**, 8329–8335.
26 Y. Song, N. Iyi, T. Hoshide, T. C. Ozawa, Y. Ebina, R. Ma, N. Miyamoto and T. Sasaki, *Chem. Commun.*, 2015, **51**, 17068–17071.
27 J.-C. P. Gabriel, F. Camerel, B. J. Lemaire, H. Desvaux, P. Davidson and P. Batail, *Nature*, 2001, **413**, 504–508.
28 L. Boldon, F. Laliberte and L. Liu, *Nano Rev.*, 2015, **6**, 25661.
29 M. Asgari and U. Sundararaj, *Appl. Clay Sci.*, 2018, **153**, 228–238.
30 W. F. Jaynes, S. J. Traina, J. M. Bigham and C. T. Johnston, *Clays Clay Miner.*, 1992, **40**, 397–404.
31 C. Decker and K. Moussa, *J. Appl. Polym. Sci.*, 1987, **34**, 1603–1618.
32 M. Sangermano, N. Lak, G. Malucelli, A. Samakande and R. D. Sanderson, *Prog. Org. Coat.*, 2008, **61**, 89–94.
33 N. B. Colthup, L. H. Daly and S. E. Wiberley, *Introduction to Infrared and Raman Spectroscopy*, Academic Press, 3rd edn, 1990.
34 J. Lange and Y. Wyser, *Packag. Technol. Sci.*, 2003, **16**, 149–158.
35 S. Förster, S. Fischer, K. Zielske, C. Schellbach, M. Sztucki, P. Lindner and J. Perlich, *Adv. Colloid Interface Sci.*, 2011, **163**, 53–83.

Electronic Supplementary Material (ESI) for Nanoscale.

Supporting Information

Fabrication of Bragg Stack Films of Clay Nanosheets and Polycations via Co-polymerization of Intercalated Monomers and Functional Interlayer Cations

Dominik Schuchardt [a], Sabine Rosenfeldt [a], Hussein Kalo [b] and Josef Breu [a]*

[a] Bavarian Polymer Institute and Department of Chemistry, University of Bayreuth, Universitätsstr. 30, 95447, Bayreuth, Germany; dominik.schuchardt@uni-bayreuth.de (D.S.), sabine.rosenfeldt@uni-bayreuth.de (S.R.), josef.breu@uni-bayreuth.de (J.B.)

[b] BYK-Chemie GmbH, Plant Moosburg, Stadtwaldstrasse 44, 85368 Moosburg, Germany; Hussein.Kalo@altana.com (H.K.)

* Correspondence: josef.breu@uni-bayreuth.de

Table S1 Energy dispersive X-ray spectroscopy analysis of the freeze-dried vinylbenzyltrimethylammonium exchanged hectorite confirming complete exchange of Na^+.

Point	O / atom%	Na / atom%	Si / atom%
1	37.0	0.0	16.1
2	39.6	0.0	12.5
3	37.6	0.0	16.0
4	39.0	0.0	13.7

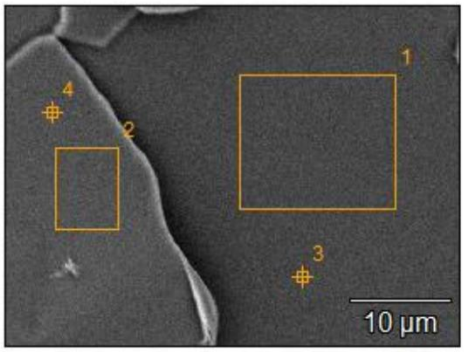

Fig. S1 Scanning electron microscope image of the EDX measurement points 1-4.

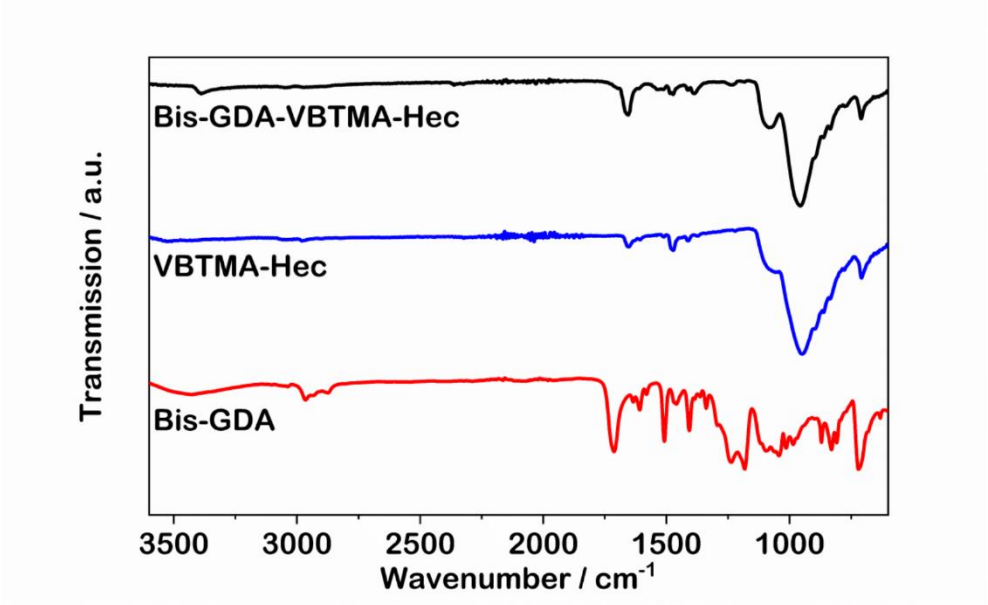

Fig. S2 Fourier-transform-infrared (FTIR) spectra of the Bis-GDA-VBTMA-Hec composite (black), VBTMA-Hec (blue) and Bis-GDA (red).

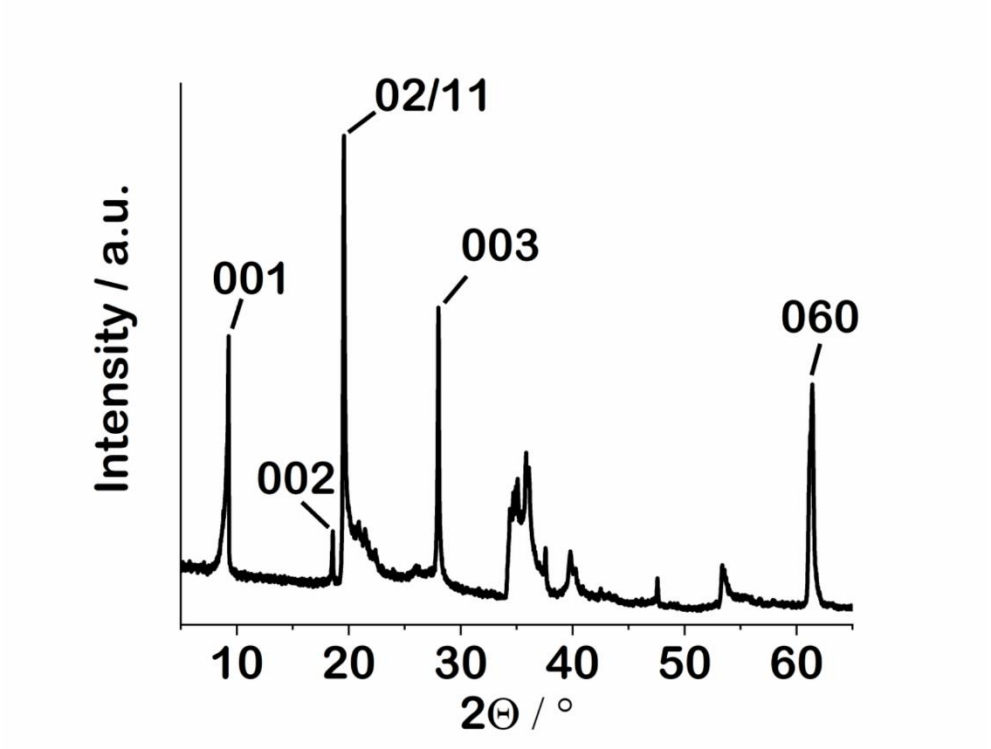

Fig. S3 X-ray pattern of dried Na-Hec indicating a d-spacing of 0.96 nm.

Thermogravimetric analysis (TGA) was measured on a Linseis STA PT 1600 (Linseis Messgeräte GmbH, Germany). The nanocomposite film was peeled off the polyethyleneterephthalat (PET) substrate and grinded to a powder by a cryogenic mill prior to the measurement. The samples were heated up to 1000 °C with a heating rate of 10 °C min^{-1} in synthetic air.

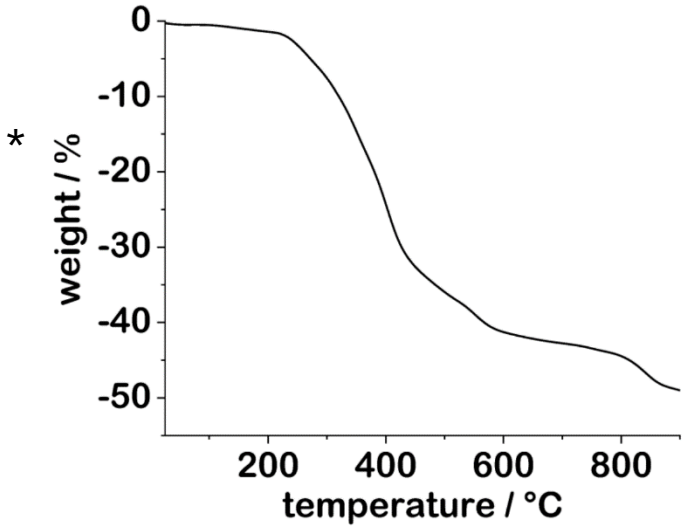

Fig. S4 TGA curve of BIs-GDA-VBTMA-Hec.

The calculation of the expected d-spacing (d001) in the polymerized and dried nanocomposite can be done using the volume content φ_{Hec} of the hectorite.

$$\varphi = \frac{wt\%\,(Hec)\cdot\rho(VBTMA+Bis\text{-}GDA)}{wt\%\,(Hec)\cdot\rho(VBTMA+Bis\text{-}GDA)+\left(100\,wt\%-wt\%\,(Hec)\right)\cdot\rho(Hec)} \quad \text{(E S1)}$$

ρ(VBTMA + Bis-GDA) can be derived through the percentage of VBTMA and Bis-GDA in the polymer matrix with With ρ(VBTMA) = 1.05 g cm^{-3} and ρ(Bis-GDA) = 1.18 g cm^{-3}.

$$\rho(VBTMA + Bis\text{-}GDA) = \frac{m(VBTMA)+m(Bis\text{-}GDA)}{\left(\frac{m(VBTMA)}{\rho(VBTMA)}\right)+\left(\frac{m(Bis\text{-}GDA)}{\rho(Bis\text{-}GDA)}\right)} \quad \text{(E S2)}$$

With ρ(Hec) = 2.7 g cm^{-3} and 54 wt% (Hec) in the dry nanocomposite, the volume content φ_{Hec} = 0.33.

$$d_{001} = \frac{1.0\ \text{nm}}{\varphi} \approx 3.0\ nm \quad \text{(E S3)}$$

*Correction: instead of “weigth / %“ please read “weight loss / %”

The cross-sectional transmission electron microscopy (TEM) image was Fourier transformed into a two-dimensional XRD pattern (Figure S5a). Then a mask was applied, and an inverse FT was done (Figure S5b). To measure the distance of the hectorite nanosheets in the cross-section a histogram was used (Figure S5c), yielding a layer distance

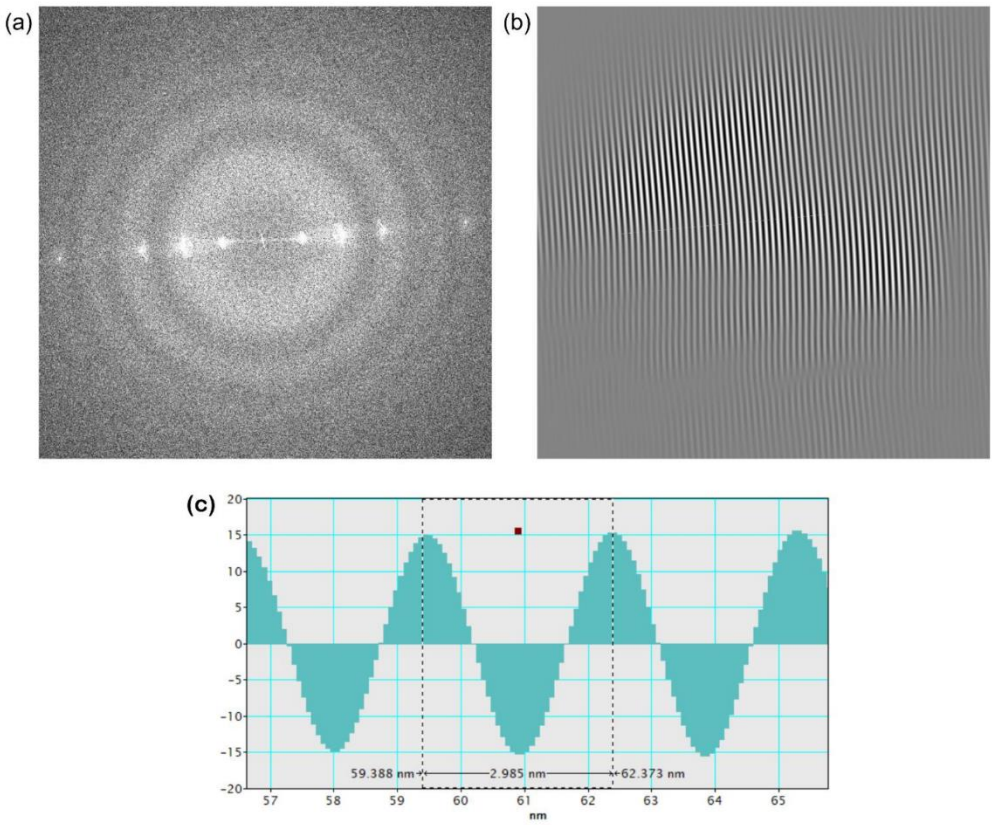

Fig. S5: (a) 2D XRD pattern of Bis-GDA-VBTMA-Hec obtained by Fourier transformation of the cross-sectional TEM image. (b) Inverse FT of the mask 2D XRD pattern of Bis-GDA-VBTMA-Hec. (c) Histogram of the grey scale analyses indicating a layer distance of 3 nm.

of 3 nm.

Preparation of neat polymer films from Bisphenol A glycerolate diacrylate (Bis-GDA)

1 g of Bis-GDA was placed in a Teflon dish and1 mol% photoinitiator were mixed and heated to 60 °C in an oven to form a homogeneous film. The sample was then polymerized by UV light for 20 minutes.

For better comparison, the oxygen transmission rate needs to be converted to the oxygen permeability (OP) by multiplying the OTR with the overall thickness of the measured sample. This is necessary because the OTR is largely influenced by the thickness of the sample. Additionally, the contribution of the PET foil to the OTR is subtracted during the conversion to the OP according to Roberts et al.2

Table S2 Oxygen (OTR) and water vapor transmission rates (WVTR) of a neat polymer film from Bis-GDA.

	relative humidity, %	Bis-GDA
Thickness, µm		976.2
OTR, $cm^3\ m^{-2}\ day^{-1}\ atm^{-1}$	50	3.80
	90	7.48
WVTR, $g\ m^{-2}\ day^{-1}$	50	0.51
	90	0.93

5

Table S3 Oxygen (OP) and water vapor permeabilities (WVP) of a neat polymer film from Bis-GDA.

	relative humidity, %	Bis-GDA-VBTMA-Hec	Bis-GDA
OP, cm^3 µm m^{-2} day^{-1} atm^{-1}	50	0.76	3.71×10^3
	90	4.41	7.30×10^3
WVP, g µm m^{-2} day^{-1} atm^{-1}	50	12.87	3.57×10^4
	90	95.52	3.59×10^4

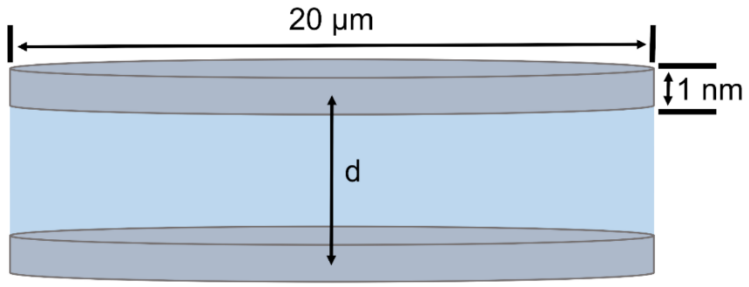

Fig. S6: Model used to fit the small-angle X-ray scattering data and to obtain the basal spacing d assuming a layer width of 20 µm (± 15 % (Gauss)) and a layer thickness of 1 nm (± 3 % (Gauss)).[1]

References

1. S. Förster, S. Fischer, K. Zielske, C. Schellbach, M. Sztucki, P. Lindner and J. Perlich, *Adv. Colloid Interface Sci.*, 2011, **163**, 53-83.
2. A. P. Roberts, B. M. Henry, A. P. Sutton, C. R. M. Grovenor, G. A. D. Briggs, T. Miyamoto, M. Kano, Y. Tsukahara and M. Yanaka, *J. Membr. Sci.*, 2002, **208**, 75-88.

6.4. Spraying transparent nanoglass coatings

Dominik Schuchardt[†], Maximilian Röhrl[†], Lukas Federer[†], Sabine Rosenfeldt[†], Hussein Kalo[‡], and Josef Breu[†]*

Submitted in: *ACS Applied Nano Materials*

[†] Bavarian Polymer Institute, Department of Chemistry, University of Bayreuth, Universitätsstraße 30, 95447 Bayreuth, Germany

[‡] BYK-Chemie GmbH, Plant Moosburg, Stadtwaldstrasse 44, 85368 Moosburg, Germany

* Corresponding author: josef.breu@uni-bayreuth.de

Spraying Transparent Nanoglass Coatings

Dominik Schuchardt[†], *Maximilian Röhrl*[†], *Lukas Federer*[†], *Sabine Rosenfeldt*[†], *Hussein Kalo*[‡], *and Josef Breu* [†,*]

[†] Bavarian Polymer Institute and Department of Chemistry, University of Bayreuth, Universitätsstraße 30, 95447 Bayreuth, Germany

[‡] BYK-Chemie GmbH, Plant Moosburg, Stadtwaldstrasse 44, 85368 Moosburg, Germany

KEYWORDS: 2D layered materials, nanosheets, clay, ion exchange, coatings, gas barrier, packaging

ABSTRACT: When coating suspensions of large aspect ratio clay monolayers upon drying the individual nanosheets self-assemble into thin nanoglass coatings due to the large overlapping areas between restacked clay nanosheets. By exchanging the films with flat-lying, hydrophobic organocations, swelling at higher relative humidity is suppressed and the interlayer space collapses to less than 3 Å, a value smaller than the kinetic diameter of oxygen. Consequently, diffusion along the interlayer space is impeded resulting in very good gas barriers. The guanidinium exchanged all-clay coating, was found to have transmission rates for oxygen as low as 0.32 cm^3 µm m^{-2} day^{-1} atm^{-1} and for water vapor as low as 3.74 g m^{-2} day^{-1}, both values determined at harsh conditions (38 °C and 90 % relative humidity). The barrier is rather insensitive to swelling with water vapor and the performance of the waterborne coatings is competitive, both in barrier performance and transparency with vapor-deposited coatings.

Introduction

Numerous packaging application areas require a high gas barrier while being flexible. Plastic foils, therefore, are a preferred choice as they are affordable, lightweight, sufficiently mechanically resistant, transparent, flexible, and protective against gas permeation.[1, 2] High-end barrier demands, however, often require lamination with thin inorganic layers, like aluminum foils or vapor-deposited aluminum coatings.[3] If transparency is an issue,[1] Al_2O_3 or glass-like SiO_x coatings in the nanometer range applied by vapor-deposition or sol-gel processes are used to enhance the barrier properties of plastic wrap.[3-7] Gas-phase processing may, moreover, be applied in industrially benign large area coatings in sufficient speed.[8] Such thin vapor-deposited barriers are, however, brittle to some extent. While an inorganic film would be expected to be impermeable, pinholes in the extended films limit the barrier performance, in particular, if the laminated barrier systems experience mechanical stress.[9]

The alternative approach taken relies on creation of a tortuous path within a polymer nanocomposite by incorporation of a platy filler. Clay minerals like montmorillonite or hectorite are such well-known platy materials capable of boosting gas barrier in polymer nanocomposites.[10-14] Due to their two-dimensional (2D) crystallinity, individual clay monolayers are impermeable to gases like oxygen or water vapor. Permeates, therefore, have to diffuse around the silicate layers. Consequently, in polymer clay nanocomposites, the permeability is determined by the extension of the diffusion path length (tortuous path), which according to Cussler scales in a highly non-linear way with aspect ratio and filler content.[15] The permeability is by large determined by the diffusion along the polymer matrix between adjacent filler platelets. Consequently, for water vapor the optimum polymer type of choice would be hydrophobic like PVDC while for oxygen or hydrogen barriers the best choice would be a polar, hydrophilic one like PVOH.[16, 17] The drawback

with polar matrix materials is, however, that they tend to swell with water vapor and as water molecules act as a plasticizer, this swelling results to a drastic breakdown of barrier that needs to be mitigated. In this line, hygroscopic interlayer cations like Na^+ are less desirable as compared to hydrophobic organocations.[18]

One of the most attractive features of nanocomposites barriers as compared to inorganic films is the fact that polymer layers intercalated between the silicate monolayers in a nacre-mimicking structure[19-21] mechanically decouple the coplanar adjacent clay nanosheets which enables sliding upon stretching while preserving the barrier. In this line recently a composite barrier system was introduced capable of tolerating up to 15 % stretch.[22]

Self-assembly of large aspect ratio, strictly monolayered nanosheets into monodomain films (Figure 1) has the potential to combine the best of the two barrier approaches sketched above: The largely overlapping nanosheets form a glass-like film extending over the complete wet-coated macroscopic area much the same as with vapor-based inorganic coatings, because the large aspect ratio forces the individual nanosheets into coplanar (textured) orientation parallel to the surface of the polymer substrate. The quality of texture and 1D periodicity is crucial and requires nanosheets of strictly one and the same thickness. Even few multilayers incorporated into the film will create severe defects in the brick (nanosheet) and mortar (interlayer cation) film. Besides assuring this 1D ordered structure via the processing, two additional issues need to be resolved with this approach. First, the interlayer cations are required to be hydrophobic enough not to trigger swelling up to harsh relative humidity (r.h.) conditions encountered in barrier applications (90 % r.h.). Second, the interlayer height as defined by the size and shape of the interlayer cation needs to be smaller than the kinetic diameter of permeates intended to be blocked by the barrier.

The idea is not completely new. Binder-free, all clay films and coatings with natural clay as well as with synthetic clay (saponite, stevensite, and mica) have been investigated by Ebina et al..[23, 24] It was shown that the interlayer cation and the aspect ratio of the clay strongly influence the formation of the film and the amount of defects in the ideal 1D structure, which in turn crucially affected the flexibility. Such self-standing all-clay films showed promising gas barriers (oxygen permeabilities for 70 -120 µm thick films were between 1690 – 18830 cm^3 µm m^{-2} day^{-1} atm^{-1}).[25] The barrier performance of the coatings fabricated most likely was hampered by limited aspect ratios offered by the clay materials applied and imperfect delamination with consequently some multilayer platelets being incorporated into the film causing defects in the brick (clay platelet) and mortar (interlayer cation) structure. It, therefore, appeared promising to explore the coating approach applying perfectly suited synthetic nanosheets.

Here we apply a melt synthesized sodium hectorite ($[Na_{0.5}]^{inter}[Mg_{2.5}Li_{0.5}]^{oct}[Si_4]^{tet}O_{10}F_2$, Na-Hec) that belongs to a group of layered materials that shows the rare phenomenon of 1D dissolution, formerly named osmotic swelling.[26] 1D dissolution resembles the dissolution of salts. The hectorite structure may be viewed as Na-salt of 2D silicate layers and therefore the dissolution is restricted to the stacking direction. When immersing the as synthesized micron-sized hectorite into water, it readily delaminates in a thermodynamically allowed spontaneous swelling. Consequently, strictly 1 nm thick monolayers are produced with median diameters of 20.000 nm. As the diameter of the coplanar nanosheets is orders of magnitude large than their separation even with dilute suspensions (< 1 wt%), the suspensions obtained upon delamination via 1D dissolution, the suspension are not isotropic but liquid crystalline, nematic phases are obtained. Recently, Röhrl et al. demonstrated the potential of this Na-Hec as binder-free clay barrier coating by applying a delaminated, aqueous dispersion to a polyethylene terephthalate (PET) foil via scalable slot-die

coating.[27] The barriers observed turned out to be mediocre. The oxygen transmission rate (OTR) was as high as 1.4 cm^3 m^{-2} day^{-1} bar^{-1} even at low r.h. of 50 % and broke down at higher r.h. because the Na^+ interlayer cations readily promoted swelling with water vapor. Clearly, the interlayer space of this all-clay barrier must be rendered less hydrophilic.

Therefore, in this work, we hydrophobized a monodomain film of Na-Hec post fabrication by spray coating nematic dispersions by ion exchange with guanidinium (Figure 1). Guanidinium salts are well soluble in water, but intercalation compounds of it in clays do not swell in humid air.[28] Moreover, reported basal spacings of guanidinium interclates (12.5 Å) indicate a flat orientation in the interlayer space resulting in a height of the interlayer space (2.9 Å) substantially smaller than the kinetic diameter of oxygen (3.5 Å).[29] This is expected to hinder diffusion along the interlayer and should result in good barrier performance even at high r.h.

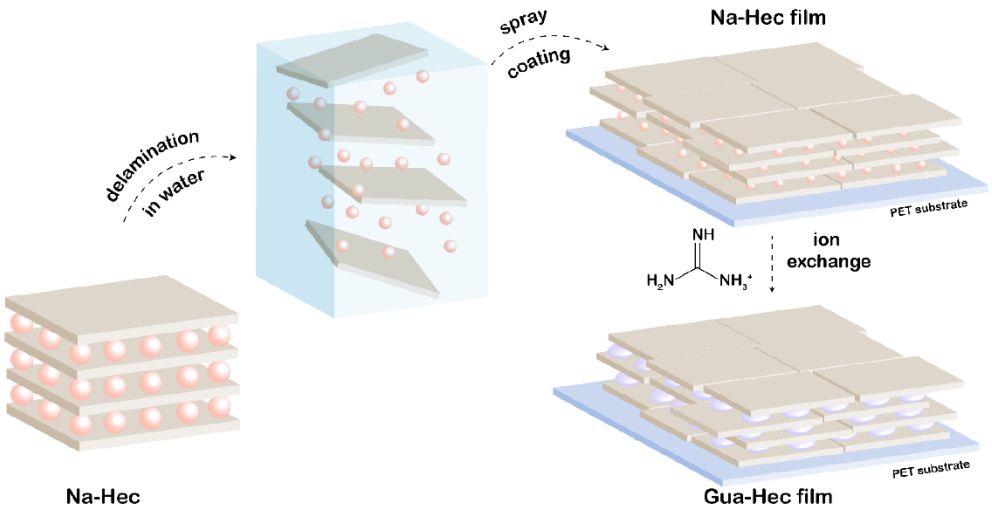

Figure 1. Schematic illustration of the manufacturing process of the hydrophobized nano-glass coating.

Results and discussion

Synthetic sodium hectorite with a nominal composition of $[Na_{0.5}]^{inter}[Mg_{2.5}Li_{0.5}]^{oct}[Si_4]^{tet}O_{10}F_2$ (Na-Hec) was obtained by melt synthesis followed by longtime annealing. The experimentally determined formula ($[Na_{0.48}]^{inter}[Mg_{2.57}Li_{0.47}]^{oct}[Si_4]^{tet}O_{10}F_2$) agreed within experimental error with the nominal composition resulting in a cation exchange capacity of 1.26 meq g^{-1}.[30] In the completely dry state, this material features a d-pacing of 9.6 Å (Figure S1) and unique charge homogeneity, purity and large platelet size (median 20000 nm).[30, 31] Delamination by 1D dissolution of Na-Hec in water into individual nanosheets is a thermodynamically driven, spontaneous process enabling easy and water-based processing.[32]

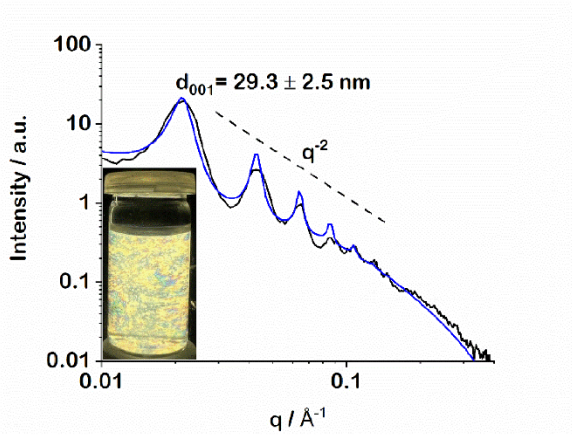

Figure 2. One-dimensional SAXS curve (black line: measurement, blue line: fit) of Na-Hec in water, indicating a homogeneous nematic, liquid crystalline dispersion with a separation of adjacent coplanar Na-Hec nanosheets of 29.3 ± 2.5 nm at 8 wt%. The inset shows the birefringence nature of a dilute dispersion of Na-Hec (0.5 wt%) in water under cross-polarized light.

Small-angle X-ray scattering (SAXS) of a concentrated gel (8 wt%), showed a separation of adjacent coplanar Na-Hec nanosheets of 29.3 ± 2.5 nm indicating a homogeneous suspension of clay monolayers of 1 nm thickness (Figure 2). Wide-angle X-ray scattering (WAXS) of dried

hectorite, a concentrated gel, and a dilute suspension corroborated the SAXS results of delamination (Figure S2).

Upon spray coating of a dilute suspension onto a corona-treated PET substrate the Na-Hec nanosheets self-assembly into a monodomain 1D crystalline Na-Hec film. Within the film, the Hec nanosheets overlap over large areas due to their huge lateral extension of 20000 nm while being oriented parallel to the substrate surface and a flexible, micron thin glass-like coating is obtained (Figure 1). The X-ray diffraction (XRD) pattern confirms the 1D crystallinity of the coating (Figure 3). Equilibrating the film at 43 % relative humidity (r.h.) gave the monohydrate[30] with a d-spacing of 12.5 Å. As indicated by a rational *00l* series and a coefficient of variation (CV) of 0.24 %, the periodicity in the restacked monodomain film is well defined and is comparably to the pristine Na-Hec material. Consequently, as with pristine bulk material, increasing the r.h. to 90 % leads triggered further swelling of the film to the two-layer hydrate with a d-spacing of 15.1 Å. At this hydration state, the *00l*-series is rational (CV = 0.23 %) indicating crystalline swelling of the restacked monodomain film to be as uniform for all interlayer spaces as in the non-delaminated pristine Na-Hec crystals. As will be discussed later, incorporation of water in the interlayer space (swelling) results in much increased transmission rates with increasing swelling. This renders Na-Hec monolayers films inappropriate for packaging applications at ambient r.h. Clearly, to mitigate detrimental swelling effects, the hygroscopic Na^+ had to be exchanged for a more hydrophobic cation. Most organocations would, however, open the interlayer space to slit heights larger than the kinetic radii of common permeants like water or oxygen. The choice of organocations yielding d-spacings smaller than 13 Å is limited. All atoms have to be sp^2 hybridized allowing for a flat arrangement in the interlayer space and the equivalent area (area requested per charge) has to be small enough to allow for complete ion exchange in a flat orientation. We chose guanidinium.

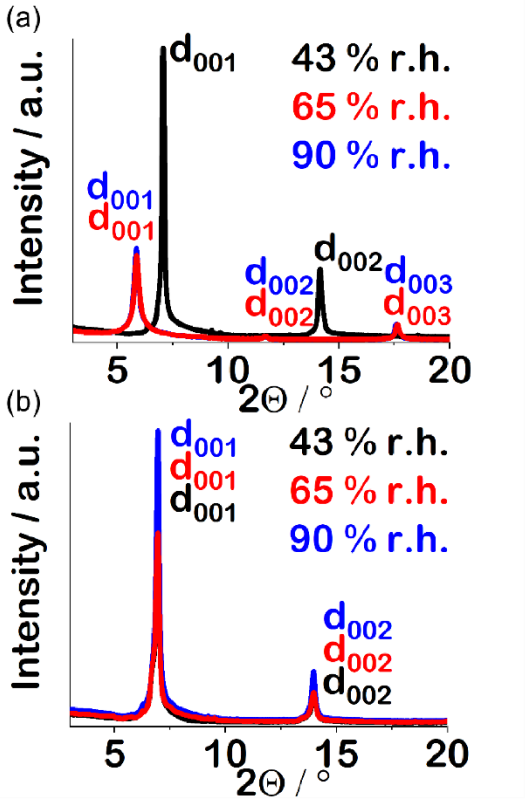

Figure 3. XRD pattern of (a) Na-Hec and (b) Gua-Hec at 43 % r.h. (black), 65 % r.h. (red), and at 90 % r.h (blue).

Therefore, the monodomain Na-Hec coating was immersed in a 1 M solution of the more hydrophobic guanidinium hydrochloride. Using a concentration higher than 0.02 M prevents 1D dissolution during the ion exchange warranting an intact coating while the guanidinium-exchange is progressing (Gua-Hec).[26] Completeness of the ion exchange was checked by energy dispersive X-ray spectroscopy (EDX) and X-ray diffraction (XRD). With EDX no residual Na^+ was found (Table S1, Figure S3). Contrary to Na-Hec, the XRD of the Gua-Hec coating showed no swelling even at 90 % r.h.. The *d*-spacing at 0 % r.h. was found to be 12.6 Å and did not increase at all upon exposure to water vapor (Figure 3b). The interlayer space of 3 Å (12.6 Å – 9.6 Å) is less than expected from the van der Waals radii of the heavy atom types (C, N, O) indicating that the

organocation is arranged lying flat parallel to the silicate surfaces. The small CV of 0.08 % of the rational *00l*-series, moreover, indicates that the interlayer height is uniform, while the resulting slit is narrow enough to hamper diffusion of oxygen and water molecules along the interlayer spaces of the restacked monodomain film. A contact angle of Gua-Hec films were found to be substantially higher (40.4 ± 1.7 °) than the value for Na-Hec films corroborating a significant hydropobization upon ion exchange (Figure S4) as already indicated by the loss of swelling capacity of Gua-Hec in humid air.

Cross-sectional transmission electron microscopy (TEM) images allowed for a more detailed insight into the coating structure and confirmed the self-assembly to produce band-like structures with individual Hec nanosheets overlapping over large areas (Figure 4).

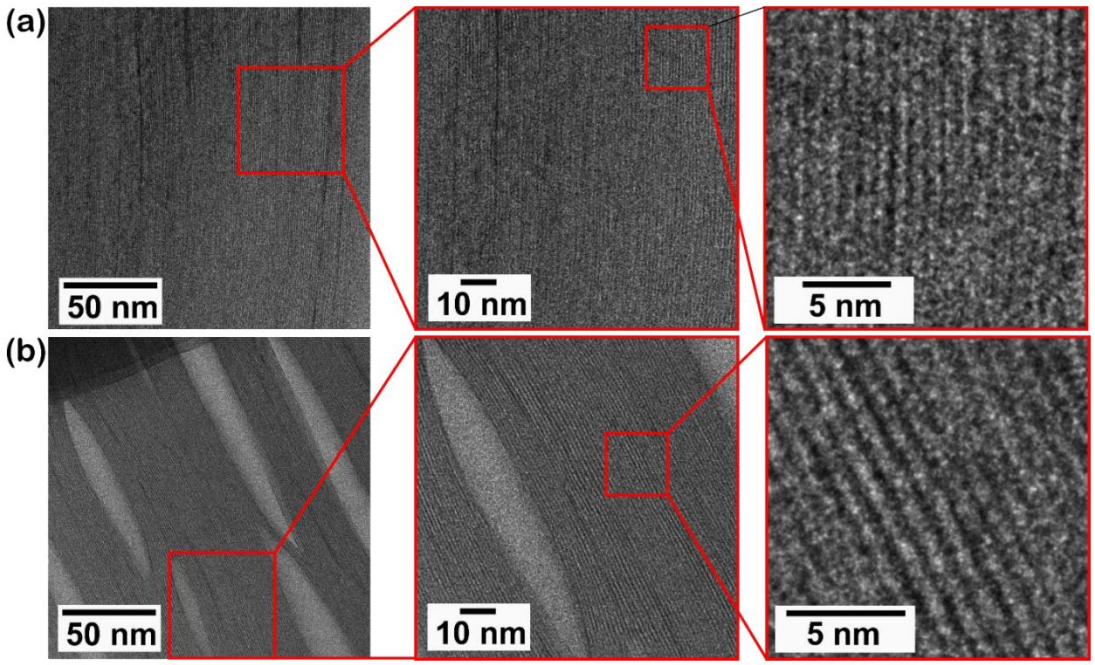

Figure 4. Cross-sectional TEM images of restacked monodomain films of (a) Na-Hec and (b) Gua-Hec.

The monodomain films looked like infinite 1D single crystals. As individual nanosheets have an irregular shape and a limited diameter of some 20000 nm, defects between to facing edges of monolayers must exist but are so scarce that they do not become apparent in the TEM images. Restacked Na-Hec films appear defect free in cross section. Apparently, upon drying the dilute wet-layers of dilute dispersion applied in a thickness of some 14 nm per spraying application allowed the water to leave the film without leaving behind voids (Figure 4a). When covering the Na-Hec with the guanidinium solution, the Na-Hec film will initially be swollen to the tri-hydrate before the Na^+ is gradually driven out of the interlayer and replaced by guadinium.[33] Upon ion exchange concomitantly the hydrophilicity is lowered eventually to a limit where the interlayer water is also completely expelled from the interlayer. As the guanidinium is applied from the top surface of the film, a gradient in interlayer composition will develop with the surface of the film being hydrophobized first. Consequently, the top of the film will collapse first and a barrier for water diffusion will gradually be built up. This in turn will hinder the interlayer water contained further down to the bottom of the film to leave the film structure and it therefore segregates into lenses being incorporated between large domains of defect free monodomain Gua-Hec films (Figure 4b). As the macroscopic defects (lenses) are invisible for X-rays, the Gua-Hec films still seem to be perfectly 1D crystalline. As after ion-exchange the Gua-Hec films were gently dried by equilibrating them at 43 % r.h. initially former interlayer water remains trapped in the lenses. In the course of storing the coating at these conditions over several weeks, eventually the water molecules will find the way out potentially creating some pinholes on their way out. These pinholes will of course affect the gas barrier performance.

As the Hec nanosheets are impermeable to gases like oxygen or water vapor and as the interlayer height is too small to allow diffusion along the slit between two restacked clay layers, ideally Gua-

Hec films would be expected to show zero transmission rates. The transmission measured experimentally must be attributed to defects and pinholes in the otherwise impermeable glass-like films.

Table 1. Oxygen and water vapor transmission rates of the Na-Hec, Gua-Hec and the uncoated PET substrate.

Sample	Coating thickness, µm	OTR, $cm^3\ m^{-2}\ day^{-1}\ atm^{-1}$		WVTR, $g\ m^{-2}\ day^{-1}$	
		23 °C, 65 % r.h.	38 °C, 90 % r.h.	23 °C, 65 % r.h.	38 °C, 90 % r.h.
PET (36 µm)	0	31.96	53.96	5.08	17.95
Na-Hec	1.4	0.23	0.42	3.90	12.31
Gua-Hec	1.6	0.12	0.32	0.93	3.74

Surprisingly, the Na-Hec showed very good oxygen transmission rates (OTR, Table 1) even at elevated r.h. where swelling of the Na-Hec has already set in opening the height of the interlayer space to 5.5 Å, a value larger than the kinetic radius of oxygen. At 23 °C and 65 % r.h. an OTR of 0.23 $cm^3\ m^{-2}\ day^{-1}\ atm^{-1}$ was observed and even at harsh conditions of 38 °C and 90 % r.h. the OTR was found to be as low as 0.42 $cm^3\ m^{-2}\ day^{-1}\ atm^{-1}$. Apparently, the transmission rate for oxygen is not too badly affected due to its limited solubility in the polar hydrated interlayer space.

After ion exchange for guanidinium the OTR of the coating is only slightly improved to 0.12 $cm^3\ m^{-2}\ day^{-1}\ atm^{-1}$ (23 °C and 65 % r.h.) and 0.32 $cm^3\ m^{-2}\ day^{-1}\ atm^{-1}$ (38 °C and 90 % r.h., Table 1). Despite suppressing swelling and despite fixing the interlayer height to a value smaller than the kinetic diameter of oxygen, Gua-Hec fails to completely block diffusion. We attribute this to structural defects as revealed in the TEM cross-sections that might act as pinholes. The

disappointing barrier apparently is limited to pinholes. Nevertheless, our binder-free, all-clay barrier competes well with methyl-Si-O-Si coatings[34] (60 - 100 nm thickness, OTR: < 1 cm^3 m^{-2} day^{-1} bar^{-1}) made by Vacuum-UV (V-UV) photo-decomposition of poly(1,1-dimethylsilazane-co-1-methylsilazane) and SiO_x coatings (7.5 nm thickness, OTR: 0.3 cm^3 m^{-2} day^{-1}) from plasma-enhanced chemical vapor deposition (PECVD) or Al_2O_3 coatings (7.5 nm thickness, OTR: 1.1 cm^3 m^{-2} day^{-1}) from plasma-enhanced atomic layer deposition (PEALD).[35] However, the best SiO_x coatings made by V-UV photodecomposition of perhydrosilazanes (150 – 300 nm thickness, OTR: < 0.05 cm^3 m^{-2} day^{-1} bar^{-1}) outperforms the binder-free clay coatings.[6]

As TR depend on sample's thickness, they need to be converted to oxygen permeability (OP) to facilitate comparison (Table 2, Figure 5). Furthermore, the influence of the PET substrate on the OTR is corrected as suggested by Roberts et al..[36]

Table 2. Oxygen and water vapor permeabilities of restacked films of Na-Hec and Gua-Hec as compared to the uncoated PET substrate.

Sample	OP, cm^3 µm m^{-2} day^{-1} atm^{-1}		WVP, g µm m^{-2} day^{-1} atm^{-1}	
	23 °C, 65 % r.h.	38 °C, 90 % r.h.	23 °C, 65 % r.h.	38 °C, 90 % r.h.
PET (36 µm)	1150.6	1942.6	10052.3	10831.4
Na-Hec	0.3	0.6	1291.3	918.7
Gua-Hec	0.2	0.5	100.2	126.7

The OP of Na-Hec films is 0.3 cm^3 µm m^{-2} day^{-1} atm^{-1}, whereas the OP of Gua-Hec films is 0.2 cm^3 µm m^{-2} day^{-1} atm^{-1} and 0.5 cm^3 µm m^{-2} day^{-1} atm^{-1}, at 23 °C and 65 % r.h. and 0.6 cm^3 µm m^{-2} day^{-1} atm^{-1} at 38 °C and 90 % r.h., respectively. Comparison to the PET substrate (1150.6 cm^3 µm m^{-2} day^{-1} atm^{-1} and 1942.6 cm^3 µm m^{-2} day^{-1} atm^{-1} at 23 °C/65 % r.h. and

38 °C/90 % r.h., respectively) shows a substantial improvement of barrier by multiple orders of magnitude. Compared to published binder-free films (70 – 120 µm) of Na-montmorillonite (2897 cm^3 µm m^{-2} day^{-1} bar^{-1}, Na-MMT), Li-montmorillonite (1690 cm^3 µm m^{-2} day^{-1} bar^{-1}, Li-MMT), or Mg-montmorillonite (18830 cm^3 µm m^{-2} day^{-1} bar^{-1}, Mg-MMT) both, Gua-Hec and Na-Hec, reveals the superiority of the synthetic hectorite over the other nanosheet materials, which is mainly based on much higher aspect ratio and perfect delamination into strict monolayers that facilitate restacking into films.[25]

Even Na-Hec coatings fabricated by a single wet-layer applied on PET by slot-die coating (2.1 cm^3 µm m^{-2} day^{-1} bar^{-1} at 23 °C and 50 % r.h.) are inferior by a factor of two, as this processing gave inferior order during restacking upon drying as compared to spray coating.[27]

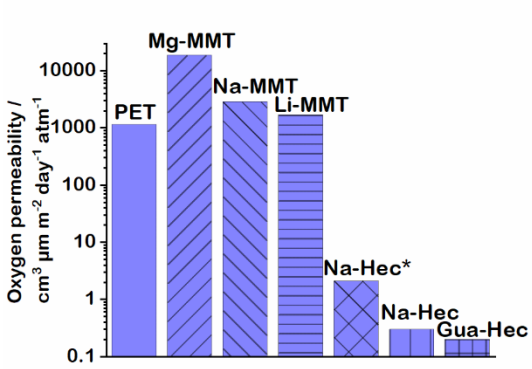

Figure 5. Comparison of the oxygen permeabilities of PET, solution casted Mg-montmorillonite (Mg-MMT), Na-montmorillonite (Na-MMT), Li-montmorillonite (Li-MMT), with Na-Hec* processed by slot-die coating, and with the spray-coated Na-Hec and Gua-Hec.[25, 27]

In contrast to OTR the WVTR measurements of Na-Hec films showed a significant break down of the water vapor barrier with increasing r.h. For Na-Hec films at 23 °C and 65 % r.h. a WVTR of 3.90 g m^{-2} day^{-1} was measured, while at 38 °C and 90 % r.h. WVTR increased to

12.31 g m^{-2} day^{-1}. The Gua-Hec films showed a substantially lower WVTR. At 23 °C and 65 % r.h. the WVTR was 0.93 g m^{-2} day^{-1} and at harsh conditions of 38 °C and 90 % r.h. the WVTR was 3.74 g m^{-2} day^{-1}.

Despite the distinctly different hydrophilicity, upon increasing the r.h. to 90 %, the WVTR of both all-clay coatings, Na-Hec and Gua-Hec, increased by a similar factor. With water vapor diffusion, increasing r.h. has several effects that are superimposed on each other: First swelling might open new diffusion pathways by widening the interlayer height. By this the mobility of interlayer species might be increased as well. Second reducing hydrophilicity will concomitantly reduce the solubility of the permeate water. Third, by increasing the r.h. the concentration of the permeate is increased. The latter is taken into account upon conversion of WVTR to WVP.

As evidenced by XRD (Figure 3) the Gua-Hec film does not swell even at higher r.h., thus, the increase of WVP with r.h. can be solely attributed to the change of solubility of water vapor in the clay film. At 23 °C and 65 % r.h. a WVP of 100.2 g µm m^{-2} day^{-1} atm^{-1} was observed (Table 2), which increased only slightly to 126.7 g µm m^{-2} day^{-1} atm^{-1} at 38 °C and 90 % r.h. indicating the the solubility increase for Gua-Hec is negligible, which in turn is in line with expectations for a hydrophobic barrier layer.

For Na-Hec coatings, at 23 °C and 65 % r.h. the WVP was 1291.3 g µm m^{-2} day^{-1} atm^{-1} (Table 2) and this decreased even slightly lower to 912.7 g µm m^{-2} day^{-1} atm^{-1} at 38 °C and 90 % r.h.. What seems counterintuitive on a first site, can be solely attributed to the higher concentration of the permeant as expressed by the water vapor partial pressure. The other two factors are negligible. This is not surprising as the interlayer height does not increase between 65 % r.h. and 90 % r.h. as indicated by a constant d-spacing (Figure 3). And as the interlayer space of the two-hydrate

structure is completely packed with interlayer cations and water molecules,[37] no voids exist that could take up more water and thus the solubility also changes only insignificantly.

The huge difference in WVP of Na-Hec and Gua-Hec coatings may therefore solely be attributed to the opening of a new diffusion avenue along the hydrated interlayers for water molecules. As such diffusion highways to not exist in condensed vapor deposited coatings, it is not surprising that the Na-Hec is by far inferior to competitors in respect to water vapor barrier performance.

Once the diffusion highway is closed by collapsing the interlayer height to less than 3 Å regardless of r.h. by ion exchange with guanidinium, the clay only coatings are rendered competitive to vapor deposited coatings. The WVTR of the aforementioned methyl-Si-O-Si coating (60 - 100 nm thickness, WVTR: < 4 g m^{-2} day^{-1}) is slightly worse than what is found for Gua-Hec.[34] Our binder-free, all-clay barrier even competes with SiO_x (70 nm thickness, WVTR: 3.5 g m^{-2} day^{-1}) and Al_2O_3 (170 nm thickness, WVTR: 0.8 g m^{-2} day^{-1}) coatings prepared by PECVD.[38] Gua-Hec is however, outperformed by the best SiO_x coatings made by V-UV photodecomposition of perhydrosilazanes (150 – 300 nm thickness, WVTR: < 10^{-2} g m^{-2} day^{-1}).[6]

For some packaging applications appealing optical properties are required. While SiO_x coatings are statistically isotropic and therefore transparent, an all-clay film consisting of individual micron-sized nanosheets might be affected by scattering. Visually, the two thin coatings appear as optically transparent as the uncoated PET substrate (Figure S5). To quantify the optical properties optical transmittance, haze, and clarity were measured (Figure 6). The PET substrate shows high optical transmittance, low haze, and high clarity. The application of Na-Hec lead to a slightly increased haze and a slightly decreased clarity mostly due to scattering at the rough surface. After the ion exchange, haze and clarity of the Gua-Hec coating were slightly increased and decreased,

respectively. A clarity of 91.4 % for Na-Hec and 90.3 % for Gua-Hec is still appropriate for transparent packaging (Figure S5).

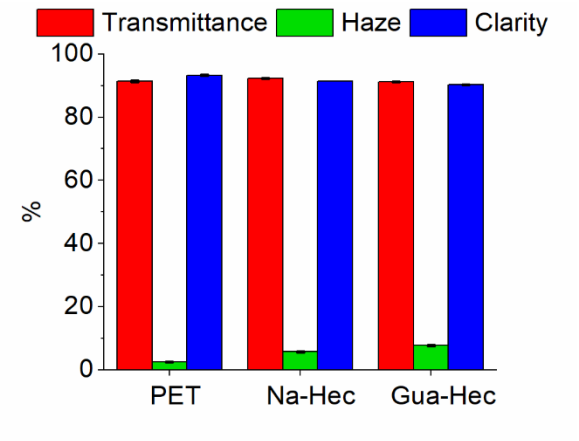

Figure 6. Optical transmittance, haze and clarity of the uncoated PET substrate and restacked monodomain films of Na-Hec and Gua-Hec.

Conclusion

Delamination of layered materials strictly into monolayers yield nematic dispersions of large aspect ratio nanosheets. When applying the suspensions to a planar substrate, the nanosheets self-assembly into 1D crystalline films. While intracrystalline reactivity and crystallographic order is comparable to the pristine layered parent compound, individual nanosheets overlap over large areas and instead of a microcrystalline powder, restacking yields monodomain films. Complete ion exchange may still be accomplished in the restacked film. Appropriate organocations like guanidinium not only block swelling with water vapor but irreversibly collapse the interlayer space to slit heights narrow enough to impede diffusion. Such water-processed films resemble nanoglass coatings obtained by physical vapor deposition methods. While such dense inorganic films would be expected to represent the ultimate barrier material, unfortunately the all-clay coatings as well as the physically deposited coatings show a limited permeability attributed to defects and pinholes.

EXPERIMENTAL

Materials and Methods.

In this study, a synthetic sodium fluorohectorite $[Na_{0.5}]^{inter}[Mg_{2.5}Li_{0.5}]^{oct}[Si_4]^{tet}O_{10}F_2$ was used. It is produced by melt synthesis followed by longtime annealing and has a cation exchange capacity of 1.26 meq g^{-1}.[31] The Guanidinium hydrochloride was purchased from Sigma Aldrich. A 36 µm thick PET foil (Bleher KG, Germany) with a corona treatment was used as substrate.

Preparation of the sodium hectorite coating

The sodium Hectorite was delaminated by immersing in double distilled water yielding a 0.5 wt% dispersion. The coating was produced using a fully automatic spray coating system with an infrared lamp drying unit. After every spray cycle, the coating is dried for 90 s at a temperature of 40 °C. After the spray coating, the Na-Hec is dried and stored at 43 % r.h. and ambient temperature.

Exchange of the sodium hectorite coating

The coated PET was placed in a 1 M aqueous solution of guanidine hydrochloride for 1 h. The solution is then exchanged for a new guanidine hydrochloride solution, and this procedure is repeated 5-times. Before drying, the film is thoroughly rinsed with water to wash an excess of guanidine hydrochloride off the coating. At the end of the exchange process, the coating is dried at 43 % r.h. and ambient temperature.

Characterization methods

Powder X-ray diffraction (XRD) measurements of the coatings were done in Bragg-Brentano-geometry using Cu $K_{\alpha 1}$ radiation (λ = 1.5406 Å). Analysis of the XRD patterns was done with Panalytical's Highscore Plus software. Na-Hec was dried under vacuum at 250 C for 4 days and filled in a glovebox into a 0.7 mm glass capillary (Hilgenberg). Powder X-ray diffraction of the

dried Na-Hec was measured in transmission geometry on a STOE Stadi P using Cu $K_{\alpha 1}$ radiation (λ = 1.5406 Å) and a MYTHENIK1K detector.

X-ray scattering measurements were performed with "Double Ganesha AIR" system (SAXSLAB/XENOCS). The X-ray source of this laboratory-based system is a rotating copper anode (MicoMax 007HF, Rigaku Corporation, Japan). A position sensitive detector (PILATUS 300 K for small-angle X-ray scattering (SAXS) and PILATUS 100 K for wide-angle X-ray scattering (WAXS), Dectris) was used for recording data. To enhance the signal-to-noise ratio in the SAXS measurements a Na-Hec suspension with a higher concentration (8 wt%) was prepared and measured in 1 mm glass capillaries (Hilgenberg). To obtain the basal spacing the SAXS data was fitted applying a model described in the SI employing the software Scatter (version 2.5, Figure S6).[39]

Oxygen transmission rates (OTR) were measured on a Mocon OX-TRAN 2/21 (Minneapolis, USA) and on a Mocon OX-TRAN 2/21 M10x. The samples were tested at 23 °C and a relative humidity of 65 % and at 38 °C and 90 % r.h. Forming gas (Linde Formiergas 95/5) was employed as carrier gas, and 100 % Oxygen (Linde Sauerstoff 3.5) as permeant. All measurements were performed after conditioning of the samples at the relevant relative humidities.

Water vapor transmission rates (WVTR) were detected on a Mocon PERMATRAN-W 3/33 (Minneapolis, USA). The samples were measured at 23 °C and r.h. of 65 % and at 38 °C and 90 % r.h.

Cross-sectional Transmission Electron Microscopy (TEM) images were measured employing a JEOL-JEM-2200FS (JEOL GmbH, Germany) microscope. Cross sections of the nanocomposite films were prepared using a JEOL EM-09100IS Cryo Ion Slicer (JEOL GmbH, Germany).

A Zeiss 1530 equipped with an EDX INCA 357 400 unit (Oxford) was used to measure energy dispersive X-ray spectroscopy (EDX) to check for a complete ion exchange with a detection limit of 1 atom%.

Contact angles were measured employing an OCA-15 (Data Physics, Germany). An average of 5 drops was taken.

Transmittance, haze, and clarity were determined using a BYK-Gardner Haze-Gard Plus (BYK-Gardner GmbH, Germany). The average of five measurements per film sample were taken.

The coating thickness was determined with a High-Accuracy Digimatic Micrometer (Mitutoyo, Japan) with a measuring range of 0 – 25 mm and a resolution of 0.1 µm. An average of 10 measurement points in the permeability area of the coated sample was taken, and the thickness of the substrate was subtracted.

ASSOCIATED CONTENT

Supporting Information.

The following files are available free of charge.

1D XRD pattern of dried Na-hectorite, 2D WAXS pattern of dried Na-hectorite, a concentrated gel in water, and a dilute suspension in water, EDX data of the exchanged hectorite coating and a SEM image of the measurement points, images of water drops on the coatings for determination of the contact angles, photographs of the PET substrate and the coated samples, fitting model applied to the SAXS data to obtain the basal spacing of the Na-hectorite dispersion (PDF).

AUTHOR INFORMATION

Corresponding Author

*Josef Breu – Bavarian Polymer Institute and Department of Chemistry, University of Bayreuth, Bayreuth 95447, Germany; orcid.org/0000-0002-2547-3950; Email: josef.breu@uni-bayreuth.de

Author Contributions

The manuscript was written through the contributions of all authors. All authors have given approval for the final version of the manuscript.

Funding Sources

This work was funded by the ALTANA Institute.

Notes

The authors declare no competing financial interest.

ACKNOWLEDGMENT

We appreciate the support of the Keylab "Mesoscale Characterization: Scattering Techniques", of the Keylab "Polymer Additives and Fillers", of the Keylab "Surface and Interface Characterization", and of the Keylab for "Optical and Electron Microscopy" of the Bavarian Polymer Institute. The authors thank Florian Puchtler for synthesizing the synthetic sodium hectorite and Marco Schwarzmann for the SEM measurements, as well as for preparing the TEM samples by cryo-ion-slicer and their measurements. We thank Jannik Thanner for helping with XRD sample preparation and Olena Khoruzhenko for designing graphics. We are thankful for

multiple stimulating discussions with people involved in the ALTANA Institute (Christian Schaumberg, Hubert Schießling, Ralf Hoffmann, and Udo Krappe).

REFERENCES

1. Lange, J.; Wyser, Y., Recent innovations in barrier technologies for plastic packaging?a review. *Packag. Technol. Sci.* **2003,** *16* (4), 149-158.
2. Zabihzadeh Khajavi, M.; Ebrahimi, A.; Yousefi, M.; Ahmadi, S.; Farhoodi, M.; Mirza Alizadeh, A.; Taslikh, M., Strategies for Producing Improved Oxygen Barrier Materials Appropriate for the Food Packaging Sector. *Food Eng. Rev.* **2020,** *12* (3), 346-363.
3. Muñoz-Rojas, D.; Maindron, T.; Esteve, A.; Piallat, F.; Kools, J. C. S.; Decams, J. M., Speeding up the unique assets of atomic layer deposition. *Mater. Today Chem.* **2019,** *12*, 96-120.
4. Hirvikorpi, T.; Vähä-Nissi, M.; Harlin, A.; Karppinen, M., Comparison of some coating techniques to fabricate barrier layers on packaging materials. *Thin Solid Films* **2010,** *518* (19), 5463-5466.
5. Dukalska, L.; Ungure, E.; Augspole, I.; Muizniece-Brasava, S.; Levkane, V.; Tatjana, R.; Krasnova, I., Evaluation of the Influence of Various Biodegradable Packaging Materials on the Quality and Shelf Life of Different Food Products. *Proc. Latv. Univ. Agr.* **2013,** *30* (1), 20-34.
6. Prager, L.; Helmstedt, U.; Herrnberger, H.; Kahle, O.; Kita, F.; Münch, M.; Pender, A.; Prager, A.; Gerlach, J. W.; Stasiak, M., Photochemical approach to high-barrier films for the encapsulation of flexible laminary electronic devices. *Thin Solid Films* **2014,** *570*, 87-95.
7. Prager, L.; Dierdorf, A.; Liebe, H.; Naumov, S.; Stojanovic, S.; Heller, R.; Wennrich, L.; Buchmeiser, M. R., Conversion of perhydropolysilazane into a SiOx network triggered by vacuum ultraviolet irradiation: access to flexible, transparent barrier coatings. *Chem. Eur. J.* **2007,** *13* (30), 8522-9.
8. With, P. C.; Helmstedt, U.; Prager, L., Flexible Transparent Barrier Applications of Oxide Thin Films Prepared by Photochemical Conversion at Low Temperature and Ambient Pressure. *Front. Mater.* **2020,** *7*.
9. Wu, F.; Misra, M.; Mohanty, A. K., Challenges and new opportunities on barrier performance of biodegradable polymers for sustainable packaging. *Prog. Polym. Sci.* **2021,** *117*, 101395.
10. Ebina, T., Development of Clay-Based Films. *Chem. Rec.* **2018,** *18* (7-8), 1020-1032.
11. Messersmith, P. B.; Giannelis, E. P., Synthesis and barrier properties of poly(ε-caprolactone)-layered silicate nanocomposites. *J. Polym. Sci., Part A: Polym. Chem.* **1995,** *33* (7), 1047-1057.
12. Doblhofer, E.; Schmid, J.; Riess, M.; Daab, M.; Suntinger, M.; Habel, C.; Bargel, H.; Hugenschmidt, C.; Rosenfeldt, S.; Breu, J.; Scheibel, T., Structural Insights into Water-Based Spider Silk Protein-Nanoclay Composites with Excellent Gas and Water Vapor Barrier Properties. *ACS Appl. Mater. Interfaces* **2016,** *8* (38), 25535-43.
13. Eckert, A.; Rudolph, T.; Guo, J.; Mang, T.; Walther, A., Exceptionally Ductile and Tough Biomimetic Artificial Nacre with Gas Barrier Function. *Adv. Mater.* **2018,** *30* (32), e1802477.
14. Song, Y.; Gerringer, J.; Qin, S.; Grunlan, J. C., High Oxygen Barrier Thin Film from Aqueous Polymer/Clay Slurry. *Ind. Eng. Chem. Res.* **2018,** *57* (20), 6904-6909.

15. Cussler, E. L.; Hughes, S. E.; Ward, W. J.; Aris, R., Barrier membranes. *J. Membr. Sci.* **1988,** *38* (2), 161-174.
16. Röhrl, M.; Federer, L. K. S.; Timmins, R. L.; Rosenfeldt, S.; Dörres, T.; Habel, C.; Breu, J., Disorder-Order Transition-Improving the Moisture Sensitivity of Waterborne Nanocomposite Barriers. *ACS Appl. Mater. Interfaces* **2021,** *13* (40), 48101-48109.
17. Habel, C.; Tsurko, E. S.; Timmins, R. L.; Hutschreuther, J.; Kunz, R.; Schuchardt, D. D.; Rosenfeldt, S.; Altstadt, V.; Breu, J., Lightweight Ultra-High-Barrier Liners for Helium and Hydrogen. *ACS Nano* **2020,** *14* (6), 7018-7024.
18. Schuchardt, D.; Rosenfeldt, S.; Kalo, H.; Breu, J., Fabrication of Bragg stack films of clay nanosheets and polycations via co-polymerization of intercalated monomers and functional interlayer cations. *Nanoscale* **2023,** *15* (15), 7044-7050.
19. Walther, A.; Bjurhager, I.; Malho, J. M.; Pere, J.; Ruokolainen, J.; Berglund, L. A.; Ikkala, O., Large-area, lightweight and thick biomimetic composites with superior material properties via fast, economic, and green pathways. *Nano Lett.* **2010,** *10* (8), 2742-8.
20. Morits, M.; Verho, T.; Sorvari, J.; Liljeström, V.; Kostiainen, M. A.; Gröschel, A. H.; Ikkala, O., Toughness and Fracture Properties in Nacre-Mimetic Clay/Polymer Nanocomposites. *Adv. Funct. Mater.* **2017,** *27* (10).
21. Podsiadlo, P.; Kaushik, A. K.; Arruda, E. M.; Waas, A. M.; Shim, B. S.; Xu, J.; Nandivada, H.; Pumplin, B. G.; Lahann, J.; Ramamoorthy, A.; Kotov, N. A., Ultrastrong and stiff layered polymer nanocomposites. *Science* **2007,** *318* (5847), 80-3.
22. Röhrl, M.; Timmins, R. L.; Rosenfeldt, S.; Schuchardt, D. D.; Uhlig, F.; Nürmberger, S.; Breu, J., Stretchable clay nanocomposite barrier film for flexible packaging. *ACS Appl. Mater. Interfaces* **2023**.
23. Nam, H.-J.; Ebina, T.; Ishii, R.; Nanzyo, H.; Mizukami, F., Self-Standing Film Formability of Various Clays. *Clay Sci.* **2007,** *13* (4-5), 159-165.
24. Nam, H.-J.; Ishii, R.; Ebina, T.; Mizukami, F., Flexible transparent self-standing binderless clay film prepared by hydrothermally-treated synthetic clay. *Mater. Lett.* **2009,** *63* (1), 54-57.
25. Nam, H.-J.; Ebina, T.; Mizukami, F., Formability and properties of self-standing clay film by montmorillonite with different interlayer cations. *Colloids Surf. A Physicochem. Eng. Asp.* **2009,** *346* (1-3), 158-163.
26. Rosenfeldt, S.; Stöter, M.; Schlenk, M.; Martin, T.; Albuquerque, R. Q.; Förster, S.; Breu, J., In-Depth Insights into the Key Steps of Delamination of Charged 2D Nanomaterials. *Langmuir* **2016,** *32* (41), 10582-10588.
27. Röhrl, M.; Mettke, J. H.; Rosenfeldt, S.; Schmalz, H.; Mansfeld, U.; Timmins, R. L.; Habel, C.; Breu, J.; Durst, F., Shear orientation of nematic phases of clay nanosheets: processing of barrier coatings. *J. Coat. Technol. Res.* **2021,** *19* (2), 487-495.
28. Plötze, M.; Kahr, G., Diagnostic intercalation in clay minerals - use of guanidine carbonate. In *Proceedings of the 4th MECC, Mineralogia*, Zakopane, Poland, 2008; Vol. 33, pp 331-332.
29. Mehio, N.; Dai, S.; Jiang, D. E., Quantum mechanical basis for kinetic diameters of small gaseous molecules. *J. Phys. Chem. A* **2014,** *118* (6), 1150-4.
30. Stöter, M.; Kunz, D. A.; Schmidt, M.; Hirsemann, D.; Kalo, H.; Putz, B.; Senker, J.; Breu, J., Nanoplatelets of sodium hectorite showing aspect ratios of approximately 20,000 and superior purity. *Langmuir* **2013,** *29* (4), 1280-5.

31. Breu, J.; Seidl, W.; Stoll, A. J.; Lange, K. G.; Probst, T. U., Charge homogeneity in synthetic fluorohectorite. *Chem. Mater.* **2001,** *13* (11), 4213-4220.
32. Dudko, V.; Khoruzhenko, O.; Weiß, S.; Daab, M.; Loch, P.; Schwieger, W.; Breu, J., Repulsive Osmotic Delamination: 1D Dissolution of 2D Materials. *Adv. Mater. Technol.* **2022**.
33. Moller, M. W.; Handge, U. A.; Kunz, D. A.; Lunkenbein, T.; Altstadt, V.; Breu, J., Tailoring shear-stiff, mica-like nanoplatelets. *ACS Nano* **2010,** *4* (2), 717-24.
34. Prager, L.; Wennrich, L.; Heller, R.; Knolle, W.; Naumov, S.; Prager, A.; Decker, D.; Liebe, H.; Buchmeiser, M. R., Vacuum-UV irradiation-based formation of methyl-Si-O-Si networks from poly(1,1-dimethylsilazane-co-1-methylsilazane). *Chem. Eur. J.* **2009,** *15* (3), 675-83.
35. Gebhard, M.; Mitschker, F.; Hoppe, C.; Aghaee, M.; Rogalla, D.; Creatore, M.; Grundmeier, G.; Awakowicz, P.; Devi, A., A combinatorial approach to enhance barrier properties of thin films on polymers: Seeding and capping of PECVD thin films by PEALD. *Plasma Process. Polym.* **2018,** *15* (5).
36. Roberts, A. P.; Henry, B. M.; Sutton, A. P.; Grovenor, C. R. M.; Briggs, G. A. D.; Miyamoto, T.; Kano, M.; Tsukahara, Y.; Yanaka, M., Gas permeation in silicon-oxide/polymer (SiOx/PET) barrier films: role of the oxide lattice, nano-defects and macro-defects. *J. Membr. Sci.* **2002,** *208* (1-2), 75-88.
37. Kalo, H.; Milius, W.; Breu, J., Single crystal structure refinement of one- and two-layer hydrates of sodium fluorohectorite. *RSC Adv.* **2012,** *2* (22).
38. Yun, J.; Lee, S.; Jeong, Y.; Lee, H.-R.; Kwon, J.-D.; Lee, G.-H., Reduction of Defects in SiOxVapor Permeation Barriers on Polymer Substrates by Introducing a Sputtered Interlayer. *Jpn. J. Appl. Phys.* **2009,** *48* (5).
39. Förster, S.; Fischer, S.; Zielske, K.; Schellbach, C.; Sztucki, M.; Lindner, P.; Perlich, J., Calculation of scattering-patterns of ordered nano- and mesoscale materials. *Adv. Colloid Interface Sci.* **2011,** *163* (1), 53-83.

Table of Content (ToC) = Graphical Abstract

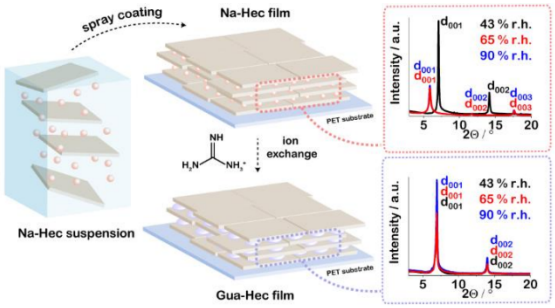

Supporting Information

Spraying Transparent Nanoglass Coatings

Dominik Schuchardt[†], *Maximilian Röhrl*[†], *Lukas Federer*[†], *Sabine Rosenfeldt*[†], *Hussein Kalo*[‡], *and Josef Breu* [†,*]

[†] Bavarian Polymer Institute and Department of Chemistry, University of Bayreuth, Universitätsstraße 30, 95447 Bayreuth, Germany

[‡] BYK-Chemie GmbH, Plant Moosburg, Stadtwaldstrasse 44, 85368 Moosburg, Germany

KEYWORDS: 2D layered materials, nanosheets, clay, ion exchange, coatings, gas barrier, packaging

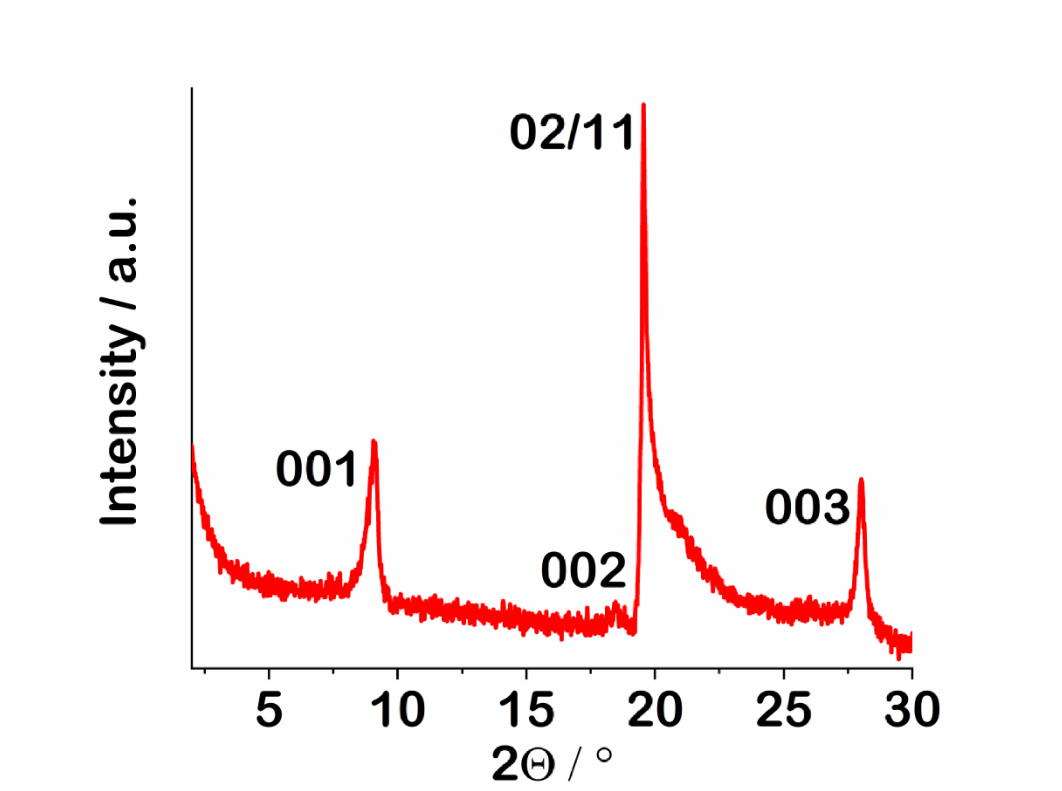

Figure S1. XRD pattern of the pristine, dried Na-hectorite powder showing a d-spacing of 9.6 Å.

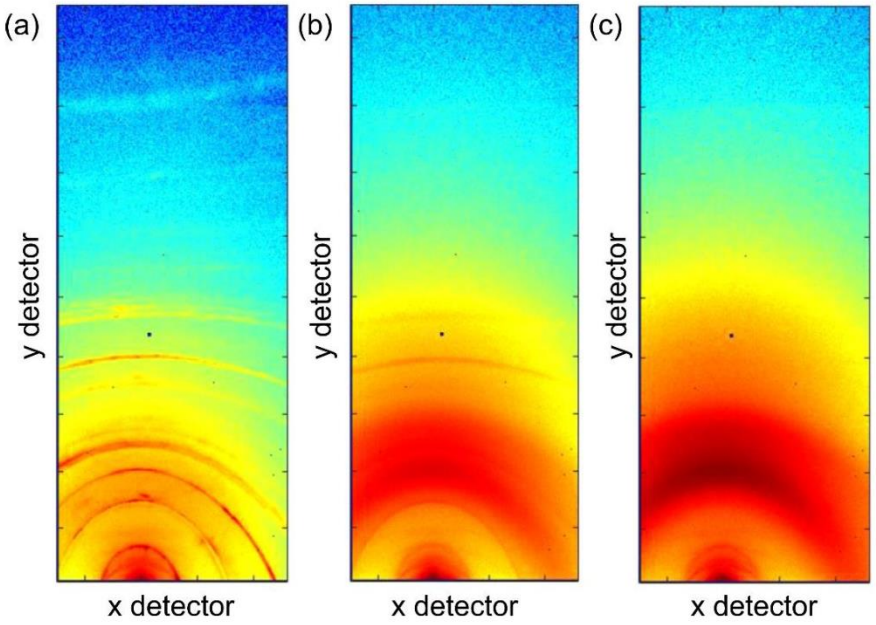

Figure S2. 2D wide-angle X-ray scattering pattern of (a) dried Na-Hec, (b) a concentrated gel of Na-Hec in water, and (c) a dilute suspension of Na-Hec in water.

Table S1. Energy dispersive X-ray analysis of Gua-Hec coating to confirm complete exchange of Na^+.

Point	O (atom%)	Na (atom%)	Si (atom%)
1	43.6	0.0	15.7
2	42.5	0.0	16.2
3	44.9	0.0	14.7
4	44.7	0.0	14.9

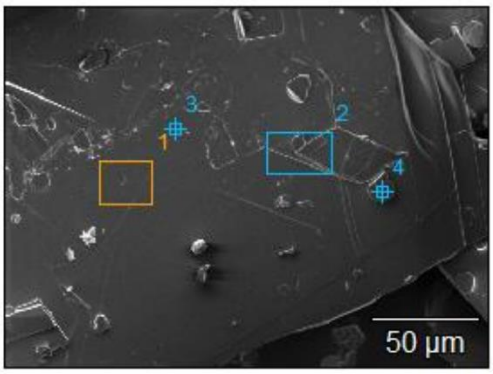

Figure S3. Scanning electron microscope image of the EDX measurement points 1-4.

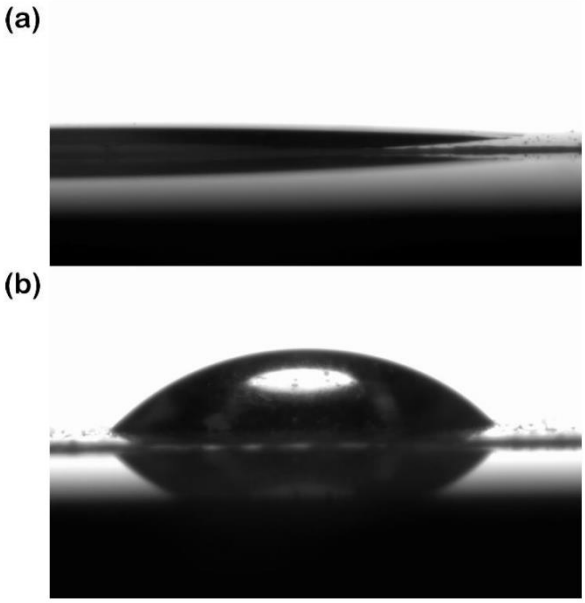

Figure S4. Images of a droplet of water on (a) Na-Hec with a contact angle of 5.3 ± 1.1 ° and (b) Gua-Hec with a contact angle of 40.4 ± 1.7 ° indicating the higher hydrophobicity of the exchanged coating.

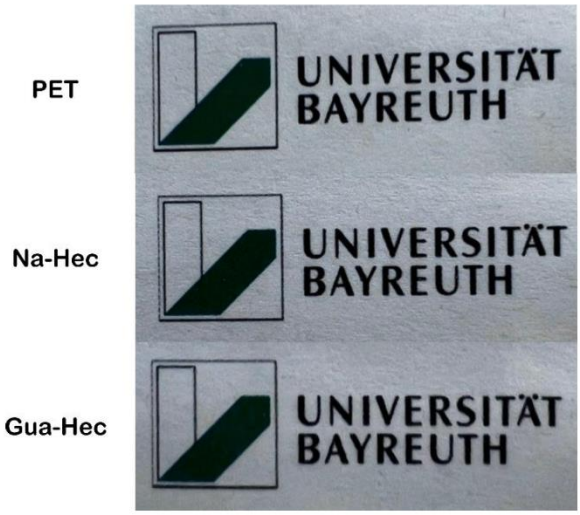

Figure S5. Photographs of the neat PET, with Na-Hec coating, and with Gua-Hec coating.

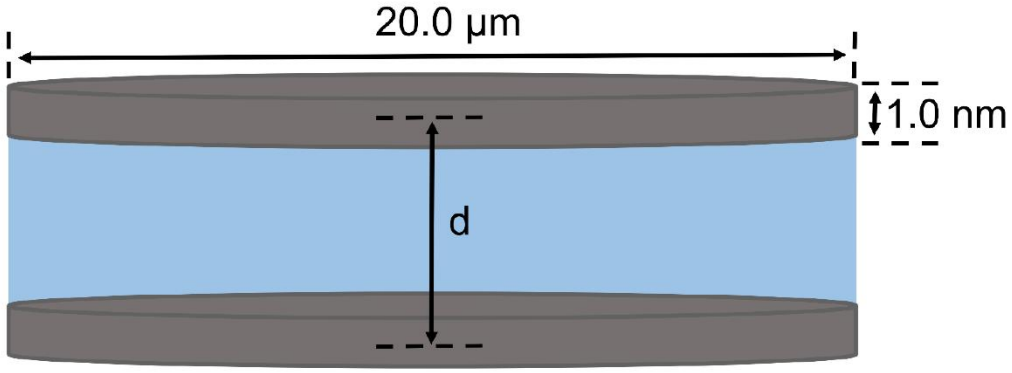

Figure S6. Fitting model used to obtain the basal spacing d from small-angle X-ray scattering data applying a layer width of 20.0 µm (± 15 %, Gaussian distribution) and a layer thickness of 1.0 nm (± 3 %, Gaussian distribution).[1]

REFERENCES

1. Förster, S.; Fischer, S.; Zielske, K.; Schellbach, C.; Sztucki, M.; Lindner, P.; Perlich, J., Calculation of scattering-patterns of ordered nano- and mesoscale materials. *Adv. Colloid Interface Sci.* **2011,** *163* (1), 53-83.

7. List of publications

7.1. Publications included in this thesis

Schuchardt, D., Röhrl, M., Federer, L., Rosenfeldt, S., Breu, J.: Spraying Transparent Nanoglass Coatings. *ACS Appl. Nano Mater.* **2023** (submitted).

Schuchardt, D., Rosenfeldt, S., Kalo, H., Breu, J.: Fabrication of Hybrid Bragg Stack Films of Clay Nanosheets and Polycations via Co-polymerization of intercalated monomers and functional interlayer cations. *Nanoscale.* **2023**, 15, 7044-7050.

Schuchardt, D., Röhrl, M., Rosenfeldt, S., Breu, J.: Gas Barriers from In Situ Polymerized Poly(ethylene glycol) Diacrylate Clay Nanocomposites for Food Packaging. *ACS Appl. Polym. Mater.* **2023**, 5, 1, 576-582.

7.2. Additional publications

Röhrl, M., Timmins, R.L., Rosenfeldt, S., Schuchardt, D.D., Uhlig, F., Nürmberger, S., Breu, J.: Stretchable Clay Nanocomposite Barrier Film for Flexible Packaging. *ACS Appl. Mater. Interfaces.* **2023**.

Loch, P., Schuchardt, D., Algara-Siller, G., Markus, P., Ottermann, K., Rosenfeldt, S., Lunkenbein, T., Schwieger, W., Papastavrou, G., Breu, J.: Nematic suspensions of a microporous layered silicate obtained by forceless spontaneous delamination via repulsive osmotic swelling for casting high-barrier all-inorganic films. *Sci. Adv.* **2022**, 8, eabn9084.

Habel, C., Tsurko, E.S., Timmins, R.L., Hutschenreuther, J., Kunz, R., Schuchardt, D.D., Rosenfeldt, S., Altstädt, V., Breu, J.: Lightweight Ultra-High-Barrier Liners for Helium and Hydrogen. *ACS Nano*. **2020**, 14, 6, 7018-7024.

Schöttle, M., Schuchardt, D., Edenharter, A., Koch, S., Senker, J., Breu, J.: Determination of the charge of Al_{13} Keggin oligocations intercalated into synthetic hectorite. *Z. Naturforsch. B.* **2019**, 71, 85-90.

8. Acknowledgements

This thesis is the product of the last few years of research and would not have been possible without the help and support of many others.

First, I want to thank my supervisor, Prof Dr. Josef Breu, for the opportunity to join his group and work on an exciting industry project. Further, I would like to express my gratitude for his guidance and trust over the years and for providing me with the freedom to conduct my research independently in well-equipped laboratories.

Next, I want to thank Christian Schaumberg, Hubert Schießling, Ralf Hoffmann, Udo Krappe, Hussein Kalo, and Fabian Gyger involved in the ALTANA Institute for all the inspiring discussions regarding my research within the cooperation with BYK and ELANTAS. In addition, I want to thank ALTANA for the opportunity to present my results at the ALTANA Summer Schools. Thanks to all other ALTANA members I have met for their support and discussions. Thanks to the ALTANA Institute for financial support.

My thanks continue to all members of ACI and ACIII. I want to thank Petra Seidler, Silke Reimann, and Iris Raithel for helping me with all kinds of administrative tasks. Thanks to Marco Schwarzmann, Florian Puchtler, and Michael Thelen for the synthesis of hectorite, all kinds of sample preparation, their measurements, and technical support. Thanks to Theresa Dörres and Maximilian Röhrl for being great lab colleagues and all the discussions work related or not. Thanks to Daniel Wagner, Patrick Loch, Natalie Eichstaedt, and many more for all the lunch and coffee breaks. Thanks to Sebastian Weiß who always had an open ear for me and for the entertaining table tennis matches. Thanks to Wolfgang Milius for his help and ideas. Thanks to Daniel and Wolfgang for commenting on this work.

Furthermore, I want to thank my volleyball teammates of the “Herren II” of the BSV Bayreuth. With you, it was always possible for me to find the necessary distraction from the university.

Probably my biggest thanks goes to my parents without their love and support I would not have made it this far.

In the end, I want to thank Lisa for her love, support, and motivation at all times.

9. Erklärung des Verfassers

(Eidesstattliche) Versicherungen und Erklärungen

(§ 9 Satz 2 Nr. 3 PromO BayNAT)

Hiermit versichere ich eidesstattlich, dass ich die Arbeit selbstständig verfasst und keine anderen als die von mir angegebenen Quellen und Hilfsmittel benutzt habe (vgl. Art. 64 Abs. 1 Satz 6 BayHSchG).

(§ 9 Satz 2 Nr. 3 PromO BayNAT)

Hiermit erkläre ich, dass ich die Dissertation nicht bereits zur Erlangung eines akademischen Grades eingereicht habe und dass ich nicht bereits diese oder eine gleichartige Doktorprüfung endgültig nicht bestanden habe.

(§ 9 Satz 2 Nr. 4 PromO BayNAT)

Hiermit erkläre ich, dass ich Hilfe von gewerblichen Promotionsberatern bzw. –vermittlern oder ähnlichen Dienstleistern weder bisher in Anspruch genommen habe noch künftig in Anspruch nehmen werde.

(§ 9 Satz 2 Nr. 7 PromO BayNAT)

Hiermit erkläre ich mein Einverständnis, dass die elektronische Fassung der Dissertation unter Wahrung meiner Urheberrechte und des Datenschutzes einer gesonderten Überprüfung unterzogen werden kann.

(§ 9 Satz 2 Nr. 8 PromO BayNAT)

Hiermit erkläre ich mein Einverständnis, dass bei Verdacht wissenschaftlichen Fehlverhaltens Ermittlungen durch universitätsinterne Organe der wissenschaftlichen Selbstkontrolle stattfinden können.

Bayreuth, ...